http://dx.doi.org/10.14755/DIS.1999.001

PREVENTION OF COPPER CORROSION USING AROMATIC SULFOXIDES AND BENZOHYDROXAMIC ACIDS

CANDIDATE THESIS

BY ABDUL IBDEWI SHABAN

This dissertation is presented as part of the requirements for the award of the Degree of Candidate of the Hungarian Academy of Sciences.

Under the supervision of Prof. Erika Kálmán

1998

http://dx.doi.org/10.14755/DIS.1999.001

Prevention of Copper Corrosion Using Aromatic Sulfoxides and Benzohydroxamic Acids

Candidate Thesis

By

Abdul Muttalib Shaban

This dissertation is presented as part of the requirements

for the award of the Degree of Candidate

of the Hungarian Academy of Sciences,

Budapest, Hungary

Submitted 1997

http://dx.doi.org/10.14755/DIS.1999.001

Dedication

AFFECTIONATELY DEDICATED TO

MY BELOVED PARENTS.

رَبِّ ارْحَمْهُمَا كَمَا رَبَّيَانِىْ صَغِيْرًا

O Allah ﷻ! Have mercy upon them as they had mercy upon me when I was small.

(AL-Quraan S. 17, V. 24)

http://dx.doi.org/10.14755/DIS.1999.001

Acknowledgment

I would firstly express my sincere thanks to Prof. Dr. Erika Kálmán, for her supervision, invaluable advice and encouragement throughout this research.

I am very grateful to Dr. Judit Telegdi for her assistance throughout this work. I also greatly appreciate Mr. Lajos Haklik for his technical assistance.

I wish to express my warm gratitude and thanks to the Directors of the HAS CRIC, Prof. Dr. Ferenc Márta and Prof. Dr. Gábor Pálinkás for making me more than welcome in the institute.

I express my special thanks to Dr. István Lukovits, dr. Franciska Kármán, Éva Tarlós, Andrea Jámbor, Katalin Tímár, Anna Eke, Tibor Horváth, Dr. Imre Bakó, Dr. Szabó Sandor and also to my laboratory mates Gabriella Stáhl, Ilona Felhösi, and Zsófia Keresztes, for their extensive helps in various ways.

I owe many thanks to dr. János Bácskai and Prof. Dr. György Inzelt of ELTE University for allowing me to use their laboratory cell at the early stages of the work.

Many thanks are to Mrs. Szokira Józsefné, of the MTA Doctori Tanács, for her kindness and cooperation.

I am indebted to all my friends for their moral support.

Last but not least, I would like to thank my parents and the rest of my family, only their cooperation and sacrifice make me to achieve this task in satisfactory manner.

Above all, I am very much grateful to GOD Almighty for giving me courage and good health for completing this venture.

This moment, my heart is filled with pleasant thoughts, thanks to its source.

Abdul

http://dx.doi.org/10.14755/DIS.1999.001

Declaration.

The research work reported in this thesis has been carried out under the supervision of Prof. Dr. E. Kálmán, Head of Solution Chemistry and Corrosion Research Department at Central Research Institute for Chemistry of the Hungarian Academy of Sciences.The subject matter of the thesis is original and has not previously been submitted in part or in full for any degree or diploma at this or any other tertiary educational institution.

Abdul Shaban

http://dx.doi.org/10.14755/DIS.1999.001

Table of contents:

http://dx.doi.org/10.14755/DIS.1999.001

http://dx.doi.org/10.14755/DIS.1999.001

http://dx.doi.org/10.14755/DIS.1999.001

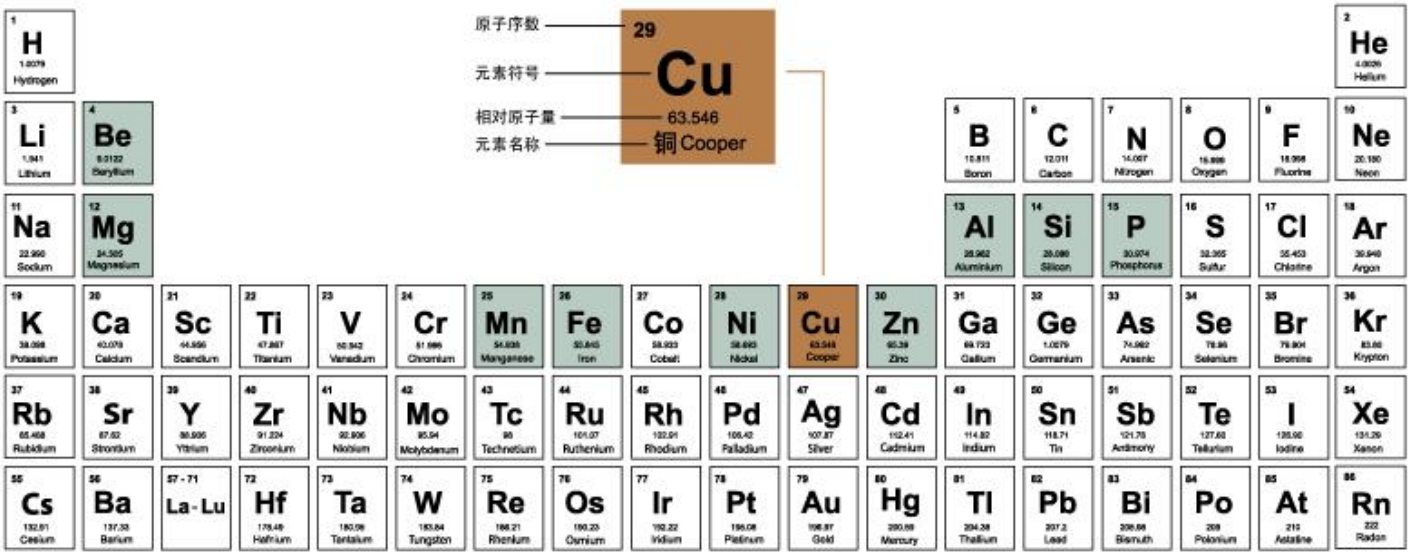

http://dx.doi.org/10.14755/DIS.1999.001

List of Abbreviations and Symbols

Abbreviations:

AC	Alternating current
AFM	Atomic force microscopy
AW	Atomic weight
BEV	Butler-Erdey-Gruz-Volmer
CE	Counter electrode
DBS	Dibenzylsulfide
DBSO	Dibenzylsulfoxide
DC	Direct current
DI	De-ionized
DPSO	Diphenylsulfoxide
DPTSO	Di-p-tolylsulfoxide
ECI	Electrochemical interface
EDX	Energy dispersive spectrometer
EIS	Electrochemical impedance spectroscopy
EQCM	Electrochemical quartz crystal microbalance
FRA	Frequency response analyzer
IE	Inhibition efficiency
M	Metal
M^{n+}	Metal cation
NLLS	Non-linear least square
o-Cl-BHA	Ortho-chloro-benzohydroxamic acid
OCP	Open circuit potential
o-M-BHA	Ortho-methyl-benzohydroxamic acid
p-Cl-BHA	Para-chloro-benzohydroxamic acid
p-N-BHA	Para-nitro-benzohydroxamic acid
ppb	Parts per billion
QCM	Quartz crystal microbalance
RDS	Rate determining step
RMS	Root mean square factor
SCE	Saturated calomel electrode
SEM	Scanning electron microscopy
TOC	Total oxygen content
UPD	Under potential deposition
WE	Working electrode
WL	Weight loss

Symbols:

$\dot{\delta}$	Thickness reduction rate
ρ	Density of copper
ω	Frequency
Ω	Ohm
η	Over-potential
θ	Phase shift
α,β	Transfer coefficients
β_a	Anodic Tafel slope
Δd	Fractional change in density
Δf	Frequency shift
Δf_l	Frequency shift caused by surface layers change (liquid effect)
Δf_m	Frequency shift caused by surface layers change (Δm)
Δm	Mass change
ρ_q	Density of quartz crystal
μ_q	Shear modulus
Δt	Time interval
$[Cl^-]$	Concentration of chloride ion

http://dx.doi.org/10.14755/DIS.1999.001

A	Piezoelectrically active area
a, b	Tafel constants
aw	Atomic weight
C_{dl}	Double layer capacitance
C_f	Differential sensitivity constant
C_{film}	Surface film capacitance
df	Differential frequency shift
E	Electrode potential
E_{corr}	Corrosion potential
F	Faradays constant
f	Resonance frequency
f_o	Frequency of crystal before mass change
I	Applied current
i	Net current density
i_{corr}	Corrosion current
i_o	Exchange current density
i_p	Applied current density
j	Square root of unity
n	Electrovalence
q	Electrical charge
R	Universal gas constant
R_{ohm}	Ohmic resistance
R_p	Polarization resistance
R_{pi}	Polarization resistance with the addition of inhibitor
R_{po}	Polarization resistance without the addition of inhibitor
R_{pore}	Surface film resistance
R_t	Charge transfer resistance
T	Absolute temperature
t	Time
W_i	Corrosion rate with the addition of inhibitor
W_o	Corrosion rate without the addition of inhibitor
Z	Vertical distance factor
$Z(j\omega)$	Impedance
Z’	Real part of the impedance
Z’’	Imaginary part of the impedance

http://dx.doi.org/10.14755/DIS.1999.001

List of figures:

http://dx.doi.org/10.14755/DIS.1999.001

http://dx.doi.org/10.14755/DIS.1999.001

List of Tables:

http://dx.doi.org/10.14755/DIS.1999.001

Chapter 1.

1. INTRODUCTION

When metals are reduced from their ores, one of nature's fundamental reactions is reversed. In most environments, metals tend to revert to compounds, which are stable; a process that is called ***corrosion***. Corrosion is derived from the Latin "***corrosus***", meaning, "***gnaw away***". Corrosion is a destructive process in most cases where metals deteriorate and unwanted damages take place.

There are several ways and means to prevent corrosion, one of which is the application of inhibitors. In the early years, mainly inorganic inhibitors were applied to protect metals in different environments.

Due to general awareness of the environmental damage, and stricter regulations, these inhibitors are increasingly restricted. Another major point to be considered is the trend towards the development of environment-friendly technologies. Though inhibitors such as chromates are effective, they are becoming environmentally unacceptable because of the health hazards associated with its use. Attention has been diverted to the study of new compounds as inhibitors.

Despite considerable advances in the study of the mechanisms of corrosion and inhibition, there are many unsolved questions. The difficulties arise because of the complexity of the factors controlling corrosion and its inhibition.

The major factors are as follows:

- the surface conditions of the metal,
- composition of the medium near to the metal surface, and
- changes of the environment.

Many new methods have been developed to the study of the electrochemical interfaces and applied in corrosion investigations in the last 10 years.

Copper is generally a relatively noble metal, however, it is susceptible to corrosion by acids and strong alkaline solutions, especially in the presence of oxygen or oxidants. One major application of copper is the acid cleaning installations. In the pH range between 2 and 5 the dissolution of copper is very rapid and the formation of a stable surface oxide layer which can passivate metal surfaces is impossible. Copper can only passivate by forming an oxide surface layer in weak acid or alkaline solutions. On the other hand, copper and its alloys are applied extensively in marine environments due to their high corrosion resistance in harsh seawaters. In

http://dx.doi.org/10.14755/DIS.1999.001

addition, copper dissolution in chloride solutions is very important in the electropolishing and electromachining industries.

Due to those reasons attention has been focused on the behavior of copper in chloride solutions. Even if copper corrosion in near neutral aqueous solutions seems to be low, the dissolved copper ions can induce corrosion of other less noble materials present in the system. Accordingly, an additive must be added to the environment in order to modify or hinder the reactions involved in the process.

Based on these facts, our attention was focused on copper corrosion in two different media. The applied electrolytes were 0.1 M Na_2SO_4 (pH=2.95) and neutral 0.5 M NaCl (pH≈7) solutions.

There is number of chemical compounds that could be applied as corrosion inhibitors for copper corrosion but only few formulations have been thoroughly investigated. It was found that inhibitors molecules containing atoms as nitrogen and sulfur are the most effective.

S-containing inhibitors such as, sulfoxide molecules specifically di-benzyl-sulfoxid (DBSO) [$(C_6H_5CH_2)_2SO$] are well known inhibitors for metal corrosion in sulfuric acid solution. However, these molecules were never tested as potential inhibitors for copper corrosion inhibition in acidic media. Some of these compounds were found effective

Among the tested inhibitor molecules, a new group compounds, hydroxamic acid derivatives (HAs), was found. Hydroxamic acids (HA's) are well known chelating agents for bivalent metal ions, such as copper.

The applied experimental techniques should provide information to determine both the corrosion rate of the copper electrode and at the same time monitor inhibitor adsorption on the electrode surface. The electrochemical quartz crystal microbalance (EQCM) was proved very useful.

Film thickness variations due to adsorption of the inhibitor or the mass loss due to corrosion can be monitored in real time. This method delivers some advantages over the classical gravimetrical method due to its high sensitivity. EQCM could detect mass changes in the nanogram range, thus a mono-molecular layer can be detected. The behavior of the copper electrode in the presence of different inhibitors in neutral environment is investigated for the first time using a quartz microbalance.

Beside this technique, AC (electrochemical impedance spectroscopy) and DC (potentiostatic polarization) electrochemical techniques, and different surface techniques (atomic force microscopy (AFM) and scanning electron microscopy (SEM-EDX)) were applied.

AFM imaging is a new applied method to monitor surface changes due to corrosion or inhibition processes. This method is very useful when applied to investigate samples in electrolytes.

Considering the above mentioned review, the present investigation focuses on the following aims:

- the development and application of quartz crystal microbalance as a rapid tool to investigate the corrosion inhibition performance of copper corrosion inhibitors, for both the acidic and neutral media
- the study of the inhibition of copper corrosion by different chemical compounds in acidic or neutral media in order to find an environmentally friendly inhibitor.

http://dx.doi.org/10.14755/DIS.1999.001

- the study of inhibition mechanisms of copper corrosion inhibition and suggesting different models to illustrate the actions.

The plan of work in this direction is schematically shown by the flow diagram in Figure 1.

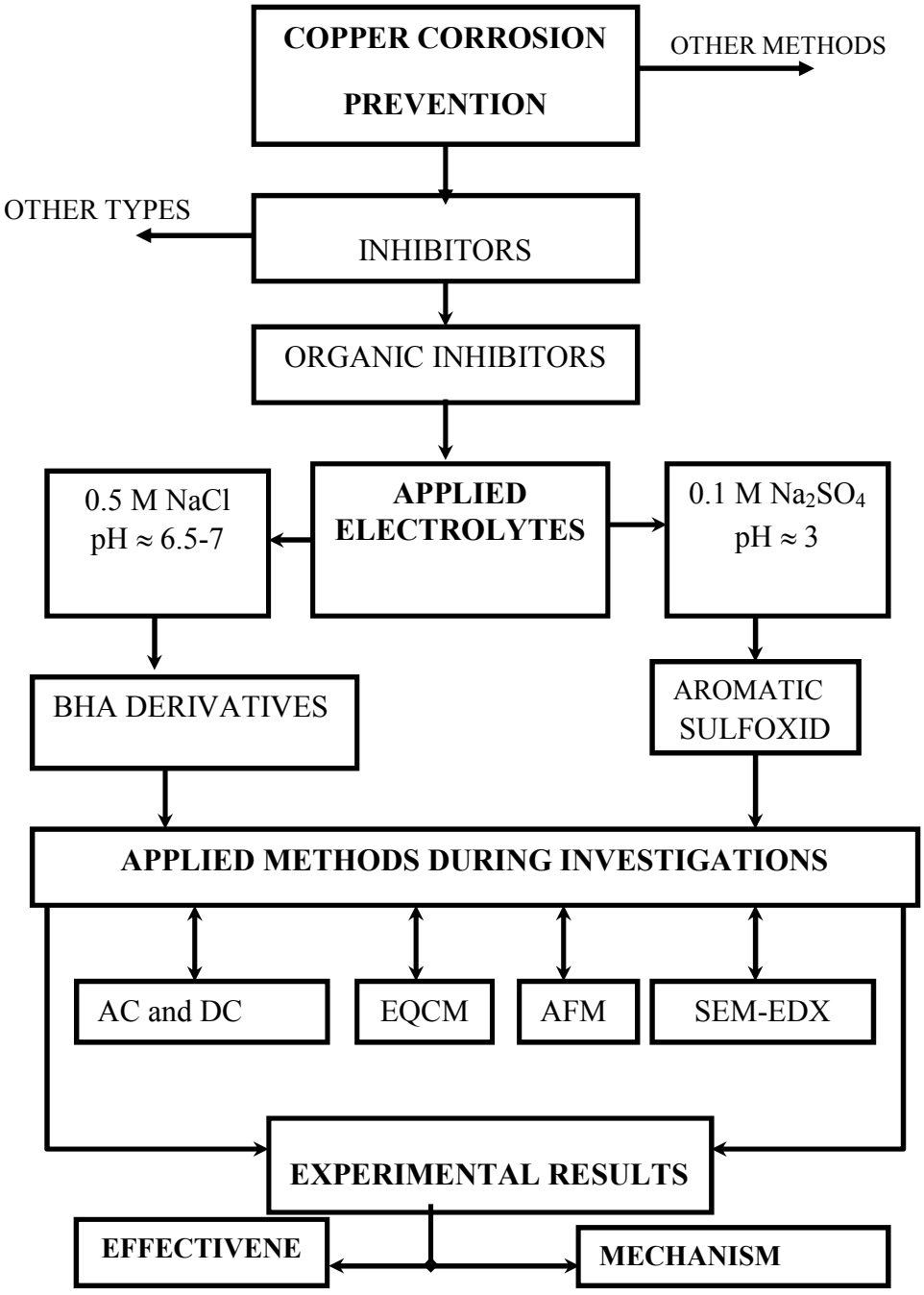

Figure 1. Flow diagram of the plan for this thesis

http://dx.doi.org/10.14755/DIS.1999.001

Chapter 2.

2. LITERATURE REVIEW

2.1. CORROSION BASICS

When metals are reduced from their ores, one of nature's fundamental reactions is reversed. In most environments, metals tend to revert to compounds, which are stable; a process that is called ***corrosion***. Corrosion is derived from the Latin "***corrosus***", meaning, "***gnaw away***". Corrosion may be further defined as a gradual destruction of a material, a substance or an entity, usually by solution or other means attributed to a chemical process [1-3]. The understanding of mechanism and kinetics of these reactions will assist in devising ways and means to minimize the losses due to corrosion.

The electrochemical corrosion, which takes place in presence of electrolyte solutions, wherein the reaction, occurs at the metal / solution interface is of great interest during this investigation.

Spontaneous corrosion of metals requires the presence of two processes: anodic and cathodic reactions.

1. The anodic reaction is the oxidation of the metal to its more stable form of ion. This is shown in general form as:

$$M \rightarrow M^{n+} + n\,e^- \quad (1)$$

2. There are several different cathodic reactions, which are frequently encountered in metallic corrosion. The most common cathodic reactions are:

- Oxygen reduction (in acidic solutions)

$$O_2 + 4H^+ + 4\,e^- \rightarrow 2H_2O \quad (2)$$

- Oxygen reduction (in neutral or alkaline solutions)

$$O_2 + 2H_2O + 4\,e^- \rightarrow 4OH^- \quad (3)$$

- Hydrogen evolution (in the absence of oxygen)

$$2H^+ + 2e^- \rightarrow H_2 \uparrow \quad (4)$$

The electrons produced in the anodic reaction are consumed by the cathodic process. The rate of electron generation must match that of electron consumption, i. e. there is not net build-up of electrons in the metal. The corroding metal attains a corrosion potential E_{corr}, somewhere between the equilibrium potentials of the anodic and cathodic processes. The rate of the corrosion reaction depends not just on the magnitude of the driving force (the difference between the two equilibrium potentials), but also on the kinetics of the anodic and cathodic processes.

The driving forces for both the hydrogen evolution and oxygen reduction processes depend on the pH of the solution [4]. Based on the chemical and electrochemical equilibrium, reactions of metals in aqueous

http://dx.doi.org/10.14755/DIS.1999.001

solutions, the potential-pH diagram, i.e. the so-called Pourbaix diagram provides the thermodynamically stable (immunity) region and areas where corrosion or passivity occurs [4].

The sites of the anodic and cathodic processes may be microscopically adjacent or they may be some distance apart. An electrically conductive path must however exist between the sites, electronically conductive path via the metal and ionically conductive path through the electrolyte. The actual areas of the anodic and cathodic sites also matter, since it is the current density (number of electrons generated per unit area per unit time) that controls the metal dissolution rate.

If the corrosion current density can be determined, then it is simple to calculate the corrosion (or penetration) rate using Faraday's law. Under freely corroding conditions the anodic and cathodic currents are equal but opposite in polarity. The corrosion potential attains a level at which this equality occurs where both the anodic and cathodic reactions are polarized from their equilibrium values towards this potential. Unfortunately, the corrosion current can not be measured directly and a few tricks have to be resorted to.

2.2. COPPER CORROSION

The corrosion rate measurements must be related to the rate-determining step (rds) of the mechanism if the results are to have a predictive or diagnosis value. Many fundamental studies were concerned with the mechanisms of copper corrosion and deposition in various media [5-14]. Rate controlling processes as well as the influence of some solution species, such as the Cl^- ion, are also elucidated. It is worth mentioning that most of the kinetic data were obtained without considering the existence of surface films (oxides, hydroxides, salts etc.), i.e. they are valid in the first moments following the immersion of the sample. It should also be pointed out that the influence of impurities in the metal phase is seldom considered in analyzing the behavior of copper.

2.2.1. Copper dissolution in water

In the absence of complexing agents (e.g. Cl^- ions, NH_3) in the corrosive medium, anodic dissolution of copper proceeds via two-step ionization of metal [7,8].

$$Cu \leftrightarrow Cu^+ + e^- \quad (5)$$

$$Cu^+ \leftrightarrow Cu^{2+} + e^- \quad (6)$$

Chemical conversion of Cu^+ ions by dissolved oxygen must be added:

$$2\,Cu^+ + \tfrac{1}{2}\,O_2 + H_2O \rightarrow 2\,Cu^{2+} + 2OH^- \quad (7)$$

The rate of reaction is more or less influenced by diffusion of the Cu^{2+} ions.

A Pourbaix diagram for copper in water system is shown in Figure 2. Different areas of the diagram indicate different equilibrium states of the metal.

http://dx.doi.org/10.14755/DIS.1999.001

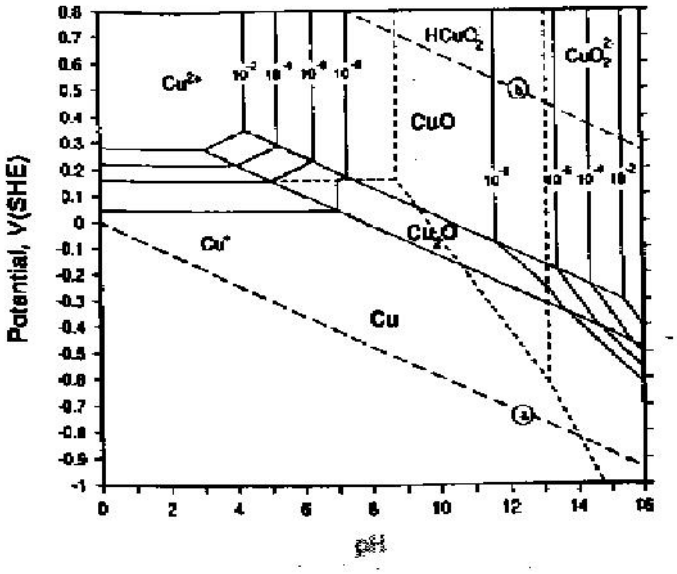

Figure 2. Equilibrium diagram for copper-water system at 25°C. Source: Ref. [13]

2.2.2. Copper dissolution in sulfate solutions

Anodic dissolution of copper is involved in electrorefining, electropolishing, corrosion phenomena, and maintaining the supply of electroless deposition processes. Bockris [9] and Kiss [10,12] employed a galvanostatic-transient polarization method to study the kinetics of deposition and dissolution of copper in $CuSO_4$ solution. According to these studies, the dissolution of copper takes place in a step-wise route in which Cu^+ ion is the intermediate species as previously shown by Equations (5,6).

In this model, the redox process between Cu^+ and Cu^{2+} , (Equation 6), is regarded as the rate-controlling step and the reaction steps relating to k_1/k_{-1}, (equilibrium constants for Equation 5), are supposed to equilibrate very quickly compared to those relating to k_2/k_{-2} , (equilibrium constants for Equation 6).

A Pourbaix diagram of the Cu-SO_4^{2-}-H_2O system is shown in Figure 3. This diagram shows the behavior of copper in SO_4^{2-} containing environment at different pH and potential.

http://dx.doi.org/10.14755/DIS.1999.001

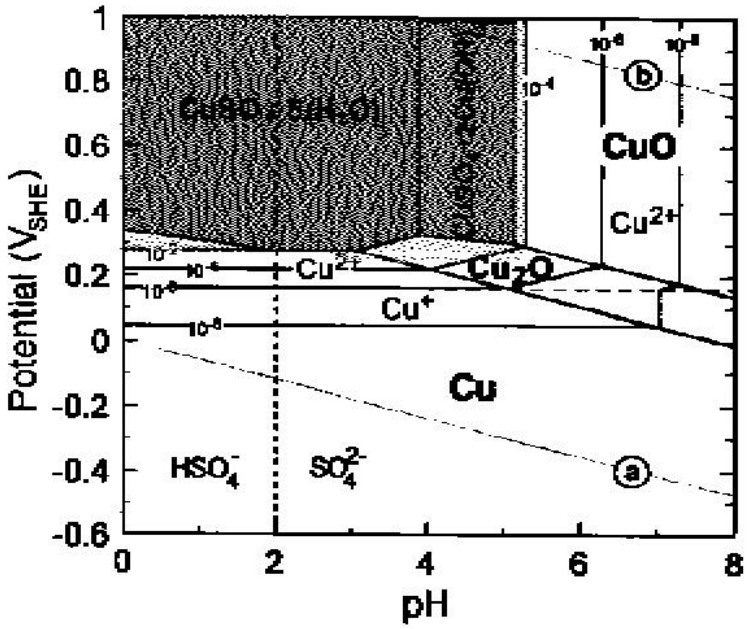

Figure 3. E-pH diagram for the Cu- SO_4^{2}-H_2O system at 25°C. Source: Ref. [13].

2.2.3. Copper dissolution in chloride solutions

The electrodissolution of copper in chloride containing solutions have been treated by several authors [8,11,12,14].The anodic reaction can be represented by the two-step sequence:

$$Cu + Cl^- \leftrightarrow CuCl_{ads} + e^- \quad (8)$$

$$CuCl_{ads} + Cl^- \leftrightarrow CuCl_2^- \quad (9)$$

(k_1,k_{-1}) and (k_2,k_{-2})) represent the equilibrium constants for Equations. 8 and 9, respectively.

High chloride concentrations lead to higher order complexes such as $CuCl_3^{-2}$ and $CuCl_4^{-3}$. The rate of electrodissolution increases as the chloride ion concentration increases. In the [Cl^-] range of 0.1-4 M. For [Cl^-] ≤ 1 M, the reaction rate is second order with respect to Cl^- indicating that below 1 M Cl^-, $CuCl_2^-$ is the dominant cuprous species [14].

http://dx.doi.org/10.14755/DIS.1999.001

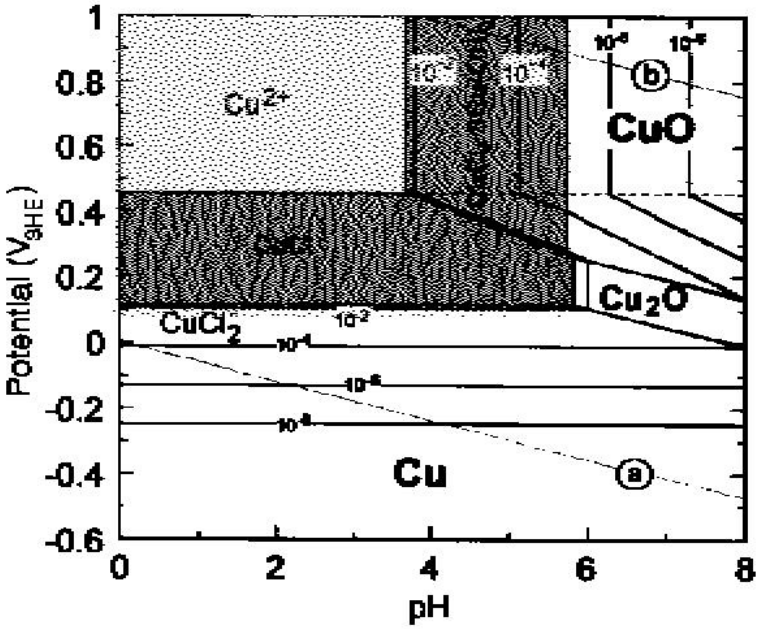

Figure 4. E-pH diagram for the Cu-Cl^--H_2O system at 25°C. Source: Ref. [13].

Figure 4 shows a Pourbaix diagram for copper in chloride containing environment.

2.2.4. Copper Oxide layers

Surface layers may interfere with corrosion reactions developing on uniformly accessible surfaces. All the processes occurring across a solid interphase are rate-controlled by a combination of faradic and non-faradic processes. Corrosion product layers grow in time. The inhibitor may interfere with the growth or dissolution process of the corrosion products. Knowledge of the nature and properties of the copper surface films is necessary in order to describe completely the mechanism of action of inhibitors. The composition and thickness of films depend on the composition of the corrosive medium and exposure time. In aqueous phase, anions determine the kind of over-layer obtained after sufficient growth time: brochantite in the presence of SO_4^{2-} ions, paratacamite with Cl^- ions etc. In all cases, it seems that Cu^+ oxide is first formed at the copper surface. For longer exposure times, salts or other oxide types are found: CuO, $Cu(OH)_2$, Cu_2O_3. In the case when only oxides are created, it has been shown that Cu^+ oxide is oxidized further to a Cu^{2+} oxide films [7,8,14]. This oxide film is not stable: therefore, it never thickens to the point where it can act as a passive film.

Cu_2O, as the initial corrosion product on copper, has been the subject of many investigations. It was often indicated that several forms of Cu_2O are likely to co-exist, depending on the formation conditions at the metal surface. Burke [15] and Arvia [16] have postulated the existence of Cu^+ species including Cu* (adatoms) and Cu (surface lattice atoms), i.e. Cu*OH, CuOH, Cu_2*O and Cu_2O. The formation of Cu^+ oxide in a NaCl solution may be due either to the precipitation of Cu_2O from the solution, or hydrolysis of $CuCl_2^-$ ions:

$$2\,CuCl_2^- + H_2O \rightarrow Cu_2O + 2H^+ + 4Cl^- \quad (10)$$

http://dx.doi.org/10.14755/DIS.1999.001

A direct oxidation of copper is also possible:

$$2Cu + H_2O \rightarrow Cu_2O + 2H^+ + 2e^- \quad (11)$$

2.3. CORROSION INHIBITORS

Inhibitor is a chemical substance which, when it is added in small concentrations to an environment, effectively checks, decreases, or prevents the reaction of the metal with the environment. To be used effectively, the inhibitor must be compatible with the expected environment, economical for the operation, amenable to treatment, and one which will contribute the greatest desired effect without any harm to the environment.

Corrosion inhibitors must be understood in light of the corrosion mechanism itself, since inhibition must either reduce the rate-determining step (rds) or create a new one.

While certain inorganic chemicals are useful for controlling corrosion, the tighter rules and restriction drew the attention to the more safe components. Organic inhibitors are increasingly applied in preventing metallic corrosion. According to the types of inhibition [17], inhibitors may be classified as:

- passivators.
- precipitators.
- vapor phase.
- cathodic, anodic or mixed type (catanodic).
- neutralizing.
- absorbents.

Lorenz and Mansfeld attempted to distinguish between interface and interphase concepts of inhibition [18]. They suggested:

Interface inhibition – two-dimensional structure (2D).

The inhibitor reacts directly with the metal surface. This type of mechanism assumes a strong interaction between the inhibitor and the corroding metal surface in the form of a barrier, because of the adsorption of the inhibitor as a two-dimensional layer. The inhibitor can behave in different ways. Geometric blocking which leads to protection of the metal surface against the solution, and coverage which deactivates the active sites of the metal surface or self-reaction of the inhibitor, which reacts instead of the metal.

Interphase inhibition – three-dimensional structure (3D).

The inhibitor reacts with the corrosion product film or by chemisorption and will form porous or nonporous 3D layers. Therefore, the inhibitor must pass through the diffusion layer and reacts with the layer beyond the surface ion shell.

http://dx.doi.org/10.14755/DIS.1999.001

Inhibitor effectiveness

The chemical structure of the inhibitor molecule plays a significant role and often determines whether a compound will effectively inhibit specific systems. Effectiveness of inhibitors has been determined in many ways and conclusions have been drawn as the determining factors contributing to effectiveness. Some general concepts are:

- the size of the organic molecule,
- the aromaticity and/or conjugated bonding,
- the hydrophobic or hydrophilic character,
- bonding strength to metal substrate,
- the type of bonding atoms or groups in the module (either π or σ)
- the ability for producing a compact layer,
- the ability to complex with the atom as a solid within the metal lattice, and
- efficient solubility.

Developing inhibitors

The theoretical explanations of inhibitor functions are in common agreement that adsorption phenomena involve:

Proton acceptors.

Organic molecules that fit this group can be generally considered as cathodic site adsorbents. Materials in this group accept the hydrogen ion or proton and migrate to the cathode. Organic inhibitors used in various acidic environments are included. Examples are anilines, urea, and aliphatic amines.

Electron acceptors.

Chemical compounds in this group are generally effective at anodic sites. They function as inhibitors due to their ability to accept electrons, and are most effective for corrosion reactions under anodic control. In addition to anodic inhibitors, passivating inhibitors are found within this group. Examples are organic peroxides, organic thiols, and the inorganic chromates and nitrates.

Mixed molecules.

These are organic molecules with more than one orienting groups attached (i.e. - NH_2 and – SH). Due to their ability to affect both anodic and cathodic processes of corrosion, these structures are classified as "ambiodic" inhibitors [19].

It appears likely that the most effective organic inhibitor is that whose electron density distribution causes inhibitor to be attracted to both anodic and cathodic areas.

Riggs and Every [19] determined why certain compounds, or groups of compounds, were effective as anodic and/or cathodic inhibitors of metallic corrosion. However, the theoretical considerations offer only guidelines,

http://dx.doi.org/10.14755/DIS.1999.001

as it was discussed previously. Interpretation of adsorbent type organic inhibitors performance data can be enhanced by "fitting" these data to one of the adsorption isotherms: Langmuir, Frumkin, Freudlich or Temkin isotherm [20].

2.3.1. Inhibitors action in acidic solutions

The effects of adsorbed inhibitors on the corrosion of metals acidic solutions are to retard either the cathodic hydrogen ion reduction and / or reaction, or the anodic dissolution process of the metal. These effects may result from the changes in the electrical double layer (EDL), from the reduction of metal reactivity, from the participation of the inhibitor in partial electrode reaction, and / or from the formation of a physical barrier.

The inhibition mechanism related to a reduction of metal reactivity does not necessarily involve the complete coverage of the metal surfaces by the adsorbed inhibitor. The inhibitor adsorbs on active sites only reducing either the anodic or the cathodic reaction or both. The reaction rate will be decreased in proportion to the extent to which the active sites are covered by the adsorbed inhibitor. The reaction mechanism does not change. In this case, the polarization curves are shifted to lower current density values without changing the Tafel slope values [21].

It is generally assumed that the anodic reaction of metal dissolution proceeds via steps with the formation of adsorbed intermediates on the metal surface [22]. The adsorbed additive may participate in the intermediate formation, promoting a reduction or a stimulation of the electrode reaction depending on the stability of the adsorbed surface complex.

In the presence of a surface complex, the rate of the anodic dissolution of the metal is reduced by changing the reaction mechanism; consequently, an increase in the anodic Tafel slope is observed.

Some classes of inhibitors are able to form multimolecular layers on the metal surface, such as compounds with a long hydrocarbon chain. The resulting barrier action is quite independent of the nature of adsorption forces between the inhibitor molecule and the metal surface. It interferes with the diffusion of ions to or from the metal surface. The hindering of mass transport causes the inhibition of the corrosion reaction. In this case, the corresponding polarization curves demonstrate concentration polarization and resistance polarization on the cathodic branches.

Copper corrosion inhibition in acidic solutions

Based on experimental results, S-containing inhibitors are primarily useful in sulfuric acid (SO_4^{2-}), while N-containing inhibitors exert their best efficiencies in hydrochloric acid (Cl^-) [23]. Among the S-containing inhibitors, sulphoxides, sulphides and thioureas are widely used in commercial inhibitors formulations. Dibenzyl sulphoxide, dibenzyl sulphide, thiourea and di-o-tolylthiourea are the most prominent representatives of these groups of compounds.

The corrosion of copper and brass in sulfuric acid can be inhibited using thiourea, quinoline or azoles [24]. The most common inhibitors are benzotriazole and its derivatives [25].

http://dx.doi.org/10.14755/DIS.1999.001

2.3.2. Inhibitors action in near-neutral solutions

The corrosion of metals in near-neutral aqueous solutions gives rise to the formation of surface products with low solubility, such as oxides, hydroxides or salts; the cathodic partial process is the oxygen reduction. In this situation, the action of the inhibitors will be exerted on the oxide-covered surface by maintaining or increasing the protective characteristics of the surface layer in the aggressive solution. The first step of the inhibition is the displacement of the pre-adsorbed water molecules by the adsorbed inhibitor molecule. This molecule could react at the surface. Because of the adsorption or reaction of the inhibitor at the oxide covered surface of the metal, different mechanisms can occur.

Some additives interfere with the reaction of oxygen reduction by restricting the diffusion of dissolved oxygen to the metal surface. In the presence of this type of inhibitors (restricting the diffusion of oxygen) usually thick surface layers, with poor electronic-conducting properties, are formed. Examples are phosphates, polyphosphates, silicates and borates. Some other additives, such as chromates and nitrates, act by causing self-passivation of metallic materials with active-passive anodic behavior. These additives are considered anodic inhibitors; in their presence, a passivating film is formed. Sodium salts of various organic acids, (acetate, propionate, benzoate, salicylate, phthalate, etc.), are proposed as inhibitors. According to Thomas [26] the mechanism of action of the inhibitive anions involves:

- stabilization of the passivating oxide with reduction of its dissolution rate;
- repassivating the surface with repair or reformation of the oxide film;
- plugging of pores in the oxide film by formation of insoluble surface products;
- competitive adsorption of inhibitive anions preventing the adsorption of corrosive anions.

An interesting series of compounds, which can act as efficient corrosion inhibitors, is the surface-active chelating agents [27], when insoluble surface chelates are formed. On the contrary, the formation of soluble chelates may promote corrosion stimulation. Different action mechanisms for chelating inhibitors have been suggested:

- a surface precipitation reaction of the chelate formed by the organic additive and the dissolved metallic ions. The resulting thick layer constitutes a physical barrier, hindering the contact between the constituents of the solution and the metal surface.
- initial chemisorption of the chelating agent to the metal surface, followed by interaction either with metal still bound in the crystal lattice or with metal ions already associated with the surface oxide film.

Among the surface-active chelating inhibitors for copper and copper alloys corrosion are oximes and possibly hydroxamic acids.

Potential inhibitors to be investigated.

Theoretically, there are great number of materials that could be applied as corrosion inhibitors for copper corrosion but only few formulations have been thoroughly investigated. It was found that most effective groups

http://dx.doi.org/10.14755/DIS.1999.001

contain atoms like N and S, which are able to bridge easily with other molecules. For a metal like copper, which can form multibonds, inhibitor molecules containing those atoms are strongly recommend.

Sulfoxide molecules, specifically dibenzylsulfoxide (DBSO), are well known inhibitors for the corrosion of iron and its alloys in acidic media. Several investigations have dealt with the inhibition effectiveness of DBSO in different HCl environment [28-31]. The effectiveness of aromatic sulfoxides on the copper corrosion was not investigated previously. DBSO, DPSO DPTSO are picked for their structure differences.

Hydroxamic acids (HA) are well known chelating agents for mono-, bi-, and tri-valent metal ions [32]. BHA derivatives are excellent candidates to act as inhibitors because of the presence of the amino group and the presence of a hydrophobic substituent on the benzene ring. The hydroxamate anion can exist in three possible species:

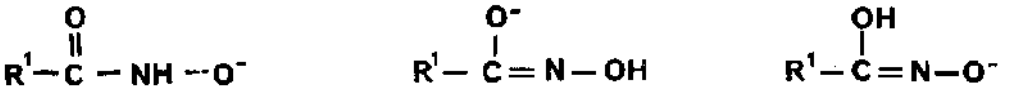

A B C

Species (A) and (B) are the reactive ones. They exist in approximately equal concentration. BHA forms different complexes with copper ions at different pH values. As shown in Figure 5, at pH of 7, the Cu-BHA complex consists of, 78% $Cu:BHA^{+}$, 11% Cu^{2+} and 11% $Cu:BHA^{++}$ [33].

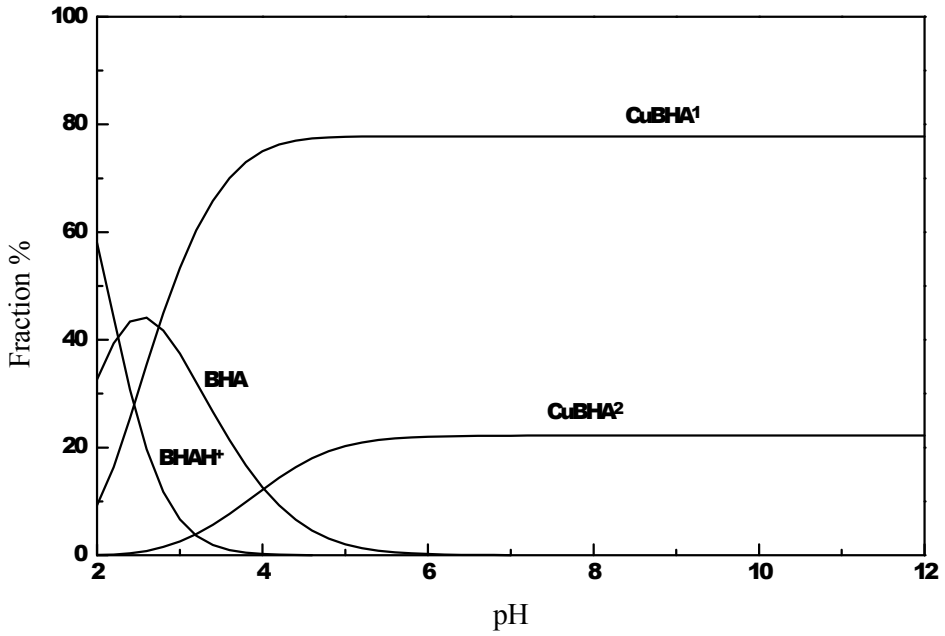

Figure 5. Complexing between copper and benzohydroxamic acid as a function of pH

The inhibition actions of these two groups of compounds on copper corrosion are investigated.

http://dx.doi.org/10.14755/DIS.1999.001

2.4. STUDYING THE ACTION OF INHIBITORS

Both corrosion and its inhibition have long been evaluated by one of several techniques: visual, soluble metal ion analysis, calipers and metal test strips. Metallic corrosion is essentially an electrochemical process and so can be studied by electrochemical techniques. Many electrochemical techniques have been developed during the past several decades for investigating the reasons and mechanisms of corrosion processes, for detecting the corrosivity of the environment and evaluating the efficiency of corrosion resistant materials etc.

Although electrochemical techniques are supposed to be versatile tools in corrosion science and engineering, their most common application is the determination of metal corrosion rate. This is due to the fact that metal corrosion rate is the most obvious and often the most important parameter in detecting the corrosivity or inhibition of the environment, in selecting corrosion inhibition formulas etc. Electrochemical techniques offer the possibility of fast, continuous, and automatic, corrosion-rate determination. The measurement of corrosion rate is, actually, equivalent to the determination of the kinetics of the electrochemical corrosion process.

During the last decade, more and more sophisticated instrumental techniques have been applied to studying electrode surface, owing to both the increased availability of powerful new tools for interfacial characterization and an increased emphasis in modern electrochemical research on detailed characterization of the structure and composition of the interface. Many methods have been newly applied to the study of electrochemical interfaces during this time [34].

2.4.1. Electrochemical Quartz Crystal Microbalance (EQCM)

One of the new methods is based on quartz crystal microbalance (QCM) technology. The QCM comprises a thin quartz crystal sandwiched between two metal electrodes that establishes an alternating electric field across the crystal at its resonant frequency. This resonant frequency is sensitive to mass changes (and other factors) on the crystal. The ability to employ one side of the QCM as a working electrode in an electrochemical cell, (EQCM), while simultaneously measuring mass changes provides a powerful approach to investigate electrochemical processes involving thin films. These studies revealed detailed mechanistic information about film deposition and dissolution, surface morphology changes, and mass changes in thin films caused by redox or other chemical processes.

EQCM and QCM are used to distinguish between electrochemical and non-electrochemical applications of QCM technology, respectively.

In its earliest form, EQCM was used in *ex-situ* experiments to measure mass change at electrode surfaces after electrodeposition of metals. Later, the experimental methods required for its use, as *in-situ* mass-sensor, for thin films on electrode surfaces so that mass changes and various other processes involving thin films on electrode surfaces could be monitored in real-time [35-38].

http://dx.doi.org/10.14755/DIS.1999.001

2.4.1.1. Basic principles of AT-cut quartz resonator

The voluminous literature on the basic principles of quartz resonators, including the quartz crystal microbalance and the complexity of the piezoelectric effect can present a substantial barrier to the experimentalist who wishes to exploit the unique mass-sensing properties of QCM. It is also worth mentioning, however, that without some fundamental understanding of these devices the experimentalist may not appreciate many of the nuances of the QCM method and in some cases may misinterpret data.

2.4.1.2. The piezoelectric effect

In 1880, Jacques and Pierre Curie discovered that a mechanical stress applied to the surfaces of various crystals, including quartz, afforded a corresponding electrical potential across the crystal whose magnitude was proportional to the applied stress. This behavior is referred to as "***the piezoelectric effect***", which is derived from the Greek word *"**piezin**"* meaning "**to press**". This property only exists in materials that are acentric; that is, those that crystallize in non-centro-symmetric space groups.

Shortly after their initial discovery, the Curies experimentally verified "*the converse piezoelectric effect*", in which application of a voltage across these crystals afforded a corresponding mechanical strain. The converse piezoelectric effect is the basis of the QCM and is illustrated in Figure 6.

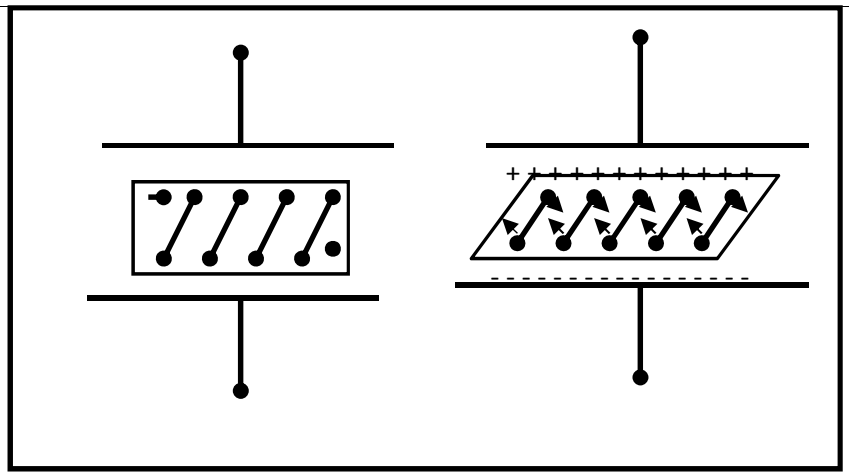

Figure 6. A diagram of the converse piezoelectric effect on shear motion.

The most suitable quartz crystals are of the AT-cut type, which consists of a thin quartz wafer prepared by slicing through a quartz rod at an angle of approximately 35° with respect to the x-axis.

Applying an alternating potential across the crystal causes a vibrational motion in the quartz crystal with amplitude parallel to the surface of the crystal. After several assumptions and simplifications, mainly that the acoustic properties of the deposited layers are identical to those of quartz, i.e. no-slip condition, Sauerbrey concluded that a fractional change in thickness (Δd) results in a fractional change in frequency (Δf) and thus producing the well-known Sauerbrey equation [39].

http://dx.doi.org/10.14755/DIS.1999.001

$$\Delta f = (- 2 f_o^2 \Delta m) / A (\mu_q \rho_q)^{1/2} \quad (12)$$

where:

Δf, is the measured frequency shift; f_o, is the frequency of the quartz crystal prior to a mass change; Δm, is the mass change; A, the piezoelectrically active area; ρ_q, the density of the quartz; μ_q, the shear modulus; and $\Delta d = \Delta m / \rho_q . A$

Sauerbrey, in deriving his equation, made the following assumptions:

- The density and the transverse velocity associated with this material are identical to those of quartz.
- Frequency shift resulting from a mass deposited at some radial distance from the center of the crystal will be the same regardless of the radial distance.
- The deposited film has a uniform thickness across the entire active region of the resonator.

The actual frequency response to an additional mass is dictated by the differential sensitivity constant, C_f, which represents the differential frequency shift for a corresponding mass change on that part of the EQCM as:

$$C_f = \Delta f / \Delta m \quad (13)$$

The sensitivity constant, C_f, is not uniform across the resonator. Studies have indicated that C_f is highest at the center of the QCM and decreases monotonically in a Gaussian-like manner, becoming negligible at and beyond the electrode boundary [39-40].

Quartz resonators, due to low losses in energy during oscillation, produce precise determination of the period of oscillation (1/f). Of course, this is equivalent to stating that the resonant frequency of a quartz crystal can be more precisely determined; this property is the basis for the use of quartz crystals in QCM investigations. The presence of damping forces can result in dramatic changes in the observed frequency and the accuracy of measurements.

2.4.1.3. Non-ideal behavior in EQCM investigations

Most reported EQCM investigations have assumed ideal rigid layer behavior, using the Sauerbrey equation when interpreting frequency changes. It is important to remember, however, that the EQCM measures frequency changes and not mass changes, although frequency change could be spontaneously converted to mass change by the instrument. While this may seem to be obvious, its importance rests on the potential for interference that can result in non-ideal behavior, defined here as a lack of conformance with the Sauerbrey equation.

Some factors that could lead to non-ideal behavior are:

http://dx.doi.org/10.14755/DIS.1999.001

1) ***Viscoelastic effects*** [41].

Examples of viscoelastic interferences in EQCM investigations have not been documented extensively, although absence of such observations probably can be attributed to a lack of attention to this aspect. This non-ideal effect gives non-real data, which could lead to misinterpretation of the results.

2) ***High mass loadings*** [39].

As mass loading is increased, the sensitivity of the EQCM decreases accordingly. This effect is also understood readily by inspection of the Sauerbrey equation. Typically, EQCM measurements are considered accurate provided that the mass of the film does not exceed 2 % of the mass of the crystal.

3) ***Surface Roughness*** [42,43].

The microscopic roughness of the EQCM electrode surface can play an important role in the behavior of the EQCM in liquid media. Trapping of liquid in surface cavities will result in an additional-mass component. Observed frequency shifts could be attributed to this effect. It is recommended therefore that the surface roughness or method of crystal preparation should be detailed when describing EQCM investigations.

4) ***Surface stress*** [43].

EQCM investigations are typically performed with one side of the AT-cut quartz crystal is in contact with liquid with the opposite side facing air. This arrangement will result in a stress on the quartz crystal due to the hydrostatic pressure exerted by the column of liquid. Strain effects arising from thick films can also affect the conformance to the Sauerbrey equation.

5) ***Interfacial slippage*** [43].

The previously discussed models describing the EQCM and its mass sensing properties rely on the "non-slip" condition, which refers to the case in which the first layer of solvent at the EQCM metal electrode surface is tightly bound and does not slip against the metal surface during the shear motion of the disk. Interfacial slippage can induce small but significant frequency shifts.

6) ***Non-uniform mass distribution*** [43].

The radial sensitivity of the QCM requires a uniform mass distribution if accurate measurements are to be made using the Sauerbrey equation. The integral sensitivity constant for a given crystal frequency, electrode thickness, and electrode geometry should be determined electrochemically prior to performing any experiments, using Faraday's law.

2.4.1.4. Applications of EQCM in corrosion studies

Mass losses result in frequency increase and vice versa. The resonance frequency for a quartz crystal in a liquid is influenced by three different effects:

$$f = f_o + \Delta f_m + \Delta f_l \qquad (14)$$

http://dx.doi.org/10.14755/DIS.1999.001

where f_o, is the resonance frequency of the blank quartz crystal; Δf_m, is the frequency shift caused by mass change due to surface layers (deposition, adsorption, etc.); Δf_l, is the frequency shift caused by the damping influence of the liquid.

An additional layer on the crystal surface enlarges its oscillating mass and decreases its eigen frequency. Sauerbrey equation (Eq. 12) could be simplified in the form [39]:

$$\Delta f = - C_f \quad f_o^2 \quad \Delta m \qquad (15)$$

A specially designed oscillator circuit was used in order to power the quartz and overcome the damping effect of the aqueous electrolyte solution.

For the calibration and copper deposition experiments, an acid copper bath was used [44]. Using Faraday's low, the amount of copper to be deposited is calculated, since nearly no current loss occurs in the used acid copper bath. Thus:

$$\Delta m = [(aw \quad I \quad n \quad \Delta t) / 2 \quad F] \qquad (16)$$

where: I, is the applied current; n, is the number of transferred electrons;
F, is the Faraday's constant; and *aw*, is the atomic weight of copper.

2.4.1.5. Applications of EQCM

Investigations of thin films

The basis for studies of thin films is the high sensitivity of the EQCM. For example, under certain conditions a mass in the nanogram range could be detected, this transfers to monolayers of films. In addition, interfacial processes can be measured on a time scale of approximately 100 ms; this depends upon the frequency counter being used. The ability to determine mass changes an reasonably short time scales can facilitate examination of the kinetics of processes involving thin films, including events that accompany these processes that are otherwise transparent to other electrochemical methods.

Electrodeposition of metals

The first applications of EQCM included investigations of electrodeposition of metals onto electrode surface [44]. The capability to perform EQCM measurements of metal electrodeposition *in-situ* provides a more convenient means for investigating fundamental processes such as underpotential deposition (UPD) of metals. Accordingly, numerous *in-situ* investigations of UPD phenomena soon followed. Bruckenstein [45] used EQCM to investigate the underpotential deposition of lead and silver on gold in acetonitrile as a solvent. Schmidt et al [46] investigated metal deposition of lead and copper, from dilute solutions, using EQCM. They combined EQCM with anodic stripping analysis, which allowed the frequency changes to be compared with the change of dissolution of deposited metals.

http://dx.doi.org/10.14755/DIS.1999.001

Dissolution of metals

The electrochemical dissolution of metal films can also be examined conveniently by EQCM. Such investigations have obvious relevance to the use of piezoelectric transducers as corrosion sensors. EQCM studies are also likely to elucidate the fundamental processes involved in the anodic dissolution of metal films, which is of essential importance in corrosion processes. The high sensitivity of the EQCM provides an advantage over other methods, such as gravimetrical method solution analytical techniques for measuring dissolution rates.

Inzelt [47] used the EQCM to study the open-circuit copper dissolution in aqueous acidic $CuSO_4$ solutions. He confirmed that oscillatory behavior of copper dissolution in sulfate containing acidic media can be triggered by the increase in the concentration of Cu^{2+} ion in the solution. Copper dissolution in sulfate media was also studied by Jardy et al. [48]. By means of EQCM measurements, they established that the over-all dissolution valency of copper was dependent upon the current density. Pickering and coworkers [49] investigated the copper corrosion inhibition in neutral environment by using the benzotriazole acid-Na_2SO_4 system but some frequency shifts could not be explained. Hepel [50] utilized the EQCM to investigate the effect of BTA on the corrosion rate of copper from composite polypyrrole-copper film.

Electrovalency measurements of anion adsorption

The EQCM has also been used to measure the direct electrosorption of anions on an electrode surface. Inzelt et al. [51] studied the sorption of ions and solvent molecules in poly-(aniline) films on electrodes under potentiostatic conditions using EQCM.

Hydrogen absorption in metal films

Several reports have appeared recently describing the use of the EQCM to measure electrochemically induced hydrogen or deuterium uptake in palladium films. This focussed attention was ignited by claims of cold fusion under these conditions [52].

Other applications

These include:

- semiconductors;
- molecular charge transfer salts;
- nucleation and Growth;
- thin film catalytic systems;
- vapor phase inhibitors;
- reaction kinetics; and
- redox and conducting polymer films.

So, the already large and steadily increasing number of papers, dedicated to the application of EQCM methods to study interfacial processes at electrode surfaces, reveals the power of the EQCM method for

http://dx.doi.org/10.14755/DIS.1999.001

characterizing interfacial processes which occur prior to, during, or after the fundamental electron-transfer event.

2.4.2. ELECTROCHEMICAL TECHNIQUES

2.4.2.1. Electrochemical *dc* methods

The fundamental formula for describing the kinetics of an electrochemical reaction is the Butler-Erdey-Gruz-Volmer (BEV) equation [53,54]. According to mixed-potential theory, for corrosion in the absence of externally applied potentials, the oxidation and the reduction processes occur simultaneously at the same metal-electrolyte interface and there can be no net electrical charge accumulation. Under these circumstances the net measurable current is zero, i.e. the corrosion current can not be measured directly. For determining electrochemical corrosion kinetics, a perturbation of the corroding electrode by an externally imposed polarization potential, E, is needed to shift the corrosion system from the corrosion potential E_{corr}. If the anodic and cathodic reactions on the working electrode are totally activation-controlled and the corrosion potential is far away from the equilibrium potential of the individual anodic and cathodic reactions, then the Butler-Erdey-Gruz-Volmer equation can be applied:

$$i = i_o[\exp(\frac{\alpha nF}{RT}\eta) - \exp(\frac{-(1-\beta)nF}{RT}\eta)] \quad (17)$$

Where η is the over potential; i, is the net current density; i_o is the exchange current density; F, is Faraday's constant; R, is the universal gas constant; T, is the absolute temperature; n, is the number of electrons transferred in the anodic or cathodic reactions; and α and β, are transfer coefficients. The BEV equation must be simplified in order to be applied into practical applications to calculate the electrochemical corrosion current.

Direct measurements of the corrosion current is usually not possible. The corrosion current is the current between the anodic and the cathodic sites and normally both the anodic metal dissolution and the supporting cathodic process occur at microscopically adjacent sites on the metal surface.

The most commonly used simplified form of the BEV equation is the Tafel equation. It can be derived from BEV equation (equation 17) for sufficiently high values of the applied potential. The Tafel equation has the following general form:

$$|\eta| = a + b\log i \quad (18)$$

where a and b, are the Tafel constants.

http://dx.doi.org/10.14755/DIS.1999.001

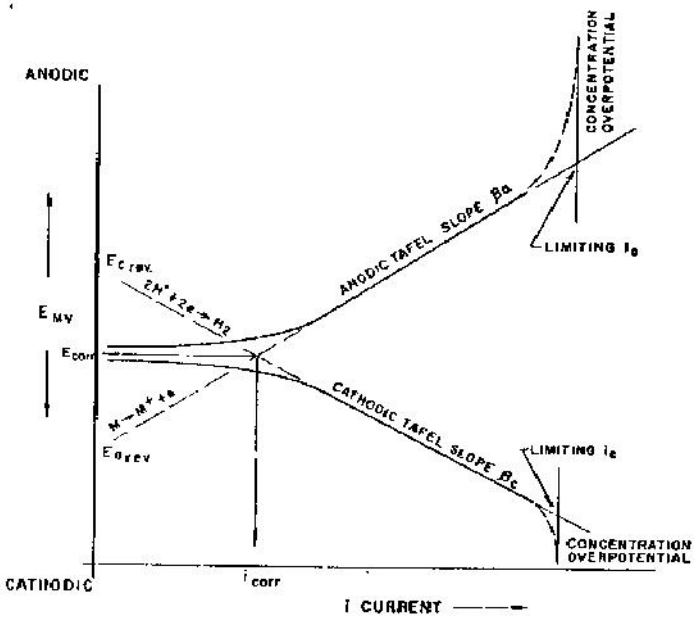

Figure 7. Polarization curve showing Tafel lines

However, the Tafel method (also referred to as the Tafel line extrapolation method) has a major disadvantage that it is destructive to test samples due to the use of high polarization potentials. Thus, the Tafel method is therefore of only limited value for continuous corrosion rate monitoring.

A polarization representation indicating the Tafel lines is shown in Figure 7. At any given potential, the measured current is the sum of the anodic and cathodic reaction currents. At potentials below the free corrosion potential E_{corr} , the response is mainly that of cathodic process. At potentials above E_{corr} the reverse occurs [55].

2.4.2.2. Electrochemical Impedance Spectroscopy (EIS)

Since Epelboin and coworkers introduced *ac* impedance techniques in electrochemistry [56], EIS has been developed into a powerful and practical tool for studying corrosion problems in various systems.

EIS offers district advantages over *dc* techniques:

- EIS uses very small excitation-potential amplitudes, generally in the range of 5 to 10 mV peak-to-peak, which causes only minimal perturbation of the electrochemical test system.
- EIS offers valuable mechanistic information because EIS can provide data on both electrode capacitance and charge transfer kinetics.
- EIS can be used for electrodes in low conductivity solutions and with organic coatings [55].

2.4.2.2.1. Fundamental aspects of EIS

Mansfeld and Lorenz, among other reviews, discussed the theory of EIS and the application of EIS in corrosion studies [57]. They suggested that two main areas of application are rapid estimates of a wide range of corrosion rate and practical insights into corrosion mechanisms, especially in the presence of an adsorbed film

http://dx.doi.org/10.14755/DIS.1999.001

or an applied organic coating. The advantage of *EIS* lies in the fact that it is essentially a steady-state technique, which is capable of accessing relaxation phenomena whose relaxation times vary over many orders in magnitude. The steady-state character permits the use of signal averaging method within a single experiment to gain the desired level of precision, and the wide frequency bandwidth permits a wide range of interfacial processes to be investigated.

Therefore, EIS can be one of the principal methods for investigating mechanisms of electrode interfacial-reaction [58]. The prerequisite conditions of EIS application are:

- the system studied is linear;
- the interface is stable over the time of sampling.

In corrosion studies using EIS, normally the corroding system under test is perturbed from an initial equilibrium state or steady state (normally the corrosion potential) by a broad band, small amplitude signal (in most cases sinusoidal). In this thesis, all EIS measurements employ a small sinusoidal signal (amplitude of 10 mV).

Impedance is commonly written in the form:

$$Z(j\omega) = Z' - jZ'' \tag{19}$$

where $j = \sqrt{-1}$, and $Z'$and Z'' are frequency-dependent real numbers, often referred to as the real and imaginary components of the impedance respectively, which are related to the magnitude of the impedance and the phase by:

$$\left|Z(j\omega)\right| = \sqrt{(Z')^2 + (Z'')^2} \tag{20}$$

$$\text{and } \tan\theta = -\frac{Z''}{Z'} \tag{21}$$

where θ is the phase angle.

Equations (20) and (21) lead directly to the two common methods for displaying impedance data: the Nyquist plot (Z' vs. Z'') and Bode plots ($\log|Z|$ vs. log ω – the Bode modulus plot, and log θ vs. log ω – the Bode phase plot). The Nyquist plot is clearer for mechanistic analysis because the number of relaxations and their mechanistic implications are often more apparent. The Bode plots employ frequency directly as the independent variable, so that more precise comparison between experimental and calculated impedance spectra can be made.

2.4.2.2.2. <u>The interpretation of EIS data</u>

The interpretation of EIS data allows one to determine the electrochemical parameters of the electrode surface and to acquire information about the corrosion process and mechanism. The corrosion rate can be

http://dx.doi.org/10.14755/DIS.1999.001

calculated by determining the polarization resistance or charge transfer resistance. Characterization of the adsorption and desorption and film formation on the electrode surface may be studied by determining its surface capacitance.

However, the interpretation of experimental EIS data is far from an easy task. In fact, the power of the EIS technique is often not fully used due to the difficulties in developing suitable models for simulating the impedance behavior and in developing fitting programs for analyzing EIS data.

For corrosion rate calculation or comparison study from experimental impedance data, it is necessary to determine the polarization resistance (R_p) or charge transfer resistance (R_t). Although R_p can be determined by the value of the intersection of the semicircle with the real axis at the low frequency part.

EIS was found quite useful in studying corrosion systems where an adsorbed film of an organic inhibitor is present. The Nyquist plot of impedance and equivalent circuit of this system is shown in Figure 8. This impedance characteristics is very common in the organic inhibitor film-metal corrosion systems and will be met a lot in this research work.

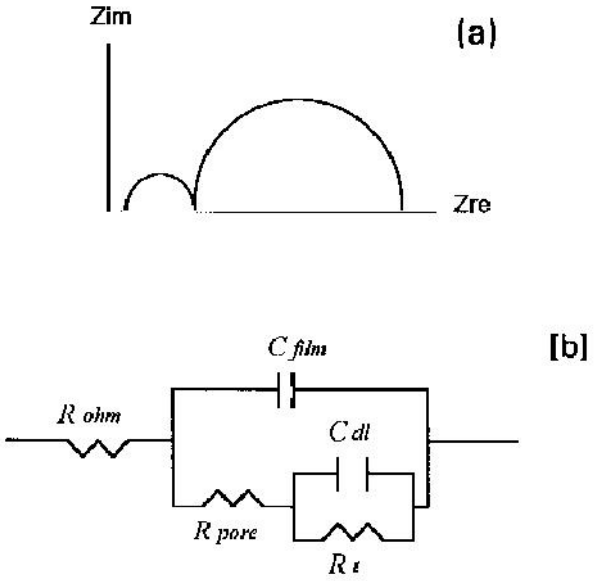

Figure 8. (a)- A typical Nyquist plot of electrode impedance, (b)-Equivalent circuit for the electrode simulation.

The two semi-circles suggest that this is a multiple time-constant system. The semicircle at the lower frequency is usually due to the electrochemical process of corrosion [59]. The semicircle into the high frequency range is due to the inhibitor film because a surface dielectric film normally has a small time-constant [57]. The impedance characteristics of this electrode surface can be simulated by an electrical circuit used by a number of workers for coated metal electrode, Figure 8.b. R_{ohm} is the solution resistance (ohmic resistance). R_{pore} is the resistance of the surface film in pore area. C_{film} is the capacitance of the surface film. R_t is the charge transfer resistance C_{dl} is the double layer capacitance. As with all other electrochemical measurement methods, EIS has to be applied very cautiously, with a prior knowledge of the system-specific corrosion behavior. A

http://dx.doi.org/10.14755/DIS.1999.001

computer software [60], which uses a non-linear least square fit (NLLS) and simulation method to fit experimental data, may help to arrive at the correct data analysis.

2.4.3. Atomic Force Microscopy (AFM)

The idea of development of scanning probe technique for imaging non-conductive surfaces led to the invention of the atomic force microscopy (AFM) [61]. Inter-atomic forces between a sharp tip and surface were proposed as the probing interactions.

There are three main types of atomic force microscopy:

- Contact AFM – based on repulsive interactions,
- Non-contact AFM – based on attractive interactions,
- Tapping mode.

The contact AFM mode up to now has been used in most applications except for soft probes. One reason is that it has much better resolution than the non-contact mode. In addition, recording changes of the repulsive force is simpler than detecting variations of the attractive interaction. Due to the strong dependence of the repulsive force on distance, surface corrugations can be precisely detected with this technique. The vertical resolution of AFM is higher than what can be achieved with the scanning electron microscopy and optical interferometer.

The registration of surface topography in the atomic scale is a unique property of contact AFM, which essentially enhances the possibilities of microscopic methods.

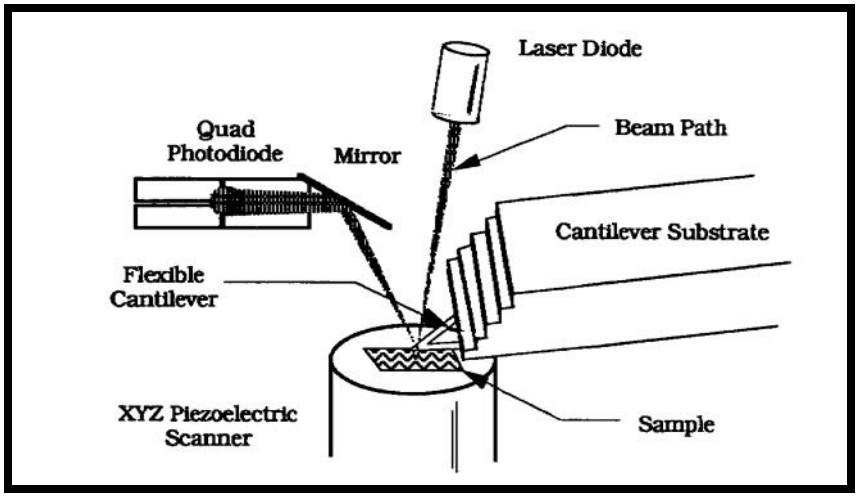

Figure 9. A schematic diagram of the contact force microscope-sensing system.

The contact force microscope is schematically shown in Figure 9. A sample is mounted on a tube piezo-scanner, which can be precisely transported in the lateral (X and Y) and vertical (Z) directions. A delicate

http://dx.doi.org/10.14755/DIS.1999.001

cantilever with a sharp microscopic stylus (both made of Si_3N_4) through a feedback circuit is the sensor of the force acting between the most advanced atoms on the probe and the surface atoms. The bending of a cantilever in the vertical up direction is proportional to the magnitude of the repulsive force. An optical lever, which consists of a laser diode, a mirror, and a four-segment photodiode, is used to register the position of the cantilever deflections.

Scanning of a sample beneath a probe starts when a sample surface encounters a stylus and the repulsive force reaches the preset value.

2.4.4. Scanning Electron Microscopy (SEM)

The scanning electron microscope is one of the methods of looking at the electrode surface. SEM uses electronics to form a magnified image of the specimen. The electron beam of the scanning electron microscope does not penetrate into the specimen. The electron beam incident on the specimen is rastered (similar to the television scan) across the object. The detector records either the secondary or the back-scattered electrons emitted from the top side of the sample, near where the electron beam strikes it. The sample does not have to be thin, but it must be reasonably conductive so that it does not charge and deflect the electron beam. Non-conductive specimens are coated with a thin layer of gold, chromium, or carbon before SEM examination. A magnification power of higher than 10^5 is achievable using SEM.

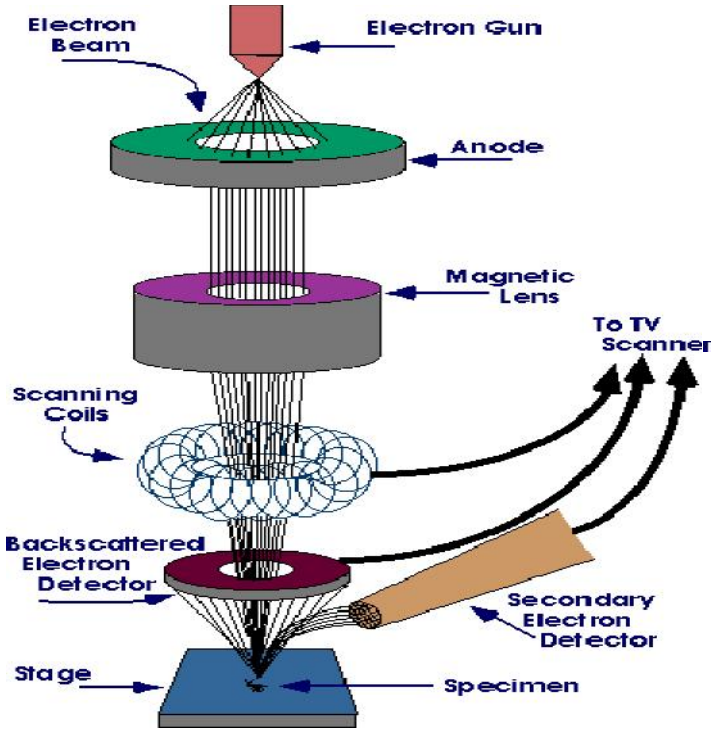

http://dx.doi.org/10.14755/DIS.1999.001

Chapter 3.

3. METHODOLOGY

3.1. ELECTROCHEMICAL QUARTZ CRYSTAL MICROBALANCE

3.1.1. Electrogravimetrical Vessel

A specially designed glass vessel with a volume of 100 ml was used as a corrosion cell, Figure 10. The working electrode (quartz crystal) was fixed to a circular hole in the sidewall of the vessel by the use of a Teflon cylinder and an elastic rubber band. The crystal holder was glued to the cell using a two-component epoxy resin (CIBA-GEIGY, HY-956 and AY-103). In order to prevent electrolyte leakage, the crystal was mounted between two rubber O-rings. Thus, only one side of the crystal blade was in contact with the aqueous electrolyte. The other cell was a 100-ml glass with a flattened side hole of 10-mm diameter. The working electrode (quartz crystal) was glued using silicone rubber glue (type General Electric Translucent RTV 108).

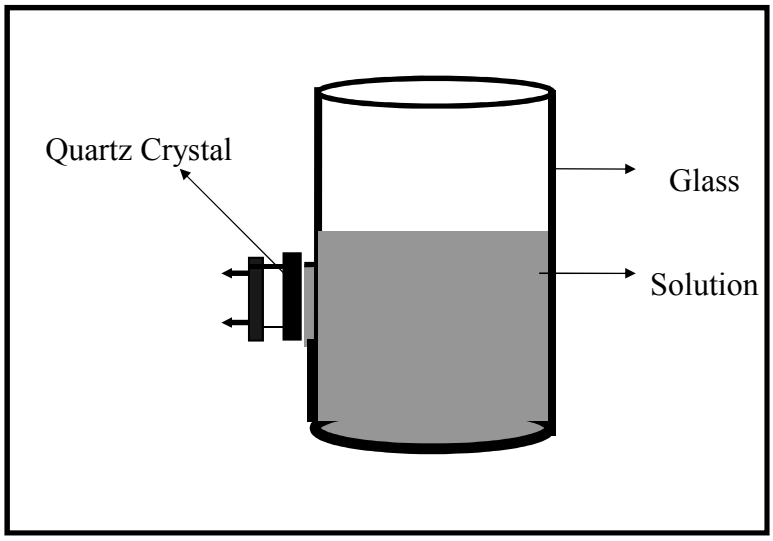

Figure 10. The electrogravimetrical vessel for EQCM measurements.

3.1.2. Electrodes

The quartz crystal was used as the working electrode, Figure 11. The crystal was coated by the manufacturer with metal layers of chromium and gold on both sides. The layers thickness are in the following range:

chromium: 15-20 nm

gold: 180-200 nm

deposited copper: 250 nm

http://dx.doi.org/10.14755/DIS.1999.001

Chromium was deposited on the crystal to serve as an adhesive layer for gold. The copper is deposited on only one side of the crystal, the side facing the solution, as shown in Figure 12.

The O-rings on both sides of the crystal produced an inner area (exposed to the solution) of 0.30 cm^2 and an outer area (exposed to air) of 1.0 cm^2. Only that part of crystal, which is between the metal layers on both sides, oscillates in a shear mode. This oscillation amplitude approaches zero within a few micrometers outside from this part. This procedure to minimize the coated area is essential in order to avoid the effects on the oscillation by the attachment of the quartz to the cell body or holder. A circular area with rectangular flags pointed to the edges of the crystal disk where golden thin wires connected the crystal to an external measuring circuit.

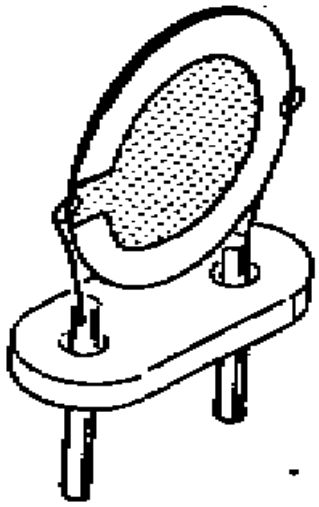

Figure 11. EQCM working electrode

Copper layers were deposited from an acidic copper sulfate bath [44]. The deposition current was 10 mA; higher currents produce more uniform surfaces but care must be taken not to damage the quartz crystal gold surface.

A saturated calomel electrode (SCE) was used as the reference electrode and all measured potential are referred to this electrode.

The oscillator was a modified Pierce-Miller circuit [60]. In order to avoid polarization effects a high impedance voltmeter (potentiostat type ELCHEMA Model PS-205) was used for the potential measurement. A schematic diagram of the apparatus is shown in Figure 13. The output was recorded by a computer and special software produced presentation of frequency and potential change in real time.

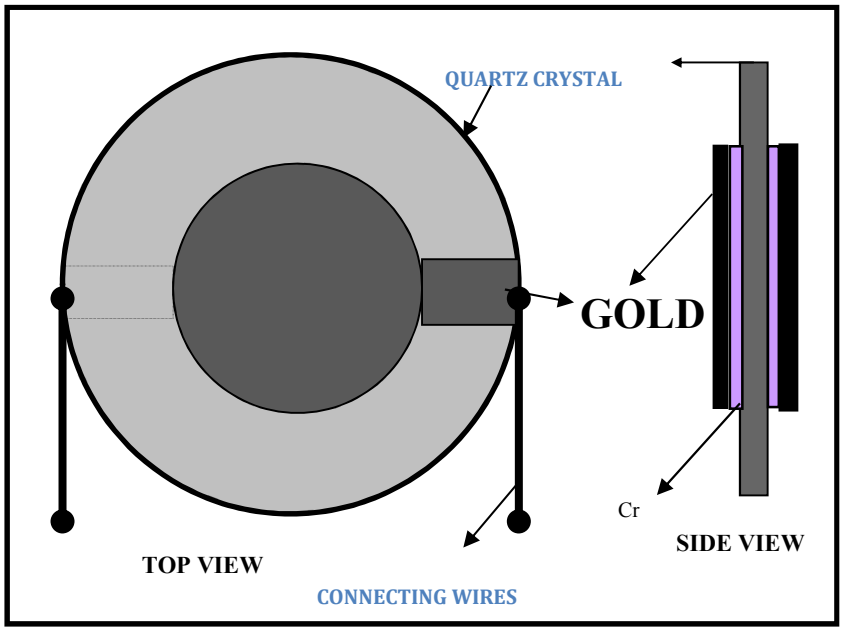

Figure 12. Top and side views of quartz crystal blade.

http://dx.doi.org/10.14755/DIS.1999.001

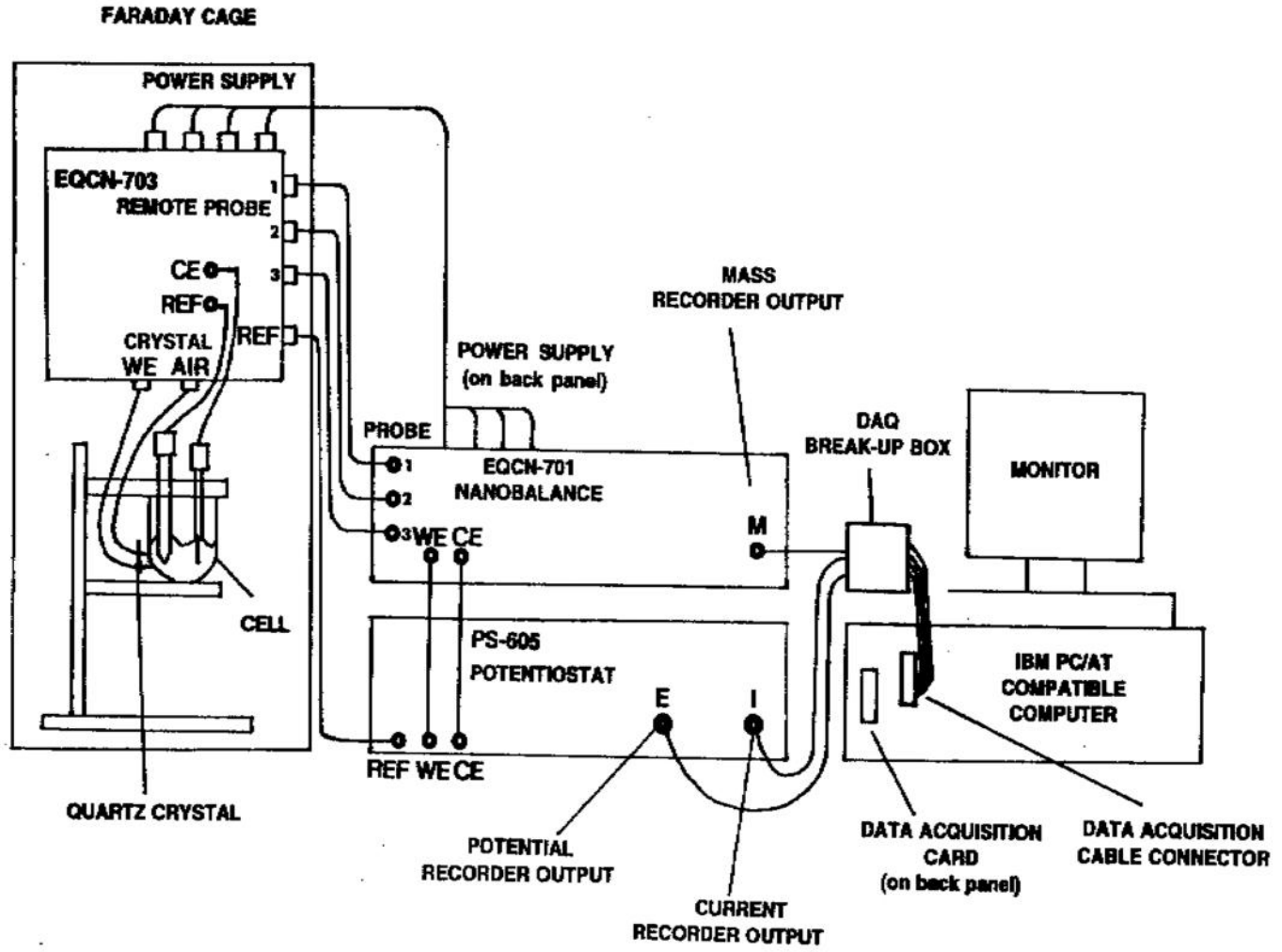

Figure 13. A block diagram of EQCM measuring system.

3.2. ELECTROCHEMICAL MEASUREMENTS

3.2.1. Electrochemical cell

A standard three-electrode glass cell was used as the electrochemical cell. The cell had a volume of 800 ml but only 500 ml was needed to cover the electrodes with the electrolytic solution. The cell had a Teflon top cover with three circular opening for working electrode (WE), SCE, and counter electrodes (CE).

3.2.2. Electrodes

In all electrochemical experiments, the working electrode was made from pure copper rod of 9.5-mm diameter. This rod was inserted into a cylindrical shape epoxy resin to limit the electrode area exposed to the solution to only the base circular face. The CE electrode was a 90-cm^2-platinum sheet. A saturated calomel electrode served as a RE. The electrodes were connected to a computer controlled electrochemical interface (Solartron ECI 1286).

http://dx.doi.org/10.14755/DIS.1999.001

For AC impedance measurements, a potentiostat (Solartron ECI 1286) to control the potential and a digital frequency response analyzer (Solartron FRA 1250) to measure electrode impedance were applied as shown in Figure 14. The FRA 1250 has two independent channels operating in parallel, one of which receives the original sinusoidal voltage signal while the other receives a voltage proportional to the current response from the test system. The FRA 1250 can cover a wide frequency range from 10μHz to 65 kHz. The used working signal amplitudes of the generator is 10 mV. The FRA 1250 was connected to ECI 1286 potentiostat and then to a microcomputer through an IEEE-488 interface board in order to store, analyze and produce a hard copy of the results using a standard software.

Potentiostatic polarization and EIS measurements were carried out using the same apparatus setup as shown in Figure 14.

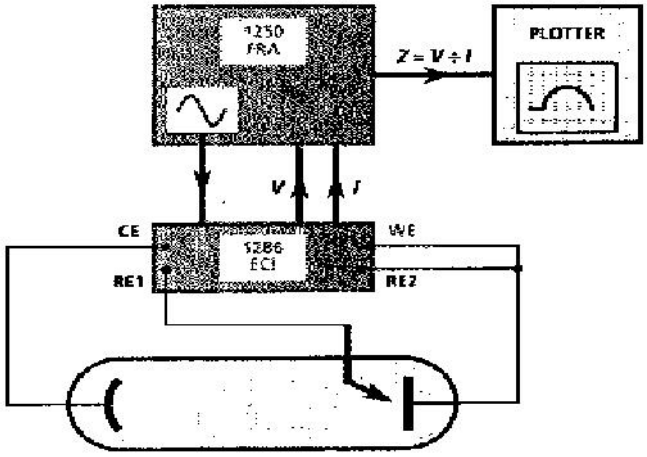

Figure 14. Schematic diagram of DC and AC electrochemical measurements setup.

3.3. SURFACE ANALYTICAL TECHNIQUES

3.3.1 ATOMIC FORCE MICROSCOPY (AFM)

Physically, the AFM consists of the optical head which houses the piezoelectric scanner and the preamplifier circuit, the base on which the sample is mounted, and the base support, which supports the base and head, see Figure 15.

There are three standard scanners built for the AFM microscope to image different areas.

- A scanner – 0.7 micron scan range
- D scanner – 12 micron scan range
- J scanner – 125 micron scan range

http://dx.doi.org/10.14755/DIS.1999.001

Two types of AFM tests were performed. Images of dried specimens after immersion in different electrolytes were captured in order to learn more about the surface morphology. Also imaging of specimens immersed in a fluid cell containing different electrolytes can be monitored for surface changes.

The specimen used for both of AFM measurements are made from the same copper rod (9.5 mm diameter) as mentioned before. Specimens were cut in the shape of coin discs of 1.5mm thickness.

For this investigation, the equipment used was Nano-Scope III AFM (system developed by Digital Instruments, Santa Barbara U.S.A.). This apparatus relies on a precise scanning technique to produce very high resolution, three-dimensional images of sample surfaces. A D-scanner, with a 12-μm^2 maximum scan range, was used throughout the measurements. The preparation of probes suitable for applications in a force microscope is one of the most important problems of AFM.

Contact AFM imaging can be conducted at ambient conditions and in liquid environments. A special cell for operations under liquids (fluid cell) was used. The fluid cell is a machined, glass cantilever mount with a compressed O-ring and sample surface that creates a closed, fluid/flow cell. Tapered channels are cut through the glass to provide flow capability and to allow insertion of other electrodes. The fluid cell can be used in place of a dry sample in a conventional AFM.

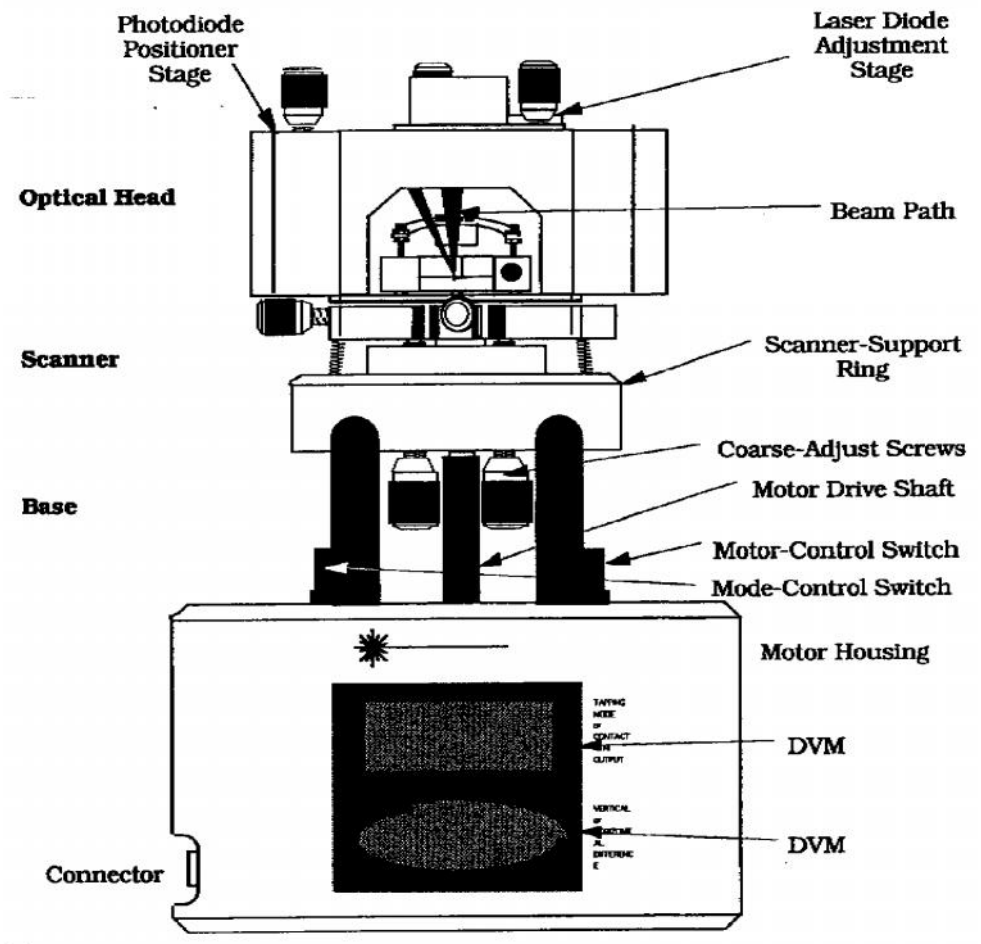

Figure 15. Schematic diagram of AFM measuring apparatus

http://dx.doi.org/10.14755/DIS.1999.001

3.3.2. SCANNING ELECTRON MICROSCOPY (SEM)

Specimens were prepared by the same method used for AFM measurements.

A Hitachi S-570 Scanning Electron Microscope, equipped with a Röntec EDX-spectrometer, was used for surface microphotography and analysis. This apparatus, which is driven by special Röntec quantitative analytical software, has a resolution of 35 Å and a magnification power of 20-200,000. A schematic diagram of the SEM-EDX measuring and analysis system is shown in Figure 16.

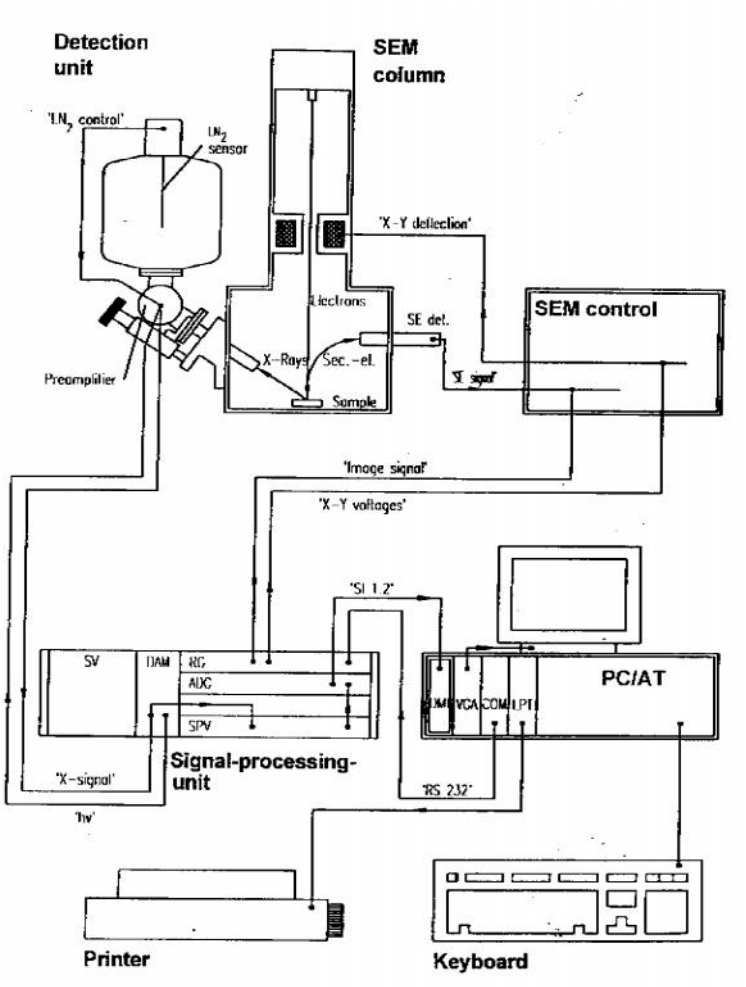

Figure 16. Schematic diagram of SEM experimental setup.

http://dx.doi.org/10.14755/DIS.1999.001

Chapter 4.

4. EXPERIMENTAL PROCEDURES

4.1 ELECTROLYTES

Ultra-pure water (DI) was produced by combining a water de-ionzer (HERCO) with a Millipore purifier system (model Milli-QRG). This system can produce water with a total oxygen content (TOC) of < 10 ppb and minimum water resistance of 18.2 M Ω.cm.

4.1.1. Sulfoxides compounds

Reagent grade chemicals (Reanal Rt., Bp. Hungary) and DI water were used to prepare the following electrolytes:

- 0.1 M Na_2SO_4 at pH = 2.95 (using sulfuric acid)
- O.1 M Na_2SO_4 at pH = 2.95 (using sulfuric acid) + 5.0 x 10^{-4} M inhibitor

Inhibitor compounds

1 - di-benzyl-sulfoxide = DBSO (Aldrich-Chemie – 98 %), MW = 230.33 g/mol.

2 - di-phenyl-sulfoxide = DPSO (Aldrich-Chemie – 97 %) MW = 202.28 g/mol.

3 – di-p-tolyl-sulfoxide = DPTSO (Aldrich-Chemie – 97 %) MW = 230.33 g/mol.

The sulfoxides were purified by recrystallization. Diluted sulfuric acid was added to adjust the pH to the desired value.

4.1.2. Benzohydroxamic acids

For this part of the experimental work, analytical reagent grade NaCl (Reanal Rt., Bp., Hungary) was used to prepare electrolyte solutions in DI water.

Benzohydroxamic acids, which were synthesized from their appropriate carboxylic acid chloride and hydroxylamin, were purified by recrystallization. Their purity was checked by elemental analysis and melting point determination.

In this series of benzohydroxamic, benzoic acid chloride and its substituted derivatives (o-Cl, p-Cl, p-NO_2, o-CH_3) provided the hydroxamic acids.

The following electrolytes were prepared:

- 0.5 M NaCl at pH ≈ 6.5-7 (using NaOH)
- 0.5 M NaCl at pH ≈ 6.5-7 (using NaOH) + 1x10^{-3}M inhibitor.

http://dx.doi.org/10.14755/DIS.1999.001

Inhibitor compounds

Inhibitor solutions were made from the BHA in DI water.

- ortho-chloro-benzohydroxamic acid (o-Cl-BHA);
- para-chloro-benzohydroxamic acid (p-Cl-BHA);
- para-nitro-benzohydroxamic acid (p-N-BHA); and
- ortho-methyl-benzohydroxamic acid (o-M-BHA).

Inhibitor	Melting point (^{o}C)	MW(g/mol)
o-Cl-BHA	147-148	171.5
p-Cl-BHA	184-185	171.5
p-N-BHA	172-173	182
o-M-BHA	163-165	151

Diluted NaOH solution is added to adjust the pH to the desired value. In all experiments, the cells were open to laboratory atmosphere at room temperature. The solutions were not deaerated.

4.2. EQCM MEASUREMENTS

The experimental work using EQCM was divided into two parts:

- Measurements in acidic 0.1 M Na_2SO_4 electrolytes without and with the addition of aromatic sulfoxides.
- Measurements in neutral 0.5 M NaCl electrolytes without and with the addition of benzo-hydroxamic acid derivatives.

4.2.1 EQCM measurements in 0.1 M Na_2SO_4 solutions

The quartz crystal used was an AT-cut disk of 12 mm diameter and nominal oscillation frequency of 5 MHz. The blank crystals were degreased with propanol before copper deposition. For the electrochemical deposition of copper, the crystal was connected to a galvanostat (Electroflex EF427 and an Electroflex EF 1808 sweep generator) and placed in the sample holder containing the insulated oscillatory circuit. The sample holder was then placed in the electrochemical glass cell containing the deposition copper bath. A platinum wire served as counter electrode. With the help of Faradays law, (Equation 16), the needed amount of copper for the desired thickness could be calculated using a current of 10 mA.

After the deposition procedure, the freshly deposited copper and the cell were rinsed with DI water. Each copper layer was freshly prepared before the experiment to be sure that no thick oxide film was formed on the electrode surface.

http://dx.doi.org/10.14755/DIS.1999.001

The electrolytes with and without the addition of the potential inhibitors (aromatic sulfoxides) were prepared as described in section 4.1.1. Due to the low solubility of the sulfoxides in 0.1 M Na_2SO_4 solution, stirring was performed for an hour at elevated temperature (≈ 45 ^oC). The solutions were then cooled to room temperature.

For the start of the measurement, the apparatus was set up as shown in Figure 13. The system was allowed to stabilize for a period of 10 minutes to assure that no thermal effects in the electronic parts would lead to frequency shifts. Upon the addition of the solution the cell containing the crystal holder, the frequency dropped by 2.5-3 kHz. This decrease reflects the effect of the high viscosity of the electrolyte in comparison to air.

All experiments were performed in three intervals and electrolytes were exchanged carefully after each interval:

- Interval I: 0.1 M Na_2SO_4 solution at pH = 2.95), (Sol. A).
- Interval II: 0.1 M Na_2SO_4 solution and $5x10^{-4}$ M inhibitor, (Sol. B).
- Interval III: same solution as in interval I, (Sol. A).

In the first interval, the freshly deposited copper surface was exposed to the corrosive solution, (Sol. A), for an hour. Then in the second interval, the solution was changed to an inhibitor-containing solution, (Sol. B), for a longer exposure period. Finally, the solution was changed back to (Sol A) and the measurement was conducted until most of the deposited copper is removed or there is no significant change in the electrode frequency.

After each interval the cell content was discharged, rinsed with DI water and refilled again. This exchange procedure took less than a minute. All solutions are kept at room temperature to minimize the temperature effect. Extra care was paid in order not to have any bubbles on the crystal, which would affect the measured frequency change. Bubbles could even cause the crystal to stop oscillating.

After each experiment, the crystal was cleaned with diluted nitric acid to remove the remaining copper and then rinsed with DI water. This was done so that the crystal could be reused again.

During all three intervals, frequency and open circuit potential changes were monitored and data were collected by special computer software.

4.2.2. Measurements in 0.5 M NaCl solutions

These experiments were used to test the effectiveness of the benzohydroxamic acids against the corrosion of copper. The quartz crystal used was an AT type with a nominal oscillation frequency of 10 MHz. The crystal was pretreated as before and then mounted to the cell. After cleaning, degreasing and rinsing with DI water, copper layer was deposited from the same bath as in section 4.2.1. Immediately, the cell was rinsed with DI water and the electrolyte was added to the cell. During the addition of the electrolyte, the cell was tilted

http://dx.doi.org/10.14755/DIS.1999.001

slightly to avoid accumulation of bubbles on the crystal. Having bubbles on the crystal during deposition could leave some parts of the gold surface uncovered by copper.

The electrolytes without and with the addition of the inhibitors (benzohydroxamic acids) were prepared in advance as described in section 4.1.2 For the start of the experiments, the apparatus was setup as shown in Figure 13.

Each experiment was performed in one interval and change of mass was then compared to the first experiment where the solution did not contain any additives. This was done because in neutral chloride containing solutions, layers of oxides and copper chlorides are formed on the electrode and it is difficult to remove them during measurements. The time interval for each experiment was 500 min. This time is long enough for inhibitors to adsorb onto the electrode.

After each run, the crystal was removed washed with nitric acid to remove the remaining copper and then rinsed with DI water.

During each experiment the mass loss in (μg) was registered at the corrosion open circuit potential by a special software (VOLTSCAN v. 3.7) and data was treated further using data analysis software (MASTER WINDOWS v 3.8). Diagrams of electrode mass loss as a function time were produced.

4.3. ELECTROCHEMICAL MEASUREMENTS

4.3.1. *DC* potentiostatic measurements

DC polarization curves were measured in different electrolyte solutions (0.5 M NaCl and 0.1 M Na_2SO_4) without and with inhibitors (sulfoxides or benzohydroxamic acids), using a copper circular electrode. The working electrode was 9.5-mm diameter and 20 mm long, rod imbedded into epoxy resin in order to restrict the contact area of the electrode. The electrode was wet-polished, using SiC emery papers (grit sizes of 800 and 1200), and mirror-like surface was produced. The electrode was then rinsed with DI water, acetone and DI water again. It was then immediately immersed into the electrolyte solution. The surface was characterized by cyclic voltammetry [11]. Each experiment was started after half an hour of immersion time and the open circuit potential (OCP) was monitored.

Measurements were conducted at room temperature (25 °C) according to the procedure described in the ASTM G-5-93 standard. A computer driven Schlumberger Solartron potentiostat (Model ECI-1286) was utilized to record the current corresponding to the applied potentials. The cathodic polarization measurement was performed, starting at a potential of 50 mV lower than the OCP. Then the electrode was removed and the same pretreatment was done again. The anodic polarization was conducted starting at a potential of 50 mV above the OCP (into the anodic region).

The applied potential scan rate was 10 mV/ 60 s, in both the anodic and cathodic directions. During measurements continuous stirring, using ceramic magnetic stirrer, was performed. At the end of each

http://dx.doi.org/10.14755/DIS.1999.001

experiment, the electrode was examined visually and any unusual findings were documented. The electrolyte solutions described in section 4.1.1 and 4.1.2 were used.

4.3.2. *AC* EIS measurements

The initial electrode preparations for the *AC* impedance experiments were the same as for the *DC* (polarization runs). The electrode surface treatment was also the same. OCP was calculated as in section 4.3.1. All of the *AC* measurements were carried out at the OCP. Experimental impedance (data) spectra were obtained in the frequency range of 0.01-10,000 Hz, with 5 points per decade, using the frequency response analyzer (FRA 1250). The working electrode was maintained at the open-circuit potential by (ECI 1286) potentiostat during the measurement. A sinus wave, with 10-mV amplitude, was used to perturb the system for impedance measurements. Data were recorded and analyzed using special software to produce Nyguist plots. The measurements were performed starting at upper frequency (10,000 Hz) and descending to the lower limit (0.01 Hz). Lower frequencies require longer measuring time, in this case the lower range value of 0.01 Hz was sufficient.

4.4. AFM MEASUREMENTS

In-situ AFM experiments were carried out using a NanoScope III AFM equipped with a fluid cell and a 12-μm scanning head. The specimens were circular disc (9.5 mm diameter) sandwiched by O-rings in order to limit the area.

The electrode was wet polished by SiC paper (grit 1200) then further polished down to 0.1 μm polycrystalline diamond paste (DP-Struers and DP-Nap) rinsed with DI water. Aqueous solutions of 0.1 M Na_2SO_4 without and with the addition of $5x10^{-4}$ M DBSO (pH = 2.95) and 0.5 M NaCl without and with the addition of $1x10^{-3}$ M of p-Cl-BHA were investigated. The sample surface was first imaged under ambient conditions then the solution was injected into the fluid cell and imaging was started as soon as a sharp image was produced. Images were recorded at different time intervals in order to register the changes taking place due to corrosion and inhibition processes. Contact AFM mode was used for imaging the surface.

Other type of AFM measurements was also conducted for all tested potential inhibitors in both acidic and neutral media. The samples as well as the surface pretreatment were the same as before. After polishing, the samples were immersed in solutions without and with the addition of DBSO or p-Cl-BHA, for 24 hrs. The samples were removed from the cell, dried and placed on the AFM sample holder for imaging. Images were collected, analyzed, and 2D and 3D images of the surface were produced.

http://dx.doi.org/10.14755/DIS.1999.001

4.5. SCANNING ELECTRON MICROSCOPY (SEM and EDX)

The circular copper specimens were mounted to a disc of araldite resin. The samples were examined under different magnifications. The specimens were analyzed by energy dispersive spectrometer (EDX). The spectrometer (EDR 288) measures the x-ray radiation, from the interaction of the electron beam with the sample surface products, and displays it as a pulse height spectrum. The analytical software allows the qualitative and quantitative analysis of elements. Morphological images of the electrode surface with different magnifications were produced.

http://dx.doi.org/10.14755/DIS.1999.001

Chapter 5.

5. RESULTS

5.1. GRAVIMETRIC RESULTS

In the development of new inhibitors, it is always important, irrespective of the nature of the investigation, to estimate quantitatively the effect of the inhibitor on the corrosive process. A series of measurements of corrosion rates must be made even to answer the question, whether a given substance is, or is not, a corrosion inhibitor. The gravimetric method is that most often used to measure corrosion rate and inhibitor efficiency. Gravimetric tests have been used in this study for the following purposes:

1- Corrosion rate calculations

2- Inhibitor efficiency determinations

3- Optimization of inhibitor concentration

The results of this method are presented in corrosion rate (W) (mm/y) or inhibition efficiency (IE) for different substances. The IE is calculated using the formula, $\{IE\ \% = [(W_o - W_I)/W_o].100\}$ where W_o and W_I represent corrosion rates without and with the addition of inhibitor, respectively.

The concentration of inhibitor needed for maximum protection is also obtained. Gravimetrical results were calculated from the difference of weight before and after the immersion of the coupons in the solutions. Corrosion rates and inhibition efficiencies were calculated using self-developed software.

5.1.1. Aromatic sulfoxides in 0.1 M Na_2SO_4

The gravimetric results for this part showed that the average optimal concentration for the corrosion inhibition by the sulfoxides was $5x10^{-4}$ M. One must take into consideration that the tested aromatic sulfoxides had a low solubility and precipitation could take place as in the case of DPSO, that is why the sulfoxides were dissolved in 20 ml of ethanol first and then added to electrolyte solutions. The corrosion rate and inhibition efficiency of the tested sulfoxides are depicted in Figure 17. This figure shows that, at the optimum concentration, DBSO has the highest inhibition efficiency followed by DPTSO.

http://dx.doi.org/10.14755/DIS.1999.001

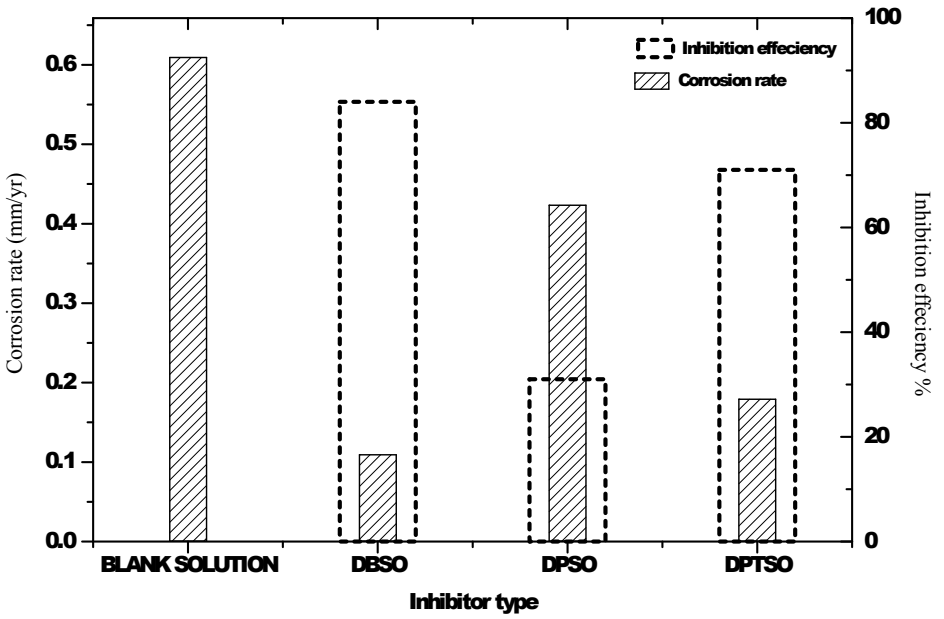

Figure 17. Corrosion rate and inhibition efficiency for the sulfoxides in 0.1 M Na_2SO_4 .

5.1.2. Benzohydroxamic Acids in 0.5 M NaCl

The optimum inhibitor concentration was found to be $1x10^{-3}$ M. This concentration will be applied for the rest of investigation. At higher concentrations, precipitation of the inhibitors could occur due to their low solubility.

The corrosion rate and inhibition efficiency of the tested BHAs are depicted in Figure 18. This figure shows that, at the optimum concentration, p-Cl-BHA has the highest inhibition efficiency.

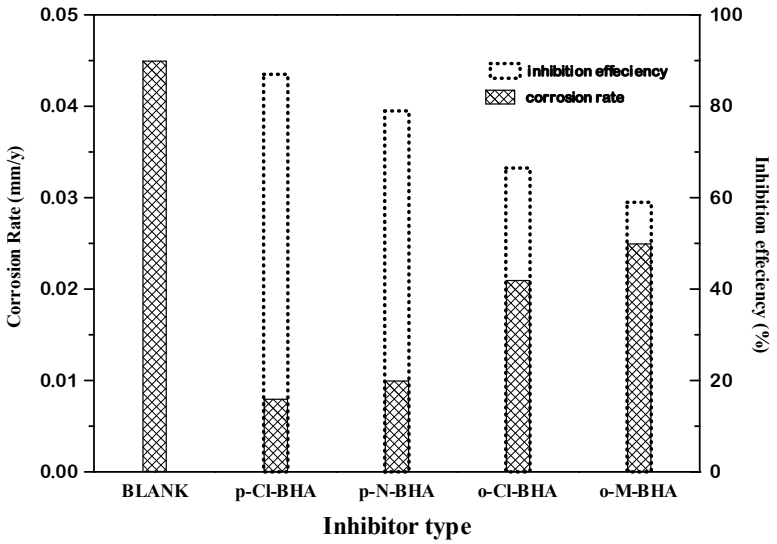

Figure 18. Corrosion rate and inhibition efficiency for the BHAs in 0.5 M NaCl.

http://dx.doi.org/10.14755/DIS.1999.001

5.2. EQCM RESULTS

Most of the classical methods in electrochemistry lack the high sensitivity in determining corrosion rates or inhibition efficiencies. The EQCM provides a very high sensitive tool to measure mass changes in real time. Although this method is considered as a density scale, nevertheless changes in the range of 10^{-10}g could be detected. The possibility to measure corrosion rates in real time is also a new dimension in monitoring corrosion. Performing long time-range experiments shows the applicability of this method in practical situations. Results of the EQCM tests are presented as mass changes in time or mass changes as a function of potential.

5.2.1. EQCM calibration experiment

During copper deposition, the frequency decreased linearly due to the copper mass increase on the gold electrode. A difference of 50 kHz was monitored for the deposition period of 180 s. This amount of copper assured the coverage of all the gold surface with copper layers.

At the start of the deposition process the electrode had a potential of (- 145 mV) which decreased sharply to a minimum value of (– 232 mV). By the end of the deposition time, the potential started to maintain a stable value of (-210 mV). The calibration curve is shown in Figure 19.

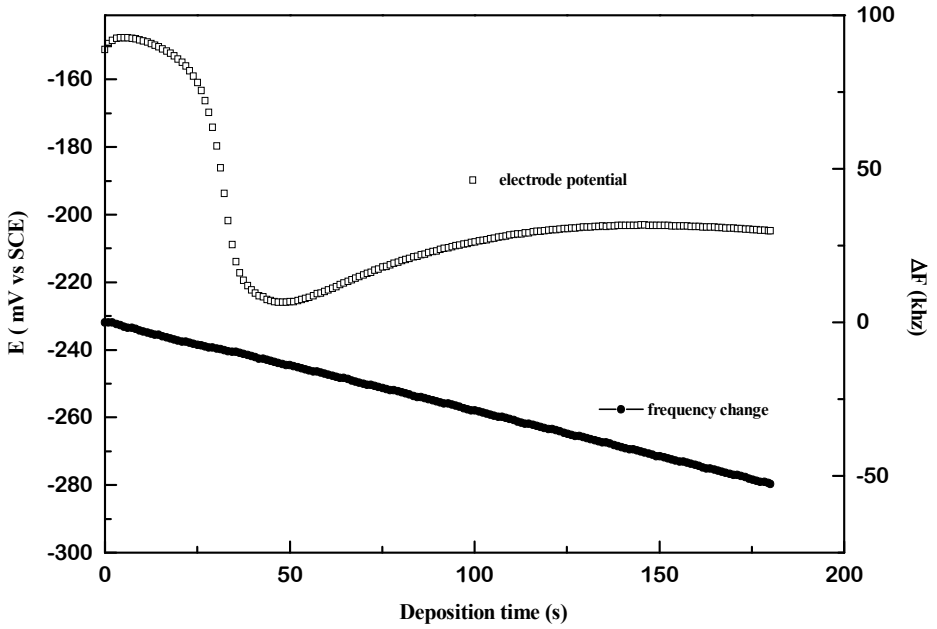

Figure 19. Calibration curve for the EQCM to determine the sensitivity.

The other EQCM results are divided into two parts, one deals with experiments of copper electrode in acidic sodium sulfate solution with the addition of aromatic sulfoxides and the other in sodium chloride solution with the addition of benzohydroxamic acid derivatives.

http://dx.doi.org/10.14755/DIS.1999.001

5.2.2. Aromatic Sulfoxides in 0.1 M Na_2SO_4

By inspecting the EQCM data of the sulfoxides, it could be shown that the data obtained are reproducible and are within small margin of error. This result could be noticed by comparing the behavior of the crystal quartz during the first interval. Figures 20, 21, and 22, show the depicted results of the frequency change and electrode potential of the working electrode (quartz crystal) in time, in the 0.1 M Na_2SO_4 solution with the addition of DBSO, DPSO, and DPTSO.

I. During the first interval (exposure to the aggressive solution), all experiments show similar behavior: a frequency increases ≈ 2.4 kHz/h, which represents a mass loss on the crystal surface, as shown in Figures 20-22. The similar results for the first interval are expected because conditions for interval I are the same for all experiments performed. Minor deviations of the frequency change during this interval could be traced back to differences in surface roughness during copper deposition. For the first interval, an open circuit potential of (-35) mV/SCE was always reached as time proceeded. All potentials were measured with respect to a saturated calomel electrode (SCE).

II. After the addition of the solutions containing inhibitors (second interval), the following observations were noticed:

♦ **Addition of DBSO**

The addition of the electrolyte containing DBSO shows a steady decrease in the quartz crystal frequency, Figure 20.

The frequency steadily became stable toward the end of this interval. The frequency increase during this interval was the lowest monitored in all of the experiments for the other chemicals.

An increase of potential to a more negative value (-30 mV) was also noticed at the end of the interval.

♦ **Addition of DPSO**

After the addition of the DPSO containing electrolyte, the observed frequency change rate did not show any decline from the first interval rate. The increase of crystal frequency continued almost at the same rate, (2.3 kHz/h). The copper electrode potential continued to drift to more negative value (-40 mV), Figure 21.

♦ **Addition of DPTSO**

The addition of DPTSO had an effect on the frequency of the crystal. The frequency decreased noticeably. During this interval, the average frequency change rate was around (900 Hz/h). After the addition of DPTSO, the potential increased (more positive) from (–40 mV) to a value of (–32 mV). Then by the end of the interval, the potential drifted slowly to a stable value of (–45 mV). This potential was the highest negative value among the tested sulfoxides, Figure 22.

III. During the third interval for all applied inhibitor, compounds showed different frequency increase rate.

http://dx.doi.org/10.14755/DIS.1999.001

- **Addition of DBSO**

In the case of DBSO, a negligible slight increase in frequency takes place just after the electrolyte is exchanged back to the aggressive solution. The average slope is constant and shows no major changes in the corrosion rate. The potential decreased (more positive) slightly and reached a stable value of (–30 mV) at the end of the interval.

- **Addition of DPSO**

For this inhibitor, the third interval was omitted because no major decrease in the dissolution rate of copper during the second interval was noticed. Therefore, the rate of frequency change would have been the same throughout all intervals.

- **Addition of DPTSO** The behavior of the quartz after the exchange of the electrolyte containing DPTSO is similar to DBSO. The frequency increases slightly at a higher rate than the second interval rate. The potential jumped from (–45 mV) to a value of (–40 mV).

http://dx.doi.org/10.14755/DIS.1999.001

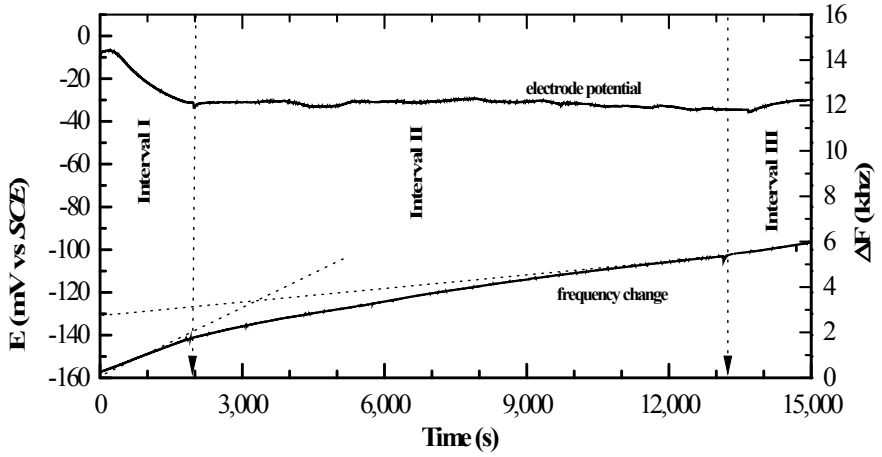

Figure 20. Mass and potential changes of copper in 0.1M Na_2SO_4 and DBSO

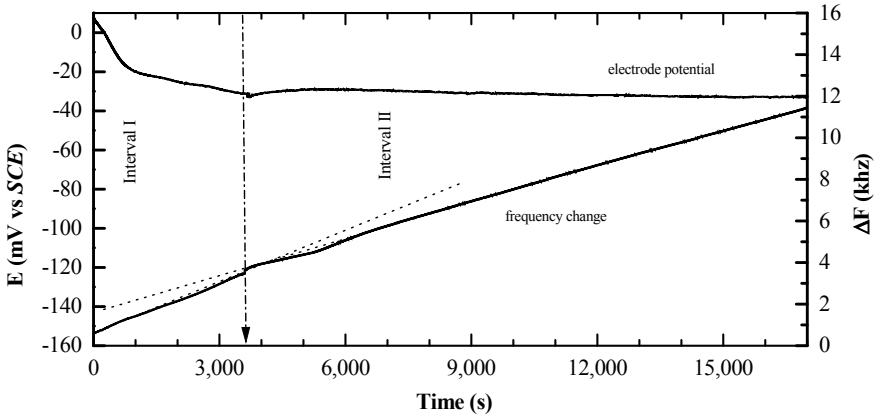

Figure 21. Mass and potential changes of copper in 0.1 MNa_2SO_4 and DPSO

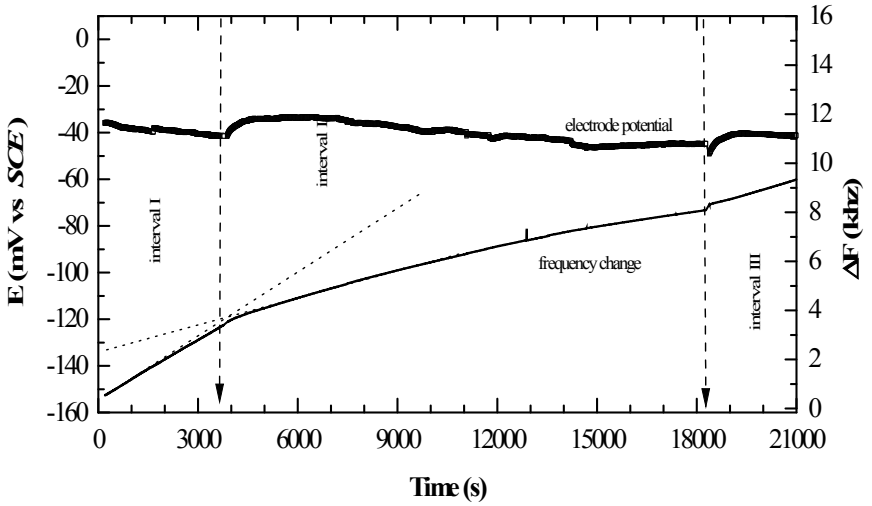

Figure 22. Mass and potential changes of copper in 0.1 MNa_2SO_4 and DPTSO

http://dx.doi.org/10.14755/DIS.1999.001

5.2.3. Benzohydroxamic acids in 0.5 M NaCl

Results of benzohydroxamic acids investigations in 0.5 M NaCl solution are depicted in Figure 23. This figure reveals the following observations:

The results are expressed as mass change in μg. cm^{-2} vs. time (min), so the corrosion rate could be represented by the slope of the curve at any particular time. At the time of addition of the different electrolytes, the mass removal or loss from the electrode surface varied.

1. **Blank solution (0.5 M NaCl)**

The aggressive solution without any additive showed very high mass decrease rate then the loss rate reached a stable value. Small increase in mass on the electrode was noticed which is due to accumulation of some corrosion products. This curve represents a net rate of dissolution and accumulation processes taking place on the electrode surface.

2. **Addition of p-Cl-BHA**

By the addition of the electrolyte containing p-Cl-BHA, the electrode mass decreased slightly and then a mass increase is noticed. This is due to corrosion products and inhibitor complexing with those products. By the end of the experiment, the electrode mass kept on increasing to a stable value.

3. **Addition of o-Cl-BHA**

The solution containing o-Cl-BHA resulted in a behavior similar to that of the p-Cl-BHA but not as efficient. A sharp increase in the copper dissolution rate was followed by a relaxation interval and then a slight increase of the electrode mass.

4. **Addition of p-N-BHA**

The addition of p-N-BHA produced the second highest dissolution rate after the aggressive solution. Similar behavior to the o-Cl-BHA was noticed.

All curves represent high mass-loss region, followed by a relaxed region and then a flattened region. Only the electrolyte containing p-Cl-BHA showed different behavior in mass increase on the electrode due probably to adsorption. The corrosion rate was the highest in the early measurement period.

http://dx.doi.org/10.14755/DIS.1999.001

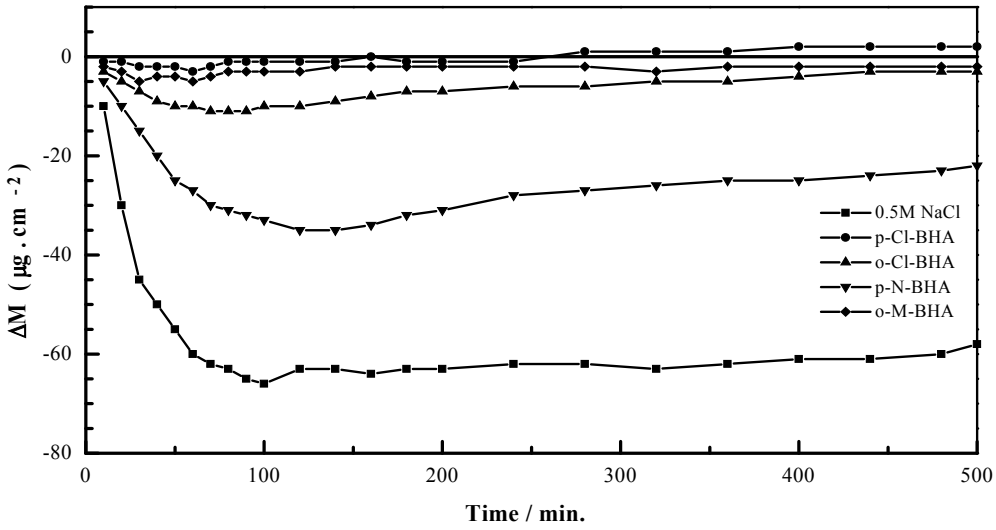

Figure 23. EQCM results for the tested BHA in 0.5M NaCl at OCP and 25°C.

5.3. ELECTROCHEMICAL RESULTS

Two electrochemical methods have been used in this study. They consist of potentiostatic polarization and AC impedance spectroscopy measurements. Results of potentiostatic polarization measurements are shown in the form of potential vs. current. These results are interpreted into polarization curves of semi-linear plot, of logarithmic value of current versus potential. The polarization curves give information on the behavior of the inhibitor in altering the corrosion current and potential. They also show the effect of the inhibitor on the anodic and cathodic parts of the polarization curve.

AC impedance measurements give results in the form of frequency {Hz}, real and imaginary values of amplitude {Ω} and phase shift {degrees}. Using these data, Nyquist plots are constructed as real vs. imaginary parts of the polarization resistance (amplitude). From the Nyquist plots relaxation time constants could be realized. The relaxation time constants could give some indication of the process type, if it is chemical, diffusion, or charge controlled. Semi-circles could be visualized and the intersection of the semicircle at low frequency and the real part axis gives the polarization resistance value. This polarization resistance value could be used to evaluate effectiveness of the inhibitors.

5.3.1. Polarization results

Polarization measurements were conducted to investigate the effect of inhibitors (sulfoxides and benzohydroxamic acids) on copper corrosion in different environments. The polarization curves are represented as log i vs. E. From these curves corrosion current density (i_{corr}) and corrosion potential E_{corr} could be obtained. The inhibition efficiency (IE %) is determined using the following formula:

http://dx.doi.org/10.14755/DIS.1999.001

$$IE(\%) = 100 . (1 - i_{corr}/i_{cor}^{o}) \quad (22)$$

where i_{cor}^{o} and i_{corr} represent the corrosion current density in the absence and the presence of the inhibitor, respectively.

5.3.1.1. Sulfoxides in 0.1 M Na_2SO_4 solution

The polarization curves of the tested sulfoxides in 0.5 M Na_2SO_4 solution are represented in Figure 24. All curves show different open circuit potentials. DBSO shifted the OCP toward more cathodic value while, DPTSO shifted it to more anodic value. DPSO did not show a significant change in behavior comparing to the blank solution.

In more details, the polarization curves could be separated into anodic and cathodic parts. In the anodic part, which represents the metal dissolution, all curves showed similar behavior at potential values higher than 400 mV. The current density decreased slightly.

The addition of DBSO influenced all regions of the graph. In the anodic region, the DBSO curve is always lower than the blank solution curve which means that the current density was lowered as a result of the addition of the inhibitor. In the cathodic region, DBSO showed the largest effect where current density was influenced the most among the tested inhibitors.

DPTSO anodically showed the largest deviation from the blank solution. At potentials higher than the OCP and lower than 400 mV, DPTSO showed two relaxed regions. The first was at ≈40 mV and the second at 100 mV. Cathodically, DPTSO did not influence the reactions. Higher current densities were observed at potentials between OCP and -300 mV.

DPSO did not significantly influence the reactions, neither anodically nor cathodically. The behavior of this curve was similar to that of copper in 0.1 M Na_2SO_4 solution. At potentials higher than 100 mV, the current densities decreased slightly. Decreasing the scale of the graph, between -400-mV and +400 mV where all the changes took place, the deviations are easily identified as shown in Figure 24. For all inhibitors, in the anodic region, the current density increased sharply and then reached a stable value at higher potentials.

Normally, one is able to observe a region where the slope is nearly constant, the so-called Tafel region. However, the presence of the inhibitors leads to a total deviation from the Tafel behavior. Between –60 mV and 300 mV all curves show erratic shifts except for DPSO. A summary of the polarization data for copper in 0.1 M Na_2SO_4 without and with the addition of the investigated sulfoxides is tabulated in Table 1.

At the end of each polarization experiment, visual observations were made. Colored surface films appeared beginning at a potential of about 450 mV. Some products grew with time and eventually fell off the electrode. These surface films could be easily rinsed off with distilled water.

http://dx.doi.org/10.14755/DIS.1999.001

Table 1. Potentiostatic polarization results for copper in 0.1M Na_2SO_4 with and without the addition of sulfoxides

Inhibitor	Corrosion current density ($\mu A/cm^2$)	IE (%)
Blank	6.61	-
DBSO	1.25	81
DPSO	4.78	27
DPTSO	2.61	60

Table 2. Visual observations after polarization measurements of copper in 0.1 M Na_2SO_4 in the absence and presence of sulfoxides.

Inhibitor	Observations
0.1 M Na_2SO_4	Greenish solution, uniform attack
DBSO	Dark gray film, washed off easily by water, uniform attack
DPSO	Black layer formed, solution was greenish
DPTSO	Dark brown layer on the electrode, some pits

5.3.1.2. BHAs in 0.5 M NaCl solution

Polarization curves of the investigated benzohydroxamic acids are depicted in Figure 25). All curves show shifts of open circuit potential OCP to more cathodic values. The curves could be divided into anodic and cathodic regions. The anodic polarization behavior of copper in 0.5 M NaCl solution without and with the addition of BHAs could be seen in Figure 25. All curves exhibit three distinct regions: the Tafel region at lower over-potentials extending to a peak current density (i_{peak}), then a region of decreasing current until a minimum value i_{min} is reached and finally, a region of sudden increase in current density leading to a limiting value (i_{lim}).

In the apparent-Tafel region, curves deviated slightly from the NaCl solution without any inhibitor. The addition of the inhibitors to the corrosive medium shifted the polarization curves toward lower i_{lim}, i_{min} and i_{peak}. The extent of the shift was maximal in the case of p-Cl-BHA. The curves were almost super-imposed on each other between i_{peak} and i_{min} expect for the p-Cl-BHA curve, which was clearly shifted to a much lower i_{min} value. In the presence of p-Cl-BHA, i_{min} was much lower than the value for the blank solution. At higher potentials than the potential corresponding to i_{min}, a decrease in current density was observed. The change in i_{lim} is noticeable for all inhibitors except for p-N-BHA.

In the cathodic region, all inhibitors reduced the current density at potential lower than the OCP. The slopes of the cathodic parts of the curves are similar. The inhibitor, p-N-BHA produced the lowest current density. The results obtained from the polarization curves are summarized in table 3.

http://dx.doi.org/10.14755/DIS.1999.001

Table 3. Corrosion inhibition parameters of Cu electrode in 0.5 M NaCl without and with the addition of different BHA's

Inhibitor	**β_a (mV/Dec)**	**(i_{peak}) ($\mu A/cm^2$)**	**(i_{min}) ($\mu A/cm^2$)**	**Polarization Res. (R_p) (k ohm cm^2)**
BLANK	65	8700	3675	3.5
p-Cl-BHA	82	5620	485	17.2
o-Cl-BHA	72	7820	3935	9.7
p-N-BHA	75	7780	2265	13.0
o-M-BHA	72	7940	4345	5.5

Visual inspection was performed at the end of each experiment and the following observations were recorded:

Table 4. Visual observations after polarization measurements of copper in 0.5 M NaCl in the absence and presence of BHAs.

Inhibitor	Observations
0.5 NaCl	thick greenish solution resulted, pits were formed on the electrode
p-Cl-BHA	light green color started at high potentials, uniform surface
o-Cl-BHA	thicker dark-greenish solution, corrosion pits were noticed
o-m-BHA	greenish solution started to form at potentials > 100 mV
p-N-BHA	white particles started to appear at potential > 0 mV.

http://dx.doi.org/10.14755/DIS.1999.001

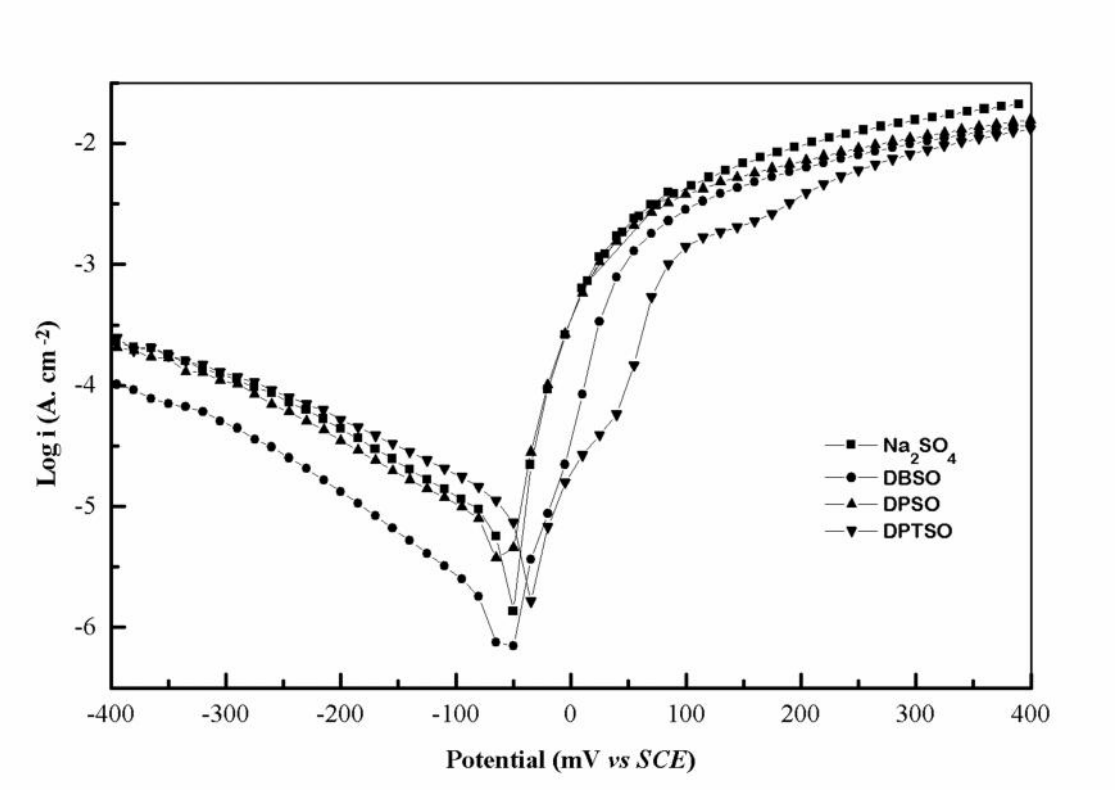

Figure 24. Polarization curves for copper electrode in 0.1 M Na_2SO_4 without and with the investigated sulfoxides at 25^{o}C.

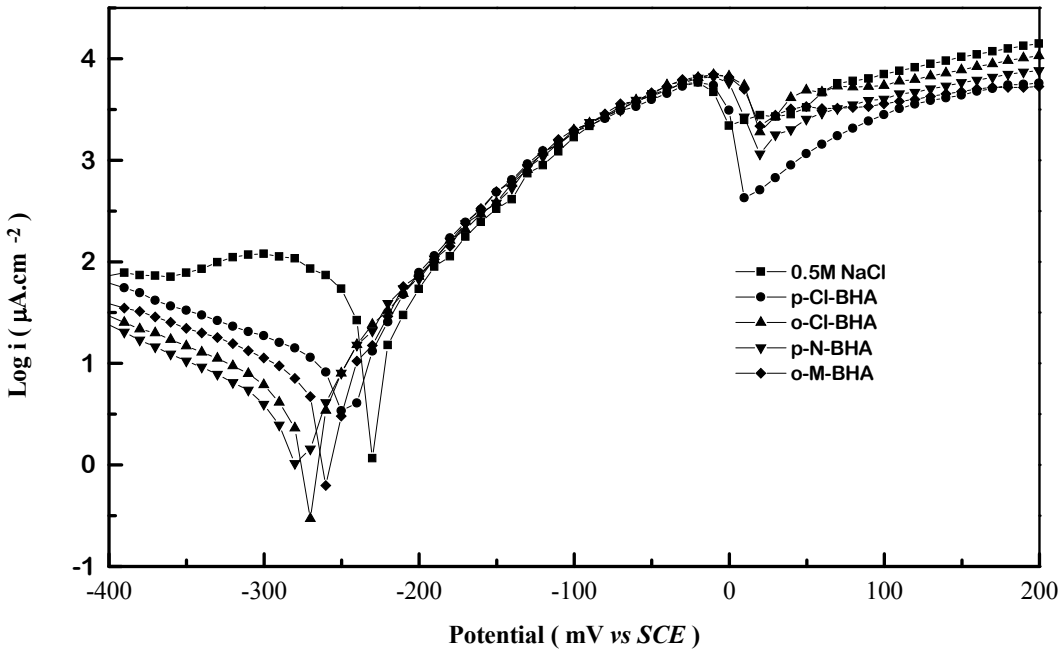

Figure 25. Anodic polarization curves for copper in 0.5 M NaCl

http://dx.doi.org/10.14755/DIS.1999.001

5.3.2 EIS Results

The EIS results are presented in the form of real vs. imaginary parts of the impedance amplitude. R_p values from the Nyquist plots are used to calculate the inhibition efficiency as:

$$IE\% = 100.(1 - R_{po}/ R_{pi}) \quad (23)$$

where R_{pi} and R_{po} are the polarization resistances with and without the presence of the inhibitor, respectively.

5.3.2.1 Copper in 0.1 Na_2SO_4 with sulfoxides

Nyquist plots of data measured of copper in 0.1 M Na_2SO_4 solution (pH=3) in the absence and presence of the tested sulfoxides, are represented in Figure 26. From Figure 26, a semicircle could be visualized, which intersects the real value axis at different values. This intersection represents the R_p value for each inhibitor curve. The inhibition efficiencies of the sulfoxides were calculated using Equation 23 and are listed in Table 5.

Table 5. Polarization resistance values (R_p) from Nyquist plot for copper in 0.1M Na_2SO_4 without and with the addition of sulfoxides.

Inhibitor	Polarization resistance R_p (ohm cm^2)	IE (%)
Blank	120	-
DBSO	440	73
DPSO	180	33
DPTSO	340	64

5.3.2.2 Copper in 0.5 M NaCl with BHA derivatives

Nyquist representation of the measured data is shown in Figure 27. The Nyquist curve for copper in NaCl, obtained at the corrosion potential, shows two more-or-less poorly separated semi-circles as seen in Figure 28. One semicircle is at high frequency range and another is at low frequency range. Data deviation or scrambling is noticed at the low frequency region due to the instability of the electrode. The radius of the low frequency semi-circle varied from one inhibitor to another. All investigated BHA produced higher R_p values than the solution without inhibitor.

http://dx.doi.org/10.14755/DIS.1999.001

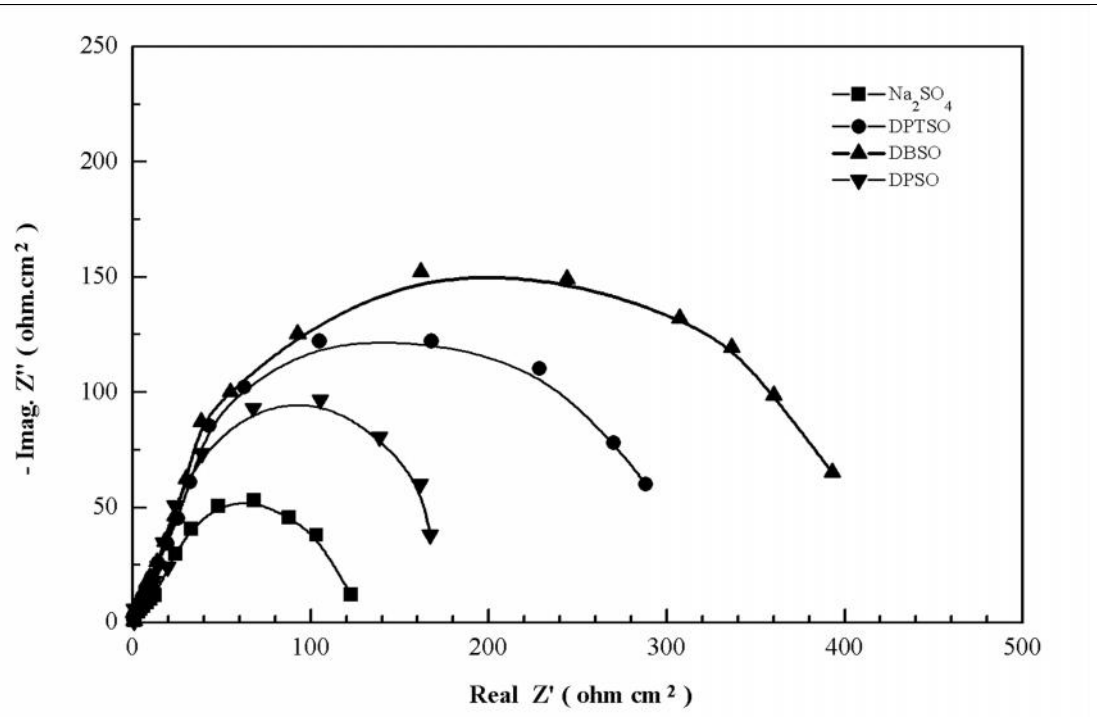

Figure 26. Nyquist plot of copper in 0.1M Na_2SO_4 and in the presence of various sulfoxides.

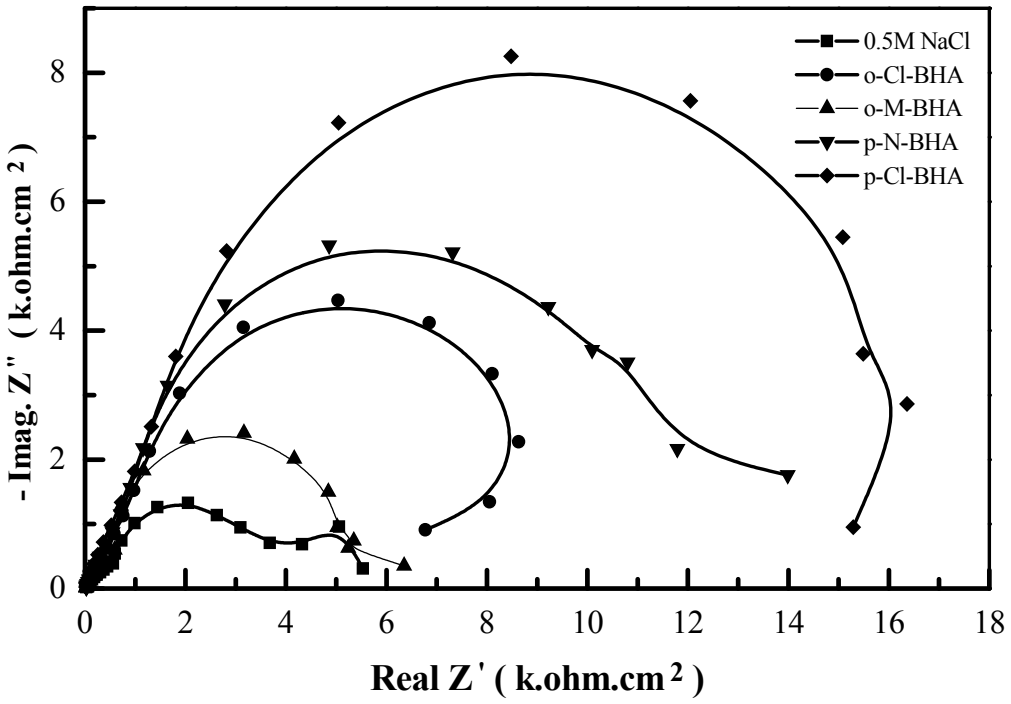

Figure 27. Nyquist plot of copper in 0.5 M NaCl and in the presence of BHAs.

http://dx.doi.org/10.14755/DIS.1999.001

Table 6. Polarization resistance values (R_p) from Nyquist plot for copper in 0.5 M NaCl without and with the addition of different BHAs

Inhibitor	Polarization resistance R_p (k ohm cm^2)	IE %
BLANK	3.5	-
p-Cl-BHA	17.2	80
o-Cl-BHA	9.7	64
p-N-BHA	13.0	72
o-M-BHA	5.5	36

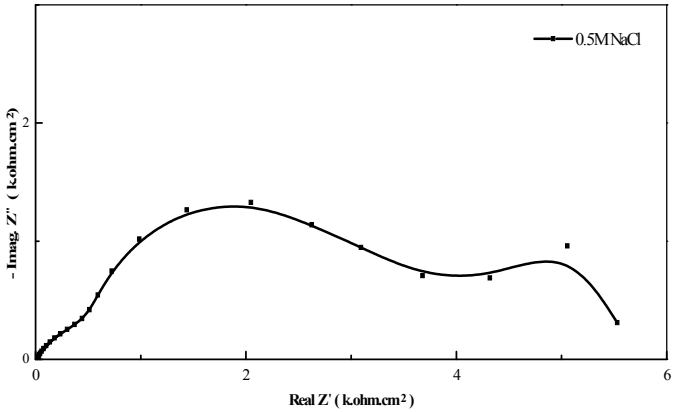

Figure 28. Nyquist plot of copper in 0.5 M NaCl, to illustrate the two semicircles at high and low frequencies.

Further information was obtained by the evaluation of the impedance data, which were fit to a model circuit that would describe the system physically. In order to fit the EIS data, a special computer software [60] which uses a non-linear least square fit (NLLS-fit) and simulation method were used.

For copper corrosion in 0.1 M Na_2SO_4 at pH=3, in the presence of DBSO, the EIS data were fitted by semicircles using the model shown in Figure 8.b. This model produced a good fit between the measured and simulated data. The electrochemical parameters: solution resistance; film resistance; corrosion products capacitance; electrochemical charge transfer resistance and the double layer capacitance were obtained.

For copper corrosion in 0.5 M NaCl at neutral pH range, Nyquist spectra were deconvolved using a model similar to the one presented by several authors [65] for an inhomogeneous 3D layer. This model can simulate organic film coating behavior (i.e. p-Cl-BHA) in the presence of pits or defects in the layer. The

http://dx.doi.org/10.14755/DIS.1999.001

transfer function consists of a parallel combination of the impedance of the covered surface areas (θ) and of the active surface area (1-θ), linked to the metal corrosion process, as shown in the next schematic diagram.

R_Ω represents electrolyte resistance, C_L and R_L are capacitance and resistance, respectively, of the covered surface areas, θ is the surface coverage by the film. $R_{\Omega por}$ represents electrolyte resistance with in the pores; R_p is corrosion polarization resistance; C_{dl} is the electrochemical double layer capacitance; (1-θ) is the active area; W is the Warburg impedance which is linked to diffusion through $W_{1-\theta}$ or to coating disbanding W_θ. For this case the values of the parameters depend on θ:

For θ=0, no coverage:

R_p = 3.5 (k Ω cm^2) , C_{dl} =0.28 (F cm^2), R_L= 6.95 (k Ω cm^2), C_L=0.39 (F cm^2)

where for θ ⇒ 1 (full coverage):

the values are: R_p = 16.8 (k Ω cm^2) , C_{dl} =0.16 (F cm^2), R_L= 32.4 (k Ω cm^2), C_L=0.001 (F cm^2).

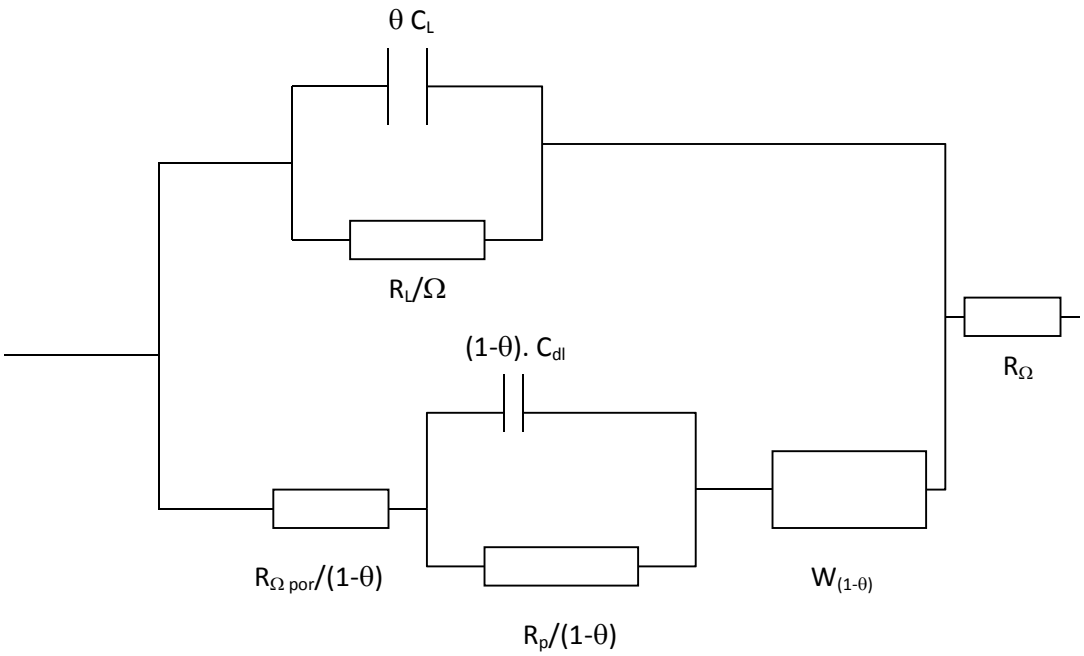

http://dx.doi.org/10.14755/DIS.1999.001

5.4. SURFACE TECHNIQUES RESULTS

5.4.1. AFM data

Surface analytical methods are becoming increasingly important in characterizing the layers formed on the electrodes. AFM imaging has an advantage to be used as an *in-situ* technique to monitor changes on the surface in time. The AFM results are represented in three different forms of images: the first is a 3D presentation of the surface image, the second is a 2D image and the third is a section analysis micrograph. The 3D presentation shows the surface morphology which is represented by the Z or the RMS factors. The section analysis data is useful in characterization of the electrode surface roughness such as: vertical distance, which is a measure of deepness of peaks. Sectional analysis was performed in different directions (x, y). This analysis is very useful in demonstrating localized attacks. The results of the AFM could be divided into two types: dry samples and in fluid cell. In both cases, the effect of DBSO on copper corrosion in 0.1 M Na_2SO_4 solution and that of p-Cl-BHA on copper corrosion in 0.5 M NaCl, were investigated.

5.4.1.1. AFM images of Dry samples

The images of copper surfaces immersed in acidic 0.1 M Na_2SO_4 in the absence and presence of DBSO are shown in Figures 29 and 30. Each figure contains two types of images, which are microscopic views of corrosion, a 3D image a section analysis presentation. As for the case of copper samples in 0.5 M NaCl solution in the absence and presence of p-Cl-BHA, images are shown in Figures 31 and 32, respectively.

http://dx.doi.org/10.14755/DIS.1999.001

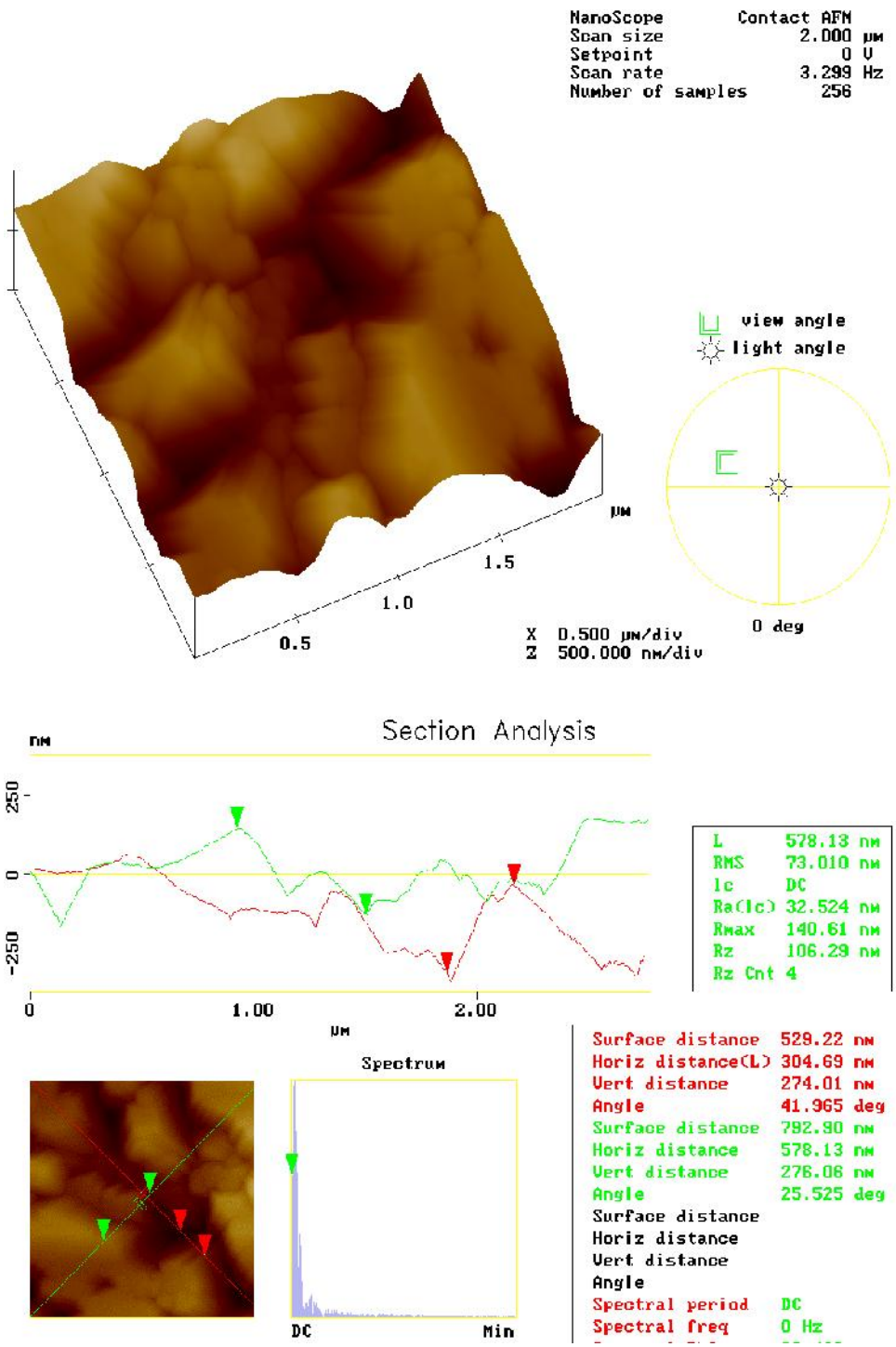

Figure 29. AFM images of copper electrode immersed in 0.1 M Na_2SO_4

http://dx.doi.org/10.14755/DIS.1999.001

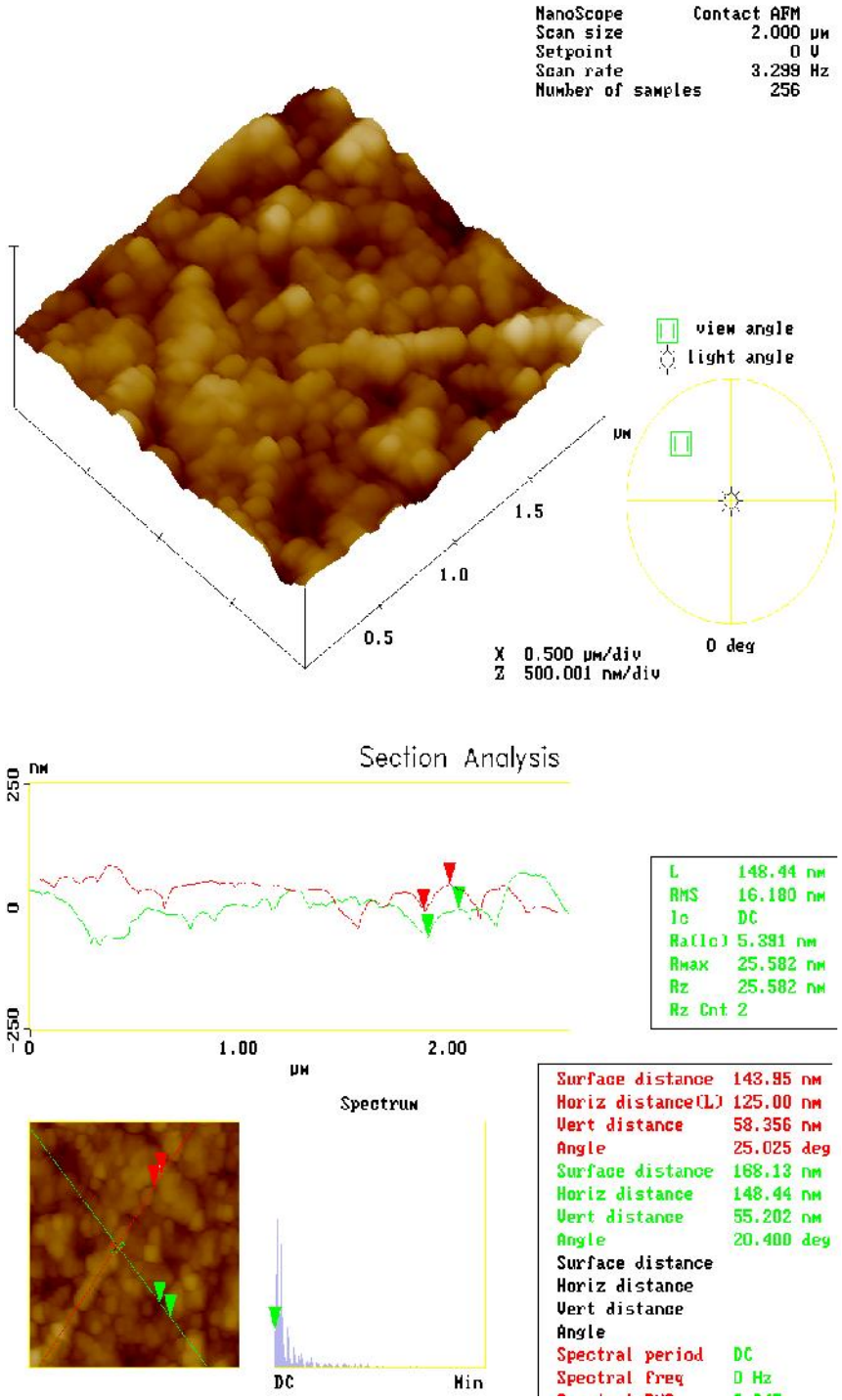

Figure 30. AFM images of copper electrode immersed in 0.1 M Na_2SO_4 and DBSO for 20 hrs; 3D presentation and section

http://dx.doi.org/10.14755/DIS.1999.001

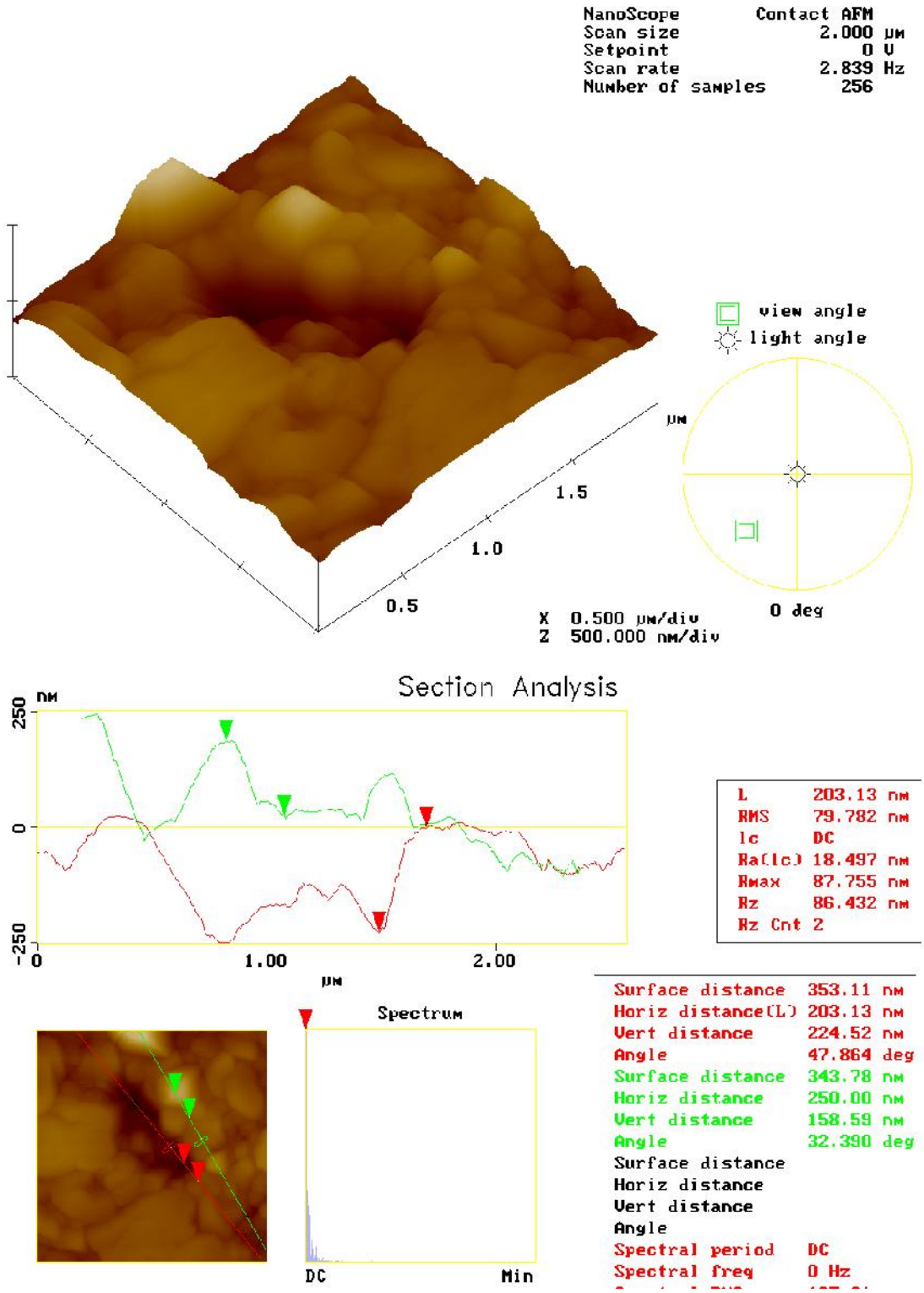

Figure 31 AFM images of copper electrode immersed in 0.5 M NaCl for 20 hrs,

http://dx.doi.org/10.14755/DIS.1999.001

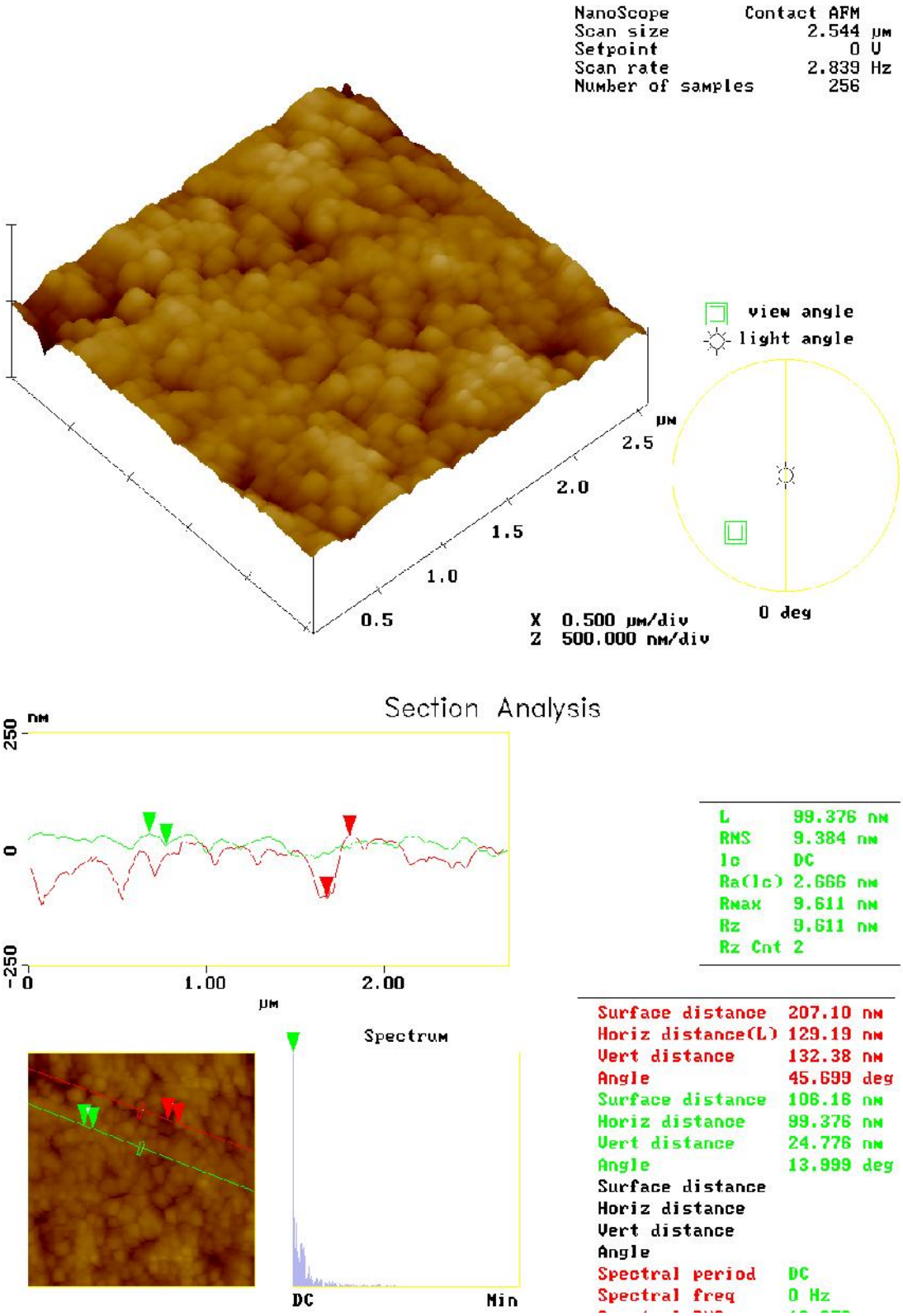

Figure 32. AFM images of copper electrode immersed in 0.5 M NaCl with p-Cl-BHA for 20 hrs; 3D presentation and sectional analysis

5.4.1.2. <u>AFM images of wet samples</u>

http://dx.doi.org/10.14755/DIS.1999.001

These results produced a series of images taken after different time intervals in order to record the changes on the electrode surfaces due to some corrosion or inhibition processes. Results of AFM in contact mode are interpreted in three types of images for each capture. Imaging of the copper surface was first done in air and then after the introduction of the solution at different times.

5.4.1.2.1. 0.1 M Na_2SO_4 with DBSO

Morphological investigations of the copper electrode captured at different times are presented Figures 33,34. Only the 3D images are included in this section for the sake of comparison. More detailed images are presented in the Appendix B. The images captured after the injection of 0.1 M Na_2SO_4 solution demonstrate some corrosion process initiating along active boundaries such as polishing groves, as shown in Figure 33. Images started to show rougher surfaces after some time, where the vertical distance (Z) of the surface increased from 4 nm for the dry sample, 6 nm after immersion for 5 min, and 27 nm after immersion for 45 min.

In the case of the presence of DBSO in the solution a layer started to form on the surface which smoothened the surface and plugged all the active site, caused by the mechanical polishing process, Figure 37. The vertical distance of this series of images decreased from a value of 11 nm after a time of 2 min, 8 nm for t = 7 min., to 6 nm for time of 45 min.. Table 7 summarizes the vertical distance value in the absence and the presence of DBSO in the solution.

Table 7. Section analysis results for copper in 0.1 M Na_2SO_4 without and with DBSO.

Time	**(min)**	0	5	15	30	45
Vertical Distance (nm)	**0.1 M Na_2SO_4**	5	7	14	17	28
	0.1 M Na_2SO_4 and DBSO	6	8	7	7	9

http://dx.doi.org/10.14755/DIS.1999.001

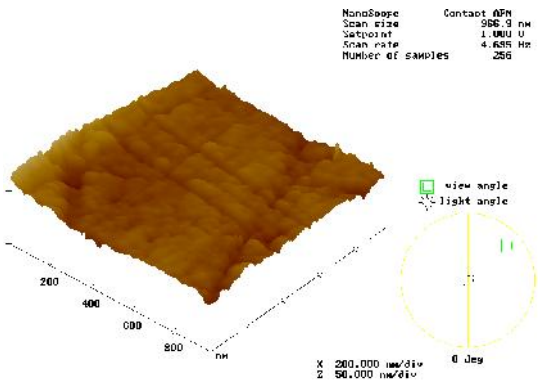

Time = 0 min.

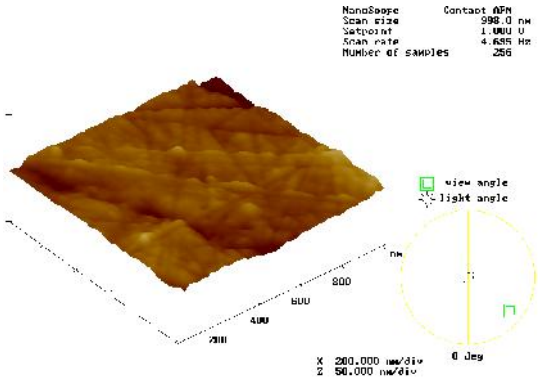

Time = 5 min.

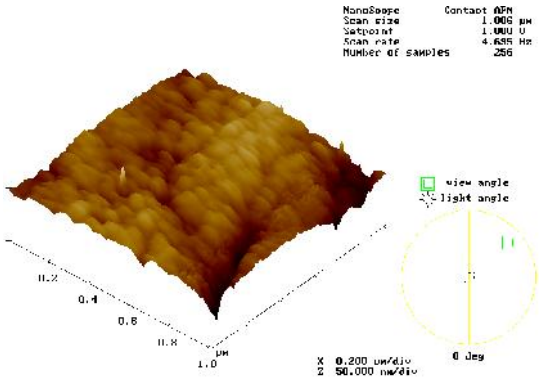

Time = 15 min.

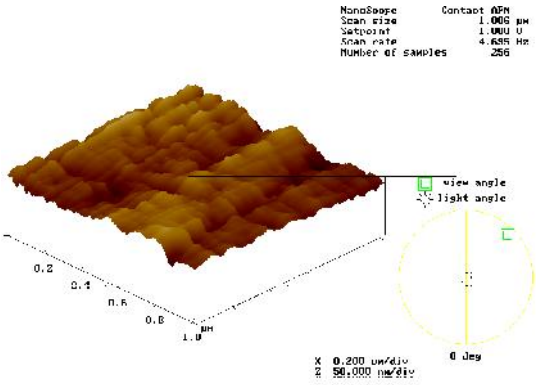

Time = 30 min.

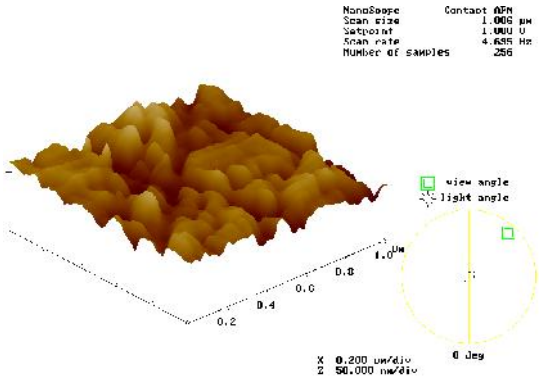

Time = 45 min.

Figure 33. A series of 3D AFM images on copper in 0.1 M Na_2SO_4 at pH = 3.

http://dx.doi.org/10.14755/DIS.1999.001

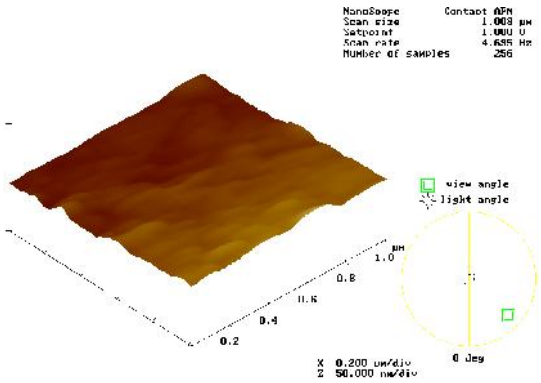

Time = 0 min.

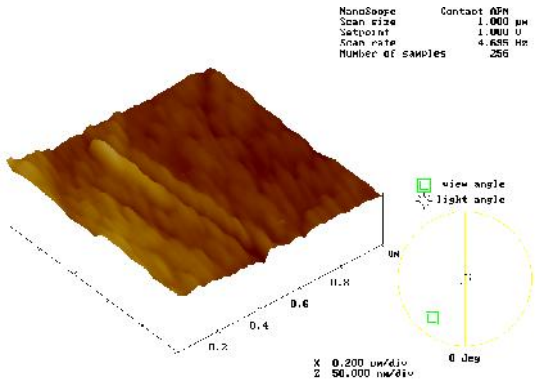

Time = 5 min.

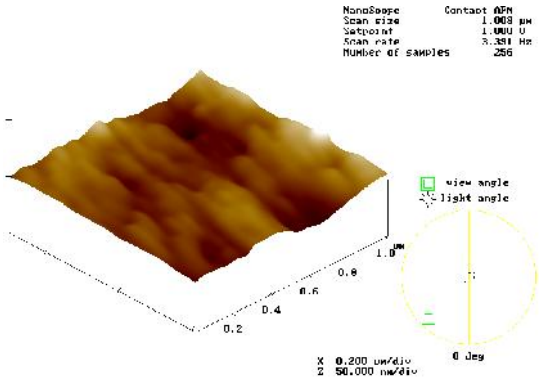

Time = 15 min.

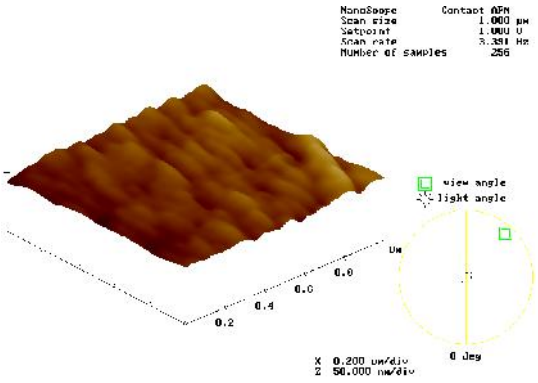

Time = 30 min.

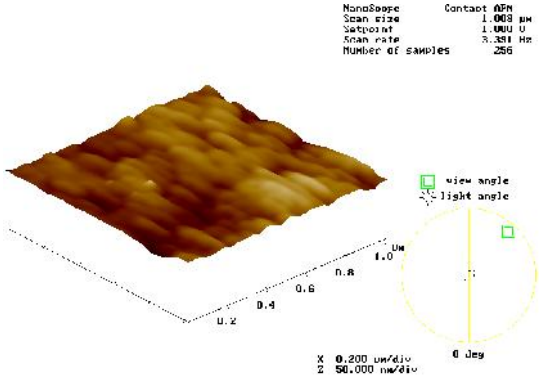

Time = 45 min.

Figure 34. A series of 3D AFM images on copper in 0.1 M Na_2SO_4 with the addition of DBSO.

http://dx.doi.org/10.14755/DIS.1999.001

5.4.1.2.2. p-Cl-BHA in 0.5 M NaCl

The results of these experiments are presented in the same format as described in the previous section. A series of 3D images measured on copper electrode surface in 0.5 M NaCl in the absence of p-Cl-BHA is shown in Figure 35.

The 3D images of copper surface in the presence of p-Cl-BHA are shown in Figure 36. For each captured image, a 3D presentation and deflected image and section analysis are prepared using special computer software and are listed in Appendix C. The effect of 0.5 M NaCl on copper showed the initiation of pitting corrosion. Pits started to develop at t = 1 min. and grew in size. Corrosion products, most likely $CuCl_2$, accumulate on the surface. Vertical distance (Z) value, which is an indication of pit deepness, increased sharply. The images in the presence of p-Cl-BHA demonstrated that p-Cl-BHA was adsorbed on the surface and plugged the active sites where pitting corrosion is most likely to take place.

Table 8. Section analysis results for copper in 0.1 M NaCl without and with BHA.

Time	**(min)**	2	7	10	15	20	30	45	60
Vertical Distance (nm)	**0.5 M NaCl**	43	71	72	83	90	91	117	104
	0.5 M NaCl + p-Cl-BHA	24	19	14	13	16	22	5	5

http://dx.doi.org/10.14755/DIS.1999.001

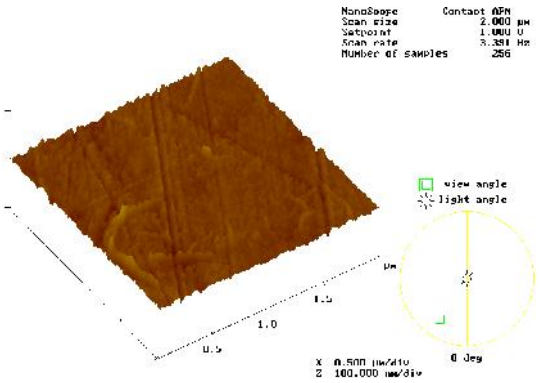

Time = 0 min

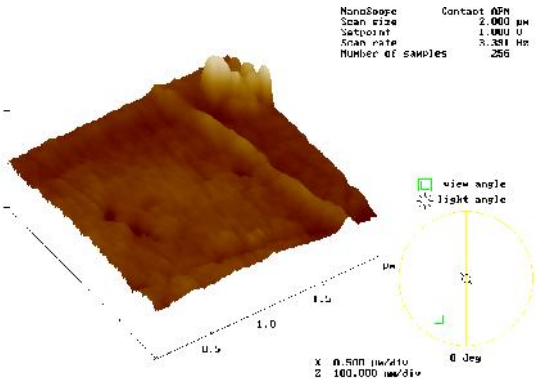

Time = 2 min

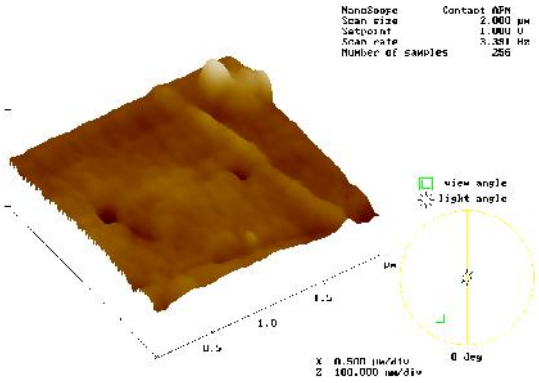

Time = 10 min

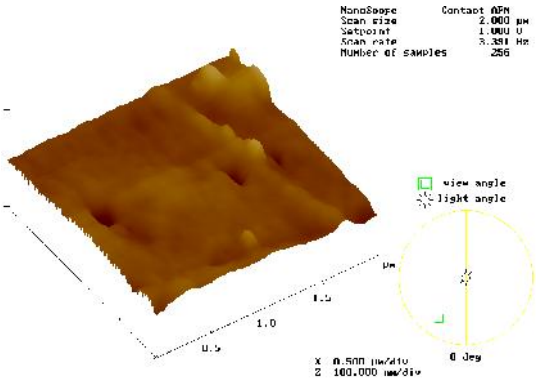

Time = 15 min

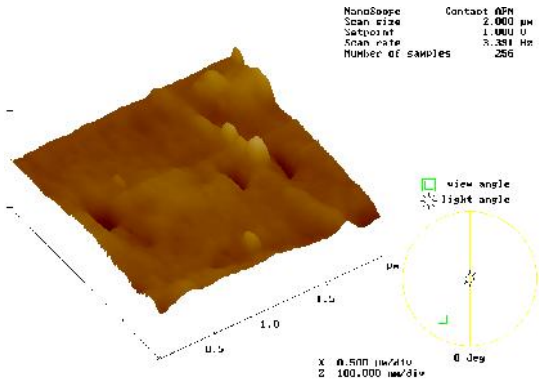

Time = 20 min

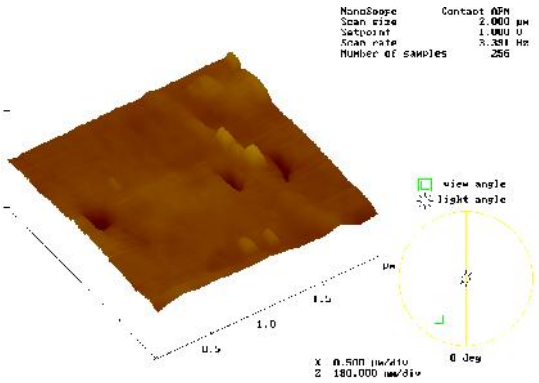

Time = 30 min

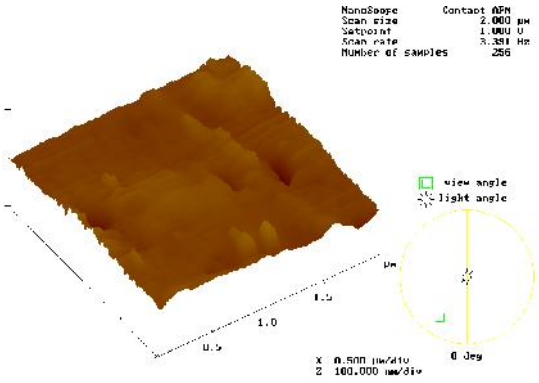

Time = 45 min

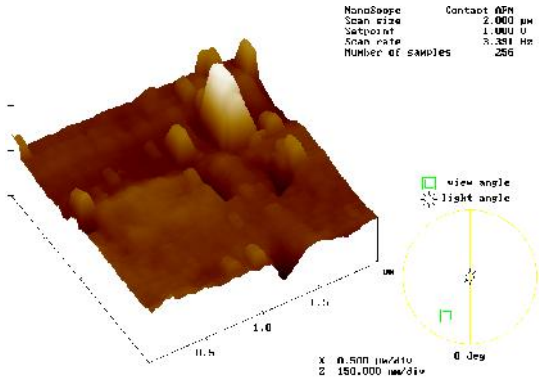

Time = 60 min

Figure 35. A series of 3D AFM images of copper in 0.5M NaCl at pH = 7.0.

http://dx.doi.org/10.14755/DIS.1999.001

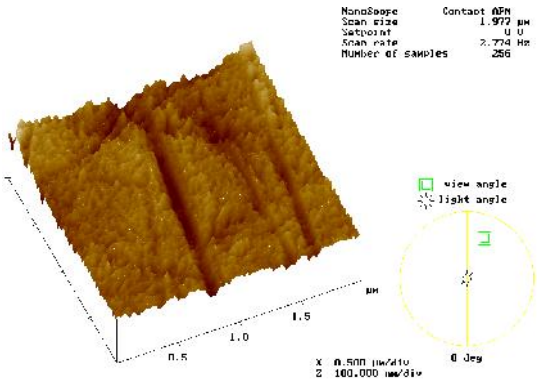

Time = 0 min

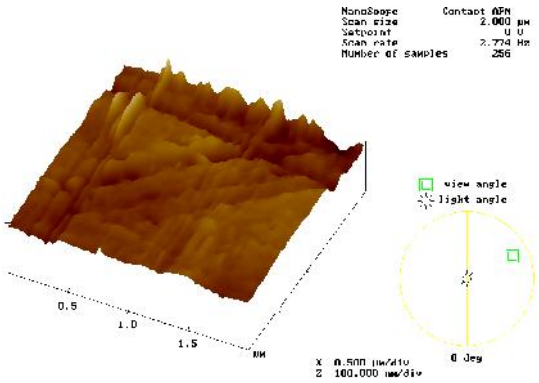

Time = 2 min

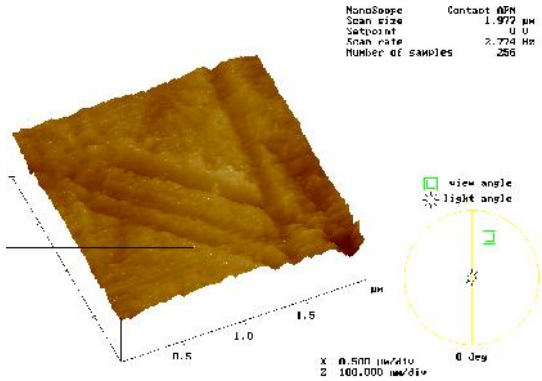

Time = 10 min

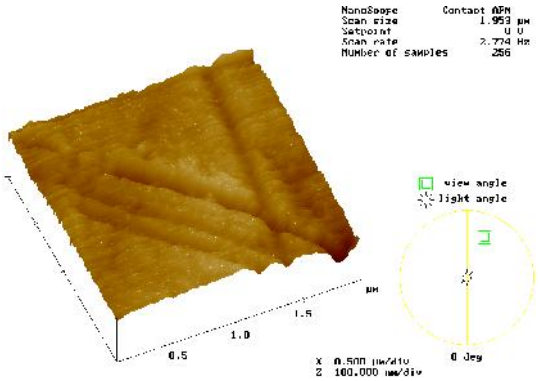

Time = 15 min

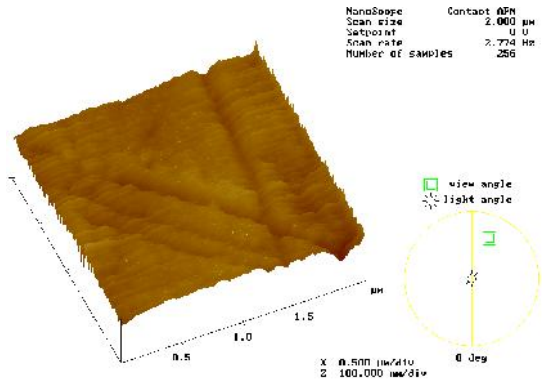

Time = 20 min

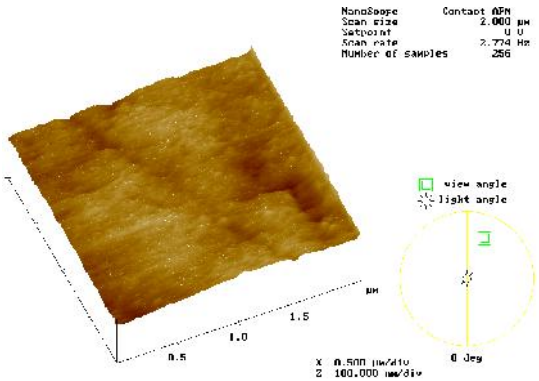

Time = 30 min

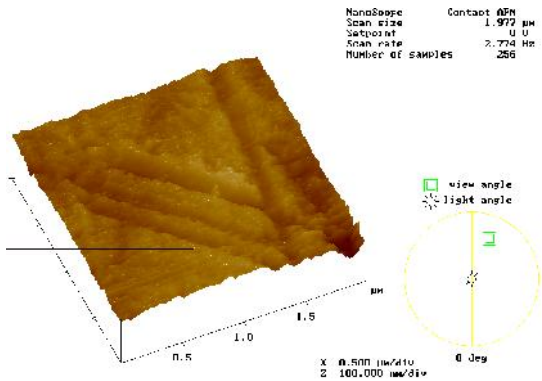

Time = 45 min

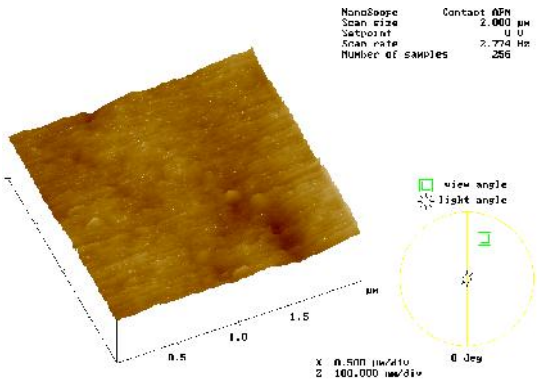

Time = 60 min

Figure 36. A series of 3D AFM images of copper in 0.5M NaCl and p-Cl-BHA, at pH = 7.0.

http://dx.doi.org/10.14755/DIS.1999.001

5.4.2. SEM-EDX RESULTS

Scanning electron microscopy (SEM) can provide photographs with high magnification of the electrode surface. This is useful to investigate the morphology of the surface after different treatments. The SEM is attached to an Energy Dispersive X-ray Spectrometer (EDX-spectrometer) which can provide quantitative analysis of the surface layer. The EDX data are presented in counts as a function of energy (KeV). The EDX spectra did not change very much due to the deep penetration of the measuring beam into the surface. High concentration of copper was measured which made the rest of the components relatively negligible. The measured spectra are listed in the appendix.

5.4.2.1. 0.1 M Na_2SO_4 and DBSO

Figure 37 shows SEM photographs of the copper electrode surface, immersed for 20 hrs in 0.1 M Na_2SO_4, at pH=2.95, in the absence of DBSO. Corrosion occurred along possible scratch lines, due to mechanical polishing, but uniformly distributed. The magnification power was 3,500. Figure 38 shows a photograph of the copper surface after corrosion in the presence of $1x10^{-3}$ M DBSO. The EDX analysis for copper in 0.1 M Na_2SO_4 in the absence and the presence of BDSO are shown in Figures **A1 and A2**, respectively **(**in Apendix A).

5.4.2.2. 0.5 M NaCl and p-Cl-BHA

Photographs of copper surfaces immersed in 0.5 M NaCl solution, at pH≈7, for 20 hrs in the absence and in the presence of p-Cl-BHA, are shown in Figures 39 and 40, respectively. EDX-analysis spectra of the surface layers are listed in Figures **A3** and **A4** of appendix A. Pits caused by corrosion grew in the absence of inhibitor. As a consequence of the addition of p-Cl-BHA, a complex multi-layer was formed on the copper surface which prevented the localized corrosion attacks.

http://dx.doi.org/10.14755/DIS.1999.001

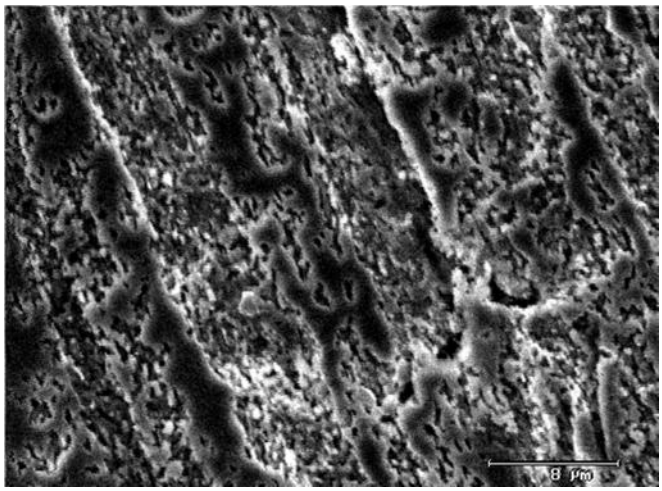

Figure 37. SEM micrograph of copper electrode, after 24 hrs. in 0.1M Na_2SO_4

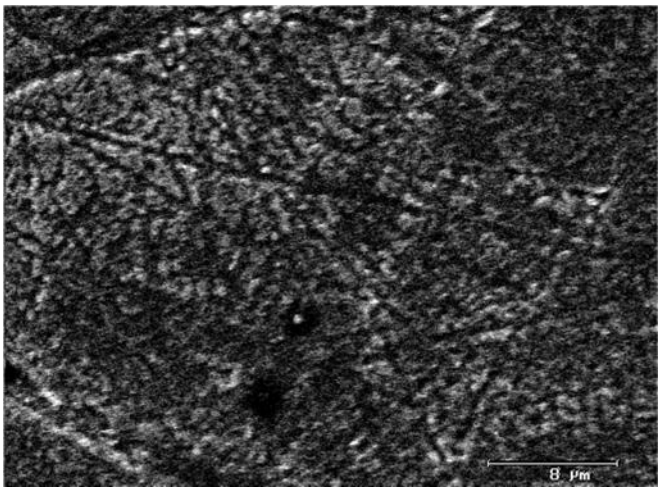

Figure 38. SEM micrograph of copper electrode after 24 hrs in 0.1MNa_2SO4 and DBSO.

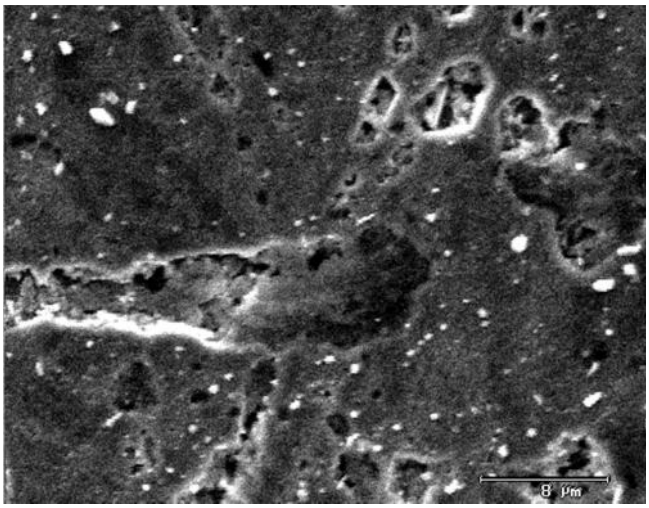

Figure 39. SEM micrograph of copper after 24 hrs in 0.5M NaCl

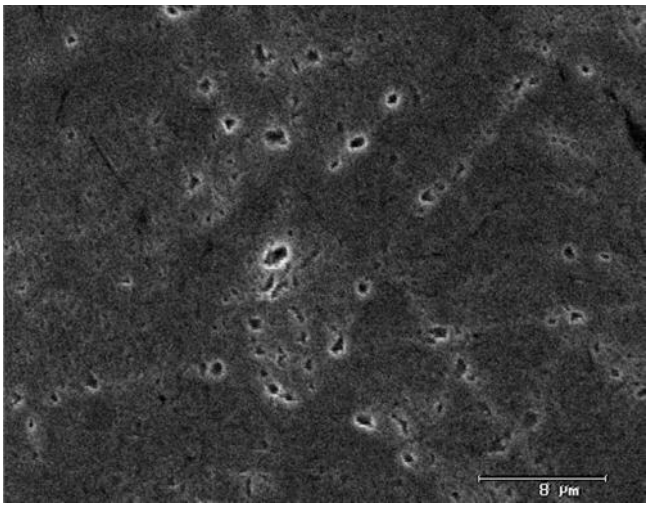

Figure 40. SEM micrograph of copper electrode after 24 hrs in 0.5M NaCl and p-Cl-BHA.

http://dx.doi.org/10.14755/DIS.1999.001

Chapter 6.

6. DISCUSSIONS

6.1. GRAVIMETRICAL RESULTS

The preliminary experiments using the gravimetrical method produced the starting step of this investigation. The initial compounds tested as potential inhibitors for copper corrosion in 0.5 M NaCl, were:

1. benzohydroxamic acid (BHA)
2. orto-chloro-benzo-hydroxamic acid (o-Cl-BHA)
3. para-chloro-benzo-hydroxamic acid (p-Cl-BHA)
4. orto-hydroxil-benzo-hydroxamic acid (o-H-BHA)
5. orto-carboxyl-benzo-hydroxamic acid (o-C-BHA)
6. para-nitro-benzo-hydroxamic acid (p-N-BHA)
7. o-methyl benzohydroxamic acid (o-M-BHA)
8. orto, orto, para-tri-methyl benzo-hydroxamic acid (o, o', p-M-BHA),

Based on the results of the preliminary experiments, four inhibitors, p-Cl-BHA, p-N-BHA, o-M-BHA, and o-Cl-BHA were selected for further investigations. A comparison between o-Cl-BHA and p-Cl-BHA shows the effect of the positioning of the substituent the inhibition effect. As the ortho and para postion from charge distribution (electronic) point of view are equivalent, the improved inhibition of p-Cl-BHA is only due to its more hydrophobic characters. The average optimum concentration for the BHAs was $1x10^{-3}$ M and that for the sulfoxides was $0.5x10^{-4}$ M.

6.2. EQCM RESULTS

6.2.1. Sulfoxides in 0.1 M Na_2SO_4

As could be observed during the first interval of each experiment of copper in 0.1M Na_2SO_4 solution the similar frequency increase rate can be explained by copper dissolution. Copper dissolves in acidic sulfate containing solutions resulting loss of the quartz crystal total mass thus resulting in an increase in the vibrating frequency. The relationship between the mass loss and the frequency change was shown by Sauerbrey equation (Equations 12,13).

http://dx.doi.org/10.14755/DIS.1999.001

During the deposition process, the mass sensitivity coefficient was derived by monitoring the frequency shift. For the crystals used in this study a sensitivity constant of $4x10^{-2}$ Hz cm^2/ng i.e. a frequency change of one Hz represents a mass change of 25 ng/cm^2.

Using Sauerbrey equation to convert ΔF to Δm resulted in quantitative copper corrosion rates. The change of mass due to dissolution could be expressed in thickness reduction rate, which is more practical for estimating the corrosion damage:

$$\dot{\delta} = \frac{\Delta m.3{,}600.24.365.10{,}000}{A.\rho.t}$$

where $\dot{\delta}$ is the thickness reduction rate (μm/yr.); ρ, is the copper density; A, is the active area.

A rate of (706) micrometer per year was calculated and this is considered very high thickness reduction rate. The rest of the calculated thickness reduction rates in the presence of different sulfoxides are tabulated in Table 9.

With the inhibitors addition at the beginning of the second interval, a decrease of the frequency change rate is observed in experiments for DBSO and DPTSO.

Table 9. Thickness reduction rate of copper in 0.1M Na_2SO_4 with the addition of different sulfoxides

	Thickness Reduction Rate (μm/yr)			IE
Sulfoxide	**Interval I**	**Interval II**	**Interval III**	**(%)**
DBSO	710	152	314	78
DPSO	705	528	528	25
DPTSO	704	239	352	66

Decrease in the frequency change rate is due to some mass gains on the electrode surface or more precisely due to the decrease of copper electrode dissolution into solution. The frequency decrease was not so great but the frequency change stabilized in time. This can be explained by the adsorption of the inhibitors on the surface of the electrode.

Taking a closer look at the copper E-pH diagram (Figure 2) reveals that the corrosion of copper immersed in deaerated acidic water is not likely to occur. The H^+/H_2 equilibrium potential indicated by line (a) is always more active than the Cu^{2+}/Cu equilibrium potential.

The E-pH diagram (Figure 3), reveals that the corrosion of copper, immersed in acidic sulfate containing electrolyte at pH=3, occurs and a stable $CuSO_4$ was the pentahydrate ($CuSO_4.5H_2O$) and that Cu^{2+} was the stable soluble copper species in the anodic region immediately preceding formation of the pentahydrate [13].

http://dx.doi.org/10.14755/DIS.1999.001

The presence of oxygen in the non-deaerated solution introduces another possible reaction, O_2/H_2O reduction, with equilibrium potential more noble than that of Cu^{2+}/Cu. The O_2/H_2O system is then a good acceptor for the electrons abandoned by copper oxidation as seen by Equation 7.

The author supports the presumption that cuprous ions are required for film formation. As in acidic solutions, (at pH=3), cuprous oxide is not stable, a special mechanism must take place. This phenomenon could be explained that at the initial stages of copper dissolution, the corrosion rate was high that a shift in the surface pH can take place, which leads to the formation of cuprous oxide. Once an oxide layer is formed, an immediate reaction with the inhibitor present in the solution occurs.

Measurements of frequency during the first interval for different inhibitors showed some deviation in frequency change, which is due to deviation in surface roughness during copper deposition. Higher deposition currents lead to smoother surfaces and lower roughness but could damage the gold surface.
The order of protection ability among these inhibitors is DBSO> DPTSO> DPSO.

6.2.2. BHAs in 0.5 M NaCl

The mechanism of copper corrosion in chloride containing solutions in the presence of BHAs differs from that in the solution containing sulfate anions. By comparing the systems of $Cu-H_2O$ (Figure 2.) and $Cu-Cl^- -H_2O$ (Figure 4), it is obvious that the formation of $CuCl_2^-$ complexes destabilizes the formation of copper oxides and extends the solubility range of copper in near-neutral solutions. Thus as predicted by the E-pH diagram, the presence of Cl^- allows the aqueous corrosion of copper to occur in near-neutral solutions without the formation of copper oxides [13].

From the results of the studied BHAs in 0.5 M NaCl, it is obvious that the curves represent a change of mass on the electrode surface. The decrease of mass, which can be calculated from the frequency increase, is due to copper corrosion. The increase of the electrode mass could mean either accumulation of corrosion products or the adsorption of the inhibitor on the electrode surface. This technique can not distinguish between the processes taking place on the electrode surface at the same time. The sudden decrease of the electrode mass due to corrosion was noticeable for all curves.

Observing the curves representing solutions in the absence and presence of BHAs could reveal the following: For the early stages of corrosion, the mass decrease could be assumed as the total mass loss. A relationship between weight loss (WL) as a function of exposure time could be derived. Inspecting the curve for the blank solution reveals that weight loss and exposure time show a parabolic relationship and can be described by:

$$WL = R\sqrt{t}.$$

This representation suggests that the dissolution process follows a transport limited mechanism, the rate of which is determined by copper diffusion. This behavior is clearly identified in the case of copper in 0.5 M

http://dx.doi.org/10.14755/DIS.1999.001

NaCl. For the solutions containing inhibitors, such as p-Cl-BHA, the corrosion films, represented by the mass loss, formed on the electrode, grew according to an asymptotic law. This suggests that film growth, in inhibitor containing solutions, is of an impervious passive complex layer that hinders diffusion. The strong decrease of copper dissolution in the presence of p-Cl-BHA, is owed to the protective power of the formed complex film. The order of protection for the tested BHAs is:

p-Cl-BHA > p-N-BHA > o-Cl-BHA > o-M-BHA.

6.3. ELECTROCHEMICAL METHODS

6.3.1. Polarization curves

6.3.1.1. Sulfoxides in 0.1 M Na_2SO_4

Results obtained from the EQCM experiments showed that the behavior of copper in 0.1 M Na_2SO_4 was modified by the addition the inhibitors. This fact can be verified by the evaluation of the OCP, Figure 24, for each experiment. These differences are caused by the formation of a thin film during the immersion time before the experiment was started. Inhibitors shift the OCP to either more anodic or cathodic values.

In the cathodic region, the polarization data showed that DBSO resulted in the best protection. Towards more anodic potentials, DPTSO was apparently more polarized and was better attracted by the surface than the other sulfoxides.

At higher potentials (400 mV) DPTSO becomes less noble than DBSO and then gradually all inhibitors become less noble. The applied potential seems to be such a great driving force for copper dissolution so that copper ions pass through the surface thin film by forming visible corrosion products such as $CuSO_4$ (greenish blue) and $Cu(OH)_2$ (blue).Considering the inhibition efficiencies of the tested sulfoxides, the inhibition efficiencies order was similar to that of EQCM.

From the visual observations during and at the end of these experiments, one can draw the conclusion that two surface layers must exist: an inner layer which is very thin and protects the metal surface and an outer layer which is very porous and loosely attached to the surface.

At the end of experiments, different colors of corrosion products were observed. These colors can be referred to the following copper compounds: [64]:

$Cu(OH)_2$ - blue color 

CuO_2 - brown to brownish black 

$CuSO_4$ - green, blue 

http://dx.doi.org/10.14755/DIS.1999.001

6.3.1.2. BHA's in 0.5M NaCl

The results for copper in NaCl in the absence and presence of BHAs showed that all curves, more or less, exhibited three distinct regions. The Tafel slopes and current densities of the maximum and minimum of these regions are listed in Table 3. The Tafel region remained linear in the absence and presence of inhibitors.

P-Cl-BHA produced the most important deviation from the Tafel behavior. However, the addition of the BHA's to the corrosive medium shifted the polarization curves toward lower current density values. The extent of the shift was maximal in the case of p-Cl-BHA. The anodic Tafel slope (βa) was evaluated for all curves and showed that p-Cl-BHA had the highest value (82 mV/Dec). Results also showed that the addition of inhibitor, especially p-Cl-BHA, lowered the overall current density to some extent but i_{peak} value remained more or less unchanged. Only in the case of p-Cl-BHA, i_{peak} decreased drastically. The occurrence of i_{peak} has been attributed to the formation of CuCl on the electrode surface [14]. In the case of p-Cl-BHA, the decrease of i_{peak} may be caused by the smaller surface area available for deposition of CuCl on the copper electrode surface. This is due to the partial coverage of parts of the electrode surface by the inhibitor molecules through adsorption or attachment.

A critical analysis of the anodic polarization curves of BHAs in 0.5 M NaCl solution showed that p-Cl-BHA acted as a potential inhibitor only beyond the anodic potential corresponding to $i_{peak,}$ (i.e. E > 0 mV vs. SCE). At higher potentials, p-Cl-BHA maintained its effectiveness.

6.3.2. EIS measurements

6.3.2.1. Sulfoxide in 0.1 M Na_2SO_4

The Nyquist plots for copper in 0.1 M Na_2SO_4 in the absence and presence of sulfoxides show the effectiveness and behavior of the inhibitors. Rp values are derived from the Nyquist plot. These values are an indication of how effective the protective films are. Among the tested sulfoxides, DBSO produced the highest Rp value of (400 ohm.cm^2).

The curves showed the presence of semi-circular arc at lower frequency values. This semicircle represents the diffusion process at the copper electrode, due to some oxides or complexes formed between the corrosion products and the inhibitors. The semi-circle at high frequency range, which is characteristic of the modulation of copper oxides adsorbed on the surface, was very small in radius (20 ohm.cm^2). This indicates that a very thin film is formed on the electrode surface and this supports the EQCM results.

6.3.2.2. BHA in 0.5M NaCl

In the case of copper in 0.5 M NaCl solution in the absence and presence of BHAs thicker layers are formed mainly as a combination of copper oxides, chloride and inhibitor molecules. The results reveal that the curve representing the aggressive solution showed two semi-circles, which are characteristics of the anodic

http://dx.doi.org/10.14755/DIS.1999.001

partial reaction involving mass transfer occurring through the Cu_2O layer. The semicircle at high frequency is due to the modulation for CuCl adsorbed at the electrode while the low frequency part represents the diffusion process at the electrode, due to $CuCl_2^-$ and other adsorbed materials. Other curves representing the inhibitors showed that the semi circle at the high frequency disappeared indicating that the inhibitors hindered the reactions taking place at the electrode surface by covering the active areas. The Rp values showed that p-Cl-BHA resulted in the highest value, thus the most protective. By comparing the Rp value, the order of inhibition is: p-Cl-BHA > p-N-BHA > o-Cl-BHA > o-M-BHA, which is in complete compliance with other results.

6.4. AFM IMAGEING

6.4.1. Long term experiments (dry specimen)

The results of the specimen, immersed in solutions in the absence and presence of inhibitors, presented the changes on the electrode surface.

In the case of copper in 0.1 M Na_2SO_4 solution, a general form of surface corrosion was observable. Corrosion products were present all over on the surface. Surface roughness represented by the vertical distance in the section analysis, was 274 nm. In the solution containing DBSO the surface was smoother and a protective layer was formed. This complex layer reduced the surface roughness and plugged the active areas where corrosion usually initiates. In this case, the vertical distance was 57 nm. In the case of copper in 0.5M NaCl solution the presence of large pits are obvious. Next to those pits, corrosion products accumulated. This confirms the results that copper corrosion in 0.5M NaCl solution is of localized type. The vertical distance of the deepest pit was about 220 nm. The addition of p-Cl-BHA to the aggressive solution changed the mechanism totally. A condensed protective layer was apparent on the surface. This layer is composed of copper corrosion products in complex with the p-Cl-BHA. The vertical distance of the highest peak was decreased to 24 nm by the addition of p-Cl-BHA.

6.4.2. Sequential AFM images

6.4.2.1. DBSO in 0.1 M Na_2SO_4

The *in-situ* sequential AFM images of copper in 0.1M Na_2SO_4 solution confirm the dynamics of copper electrode surface, which shows a general attack on the active parts of the surface. Inspecting Figure 36 reveals that copper corrosion starts at some active points and the surface roughness increases as corrosion proceeds. The formation of copper oxides is also confirmed by the presence of microcrystalline layer or products on the electrode surface. The addition of DBSO showed completely different processes. The surface was much smoother and the presence of some deposits believed to be the inhibitor was observed. The change in the shape and orientation of the surface products indicates that DBSO is first adsorbed on the surface of the electrode and then it is converted to DBS, where copper itself could play a role of a catalyst.

http://dx.doi.org/10.14755/DIS.1999.001

6.4.2.2. p-Cl-BHA in 0.5 M NaCl.

The *in-situ* sequential AFM images of copper electrode in NaCl show the progressive development of an irregular topography. This is clearly seen from both the section analyses of AFM scans at different times and the 3-D view of the images. The copper corrosion in NaCl is confirmed to be of the localized type. Etched pits were clearly monitored. Their Shape and size changed in time. The section analysis of each image could provide some information on the pit penetration rate. Beside, the *in-situ* sequential AFM imaging reveals that copper corrosion in 0.5 M NaCl is accompanied by the precipitation of copper chloride at the interface. The addition of p-Cl-BHA to the aggressive solution developed a compact covered surface.

The sequential AFM imaging showed that p-Cl-BHA compound inhibited the formation of pits on the surface. Active sites were plugged by the inhibitor thus hindering the initiation of corrosion. The electrode surface after 60 min. of measurement had a smooth compact layer which is possibly a blend of copper chloride and the inhibitor.

6.5. SEM MICROGRAPHS.

SEM micrographs were taken on the surfaces of the copper after corrosion experiments. These results confirm the type of processes taking place at the electrode. EDX-analysis of the surface layer did not produce any significant information. This can be because the protective film of the adsorbed inhibitors is very thin and the analyzing beam penetrated the bulk of the metal as well. Traces of inhibitors were detected on the surface layer, but without any quantitative results.

Combining the discussions of all different results, the following models of inhibition could be assumed:

I. A. For the DBSO effectiveness is acidic sulfate containing solutions is due to the following mechanisms:

The DBSO in acidic 0.1 M Na_2SO_4 protonizes to form cation through:

$$(C_6H_5CH_2)_2SO + H^+ \rightarrow (C_6H_5CH_2)_2SOH^+$$

This protonized species is adsorbed preferentially at the cathodic sites of the electrode and can be reduced at the electrode surface to form DBS as:

$$(C_6H_5CH_2)_2\,SOH^+ + H^+ + 2e^- \rightarrow (C_6H_5CH_2)_2S + H_2O$$

Because of the availability of the lone pair of electrons at the sulfur atom, the reduced molecule as a whole is adsorbed on the metal surface, or on some oxides, resulting in the corrosion protection effectiveness.

I. B. Other possibility that must be considered is that the dissolved Cu^{2+} form an insoluble film with DBS at the interface. These two species can combine in equi-molar amounts to form a sulfide at the interface by:

$$(C_6H_5CH_2)_2\,S + Cu^{2+} \rightarrow (C_6H_5CH_2)_2\text{-}S\text{–}Cu$$

with a coordinate type of bonding between sulfur and copper.

The reduction reaction of DBSO to DBS could be assisted by the metal itself, where it plays the role of a catalyst.

http://dx.doi.org/10.14755/DIS.1999.001

II. As for copper corrosion in NaCl solutions, p-Cl-BHA hindered the corrosion process by plugging in the active pits and producing a protective film that isolates the metal. The copper-corrosion inhibition mechanism in NaCl solution is more likely to take place on copper surface covered by oxide(s) or, eventually, on copper corrosion products. It is very difficult to assume that p-Cl-BHA could act on the electrode surface free of oxides or chlorides. It seems more realistic to consider a complementary protective effect between the inhibitor and the Cu (I) oxide.

P-Cl-BHA is likely to act by reducing processes of electronic or ionic transfer through the surface layer, or by reducing the dissolution rate of the oxide. The attachment of p-Cl-BHA, through its nitrogen atom, to the layer is most likely.

http://dx.doi.org/10.14755/DIS.1999.001

Chapter 7.

7. CONCLUSIONS

Based on all experiments results of the dissertation, the following conclusions can be drawn:

1. The quartz microbalance is a powerful technique, which allows the determination of the corrosion rate or mass loss of copper and to monitor the effectiveness of the tested inhibitors. These measurements could be performed not only in acidic media but also in neutral media where the protective film tends to be much thicker. The high sensitivity of EQCM allows distinguishing between different processes on the electrode surface.
2. EQCM has proven to be useful as a tool for long time *in-situ* measurements where corrosion monitoring is needed. The stability of the method over a long period is advantageous.
3. The EIS results provided fast and dependable method to evaluate inhibition efficiency. The results from this method were in agreement with other experimental data.
4. AFM in contact mode, a newly applied surface imaging method could be used for monitoring processes taking place on the electrode. Pit formation rate and surface roughness can be obtained from the section analysis data.
5. The different experiments have shown that among the aromatic sulfoxides used to inhibit copper corrosion in acidic media, DBSO was the most efficient. DPTSO also produced some satisfactory results.
6. The inhibition action of DBSO on copper corrosion may be considered to be a two-steps process where the sulfoxide is first converted to sulfide, which forms a badly soluble layer on the electrode surface thus hindering the metal dissolution.
7. For copper corrosion in chloride media with different BHA inhibitors, p-Cl-BHA proved effective against copper corrosion. This inhibitor could be developed into a replacement to toxic inhibitors such as azoles. The order of inhibition efficiency among the BHA derivatives is:

   p-Cl-BHA > p-N-BHA > o-Cl-BHA > o-M-BHA.
8. The inhibition action of the BHA derivatives is due to complexing actions between the inhibitors and the copper chloride products.
9. The treatment of experimental data using EQCM and AFM methods presented in this thesis constitutes the basis of further research aiming to understand the mechanism of copper inhibition in different media in terms of fundamental physical-chemical phenomena. For this purpose, imaging techniques combined with surface analysis and electro-gravimetrical techniques are very promising.

http://dx.doi.org/10.14755/DIS.1999.001

Recommendations

- Computer simulations and modeling of corrosion and inhibition processes could assist in understanding the mechanism concerned. Corrosion and inhibition are complex phenomena due to the large number of variables and factors affecting the processes.
- The effort to replace azoles must be continued. Applying some additives to inhibitors can improve the effectiveness further with the aim to develop synergistic blend. Synergism could produce some economically and environmentally favored results as the applied inhibitor concentration can be reduced drastically.

Industrial applications

- There are great needs for environmentally friendly inhibitors in the industry. In our patent, we presented the possibility to use some new chemicals as inhibitors.
- The experimental work on the development of the EQCM can add a new dimension in long term monitoring of corrosion processes.

http://dx.doi.org/10.14755/DIS.1999.001

References.

[1] **J. R. Evans**,
"The Corrosion and Oxidation of Metals", **1**st Ed, Edward Arnold, London, (1960)

[2] **H. H. Uhlig**,
"Corrosion and Corrosion Control", **4**th printing, John Wiley & Sons, Inc, New York, N.Y. 224 (1967)

[3] ASM Handbook **13**, Corrosion, (1992)

[4] **M. Pourbaix**,
Corros. Sci. **10**, 963 (1990)

[5] **M. Novak,** and **A. Szucs,**
J. Electroanal. Chem. Interfacial Electrochem. **210**, 229 (1986)

[6] **J. O. M. Bockris,** and **M. Enyo**,
Trans. Faraday Soc. **58**, 1187 (1962)

[7] **L. Kiss**,
"Kinetics of Electrochemical Metal Dissolution", (Amsterdam, NL: Elsevier, (1988)

[8] **F. K. Crundwell,**
Electrochim. Acta **37**, 2707 (1992)

[9] **E. Mattsson,** and **J. O. M. Bockris,**
Trans. Farady Soc. **55**, 1586 (1959)

[10] **L. Kiss,**
Acta Chim. Acad. Sci. Hung., **92**, 113 (1977)

[11] **C. Fiaud,**
Proc. 8th Euro. Sym. Corros. Inhi.**, 2,** Ferrara, 929 (1995)

[12] **L. Kiss, Á. Bosquez** and **M. Varsányi,**
Acta Chim. Hung., **108**, 369 (1981)

[13] **D. Tromans** and **J. C. Silva,**
Corrosion **53**, 171 (1997)

[14] **H. P. Lee** and **K. Nobe,**
J. Electrochem. Soc. **133**, (1986); pp. 2035

[15] **L. D. Burke, M. J. G. Ahern** and **T. G. Ryan,**
J. Electrochem. Soc. **137,** 553 (1990)

[16] **M. R. Gennero de Chialvo, S. L. Marchiano,** and **A. J. Arvia**,
J. Appl. Electrochem. **14**, 165 (1984)

[17] **E. S. Snavely,** and **N. Hackerman**,
Basic Corrosion Course, NACE, Houston, TX., Chapter 9, (1970)

[18] **W. J. Lorenz** and **F. Mansfeld,**
Proc. Inter. Conf. Corros. Inhib., (R. H. Hausler ed.)
Houston, TX: NACE, 7 (1987)

[19] **O. L. Riggs** and **R. L. Every**,
Corrosion **18**, 262 (1962)

[20] **R. J. Chin** and **K. Nobe,**
J. Electrochem. Soc. **118**, 4 (1971)

[21] **T. P. Hoar** and **R. D. Holliday**,
J. Appl. Chem. **3**, 502 (1953)

[22] **W. J. Lorenz** and **F. Mansfeld**,
"Corrosion Mechanisms", (F. Mansfeld, ed.) Marcel Dekker Inc,
N. Y., 1 (1987)

[23] **G. Schmitt**,
"A working party report on corrosion inhibitors", EFC Publication No. II.

http://dx.doi.org/10.14755/DIS.1999.001

64, The Institute of Materials London (1994)
[24] **D. Chadwick** and **T. Hashemi,**
Corros. Sci., **39,** 18(1), (1978)
[25] **J. Eickmans, R. Holm, D. Holtkamp**,
Proc. Eurocorr'91, **1**, 1(1991)
[26] **J. G. Thomas**,
"Corrosion", (L. Sheir, ed.) Newnes–Butterworths, London, **2**, 183 (1976)
[27] **F. Tirbonord,**and **C. Fiaud,**
Corros. Sci. **18**, 139 (1978)
[28] **G. Trabanelli**,
Corrosion'89, New Orleans, 133 (1989)
[29] **K. Aramaki, N. Ohno,** and **H. Nishihara**,
Proc. **12**th Inter. Corros. Cong., Texas, 1804 (1993)
[30] **A. Pirnat, L. Mészáros,** and **B. Lengyel**,
Proc. **7**th Euro. Sym. on Corros. Inhi., Ferrara, 885 (1990)
[31] **N. Ohno, J. Uehara,** and **K. Aramaki,**
J. Electrochem. Soc. **140**, 2512 (1993)
[32] **B. Kurzak, W. Bal** and **H. Kozlowski,**
J. Inorg. Biochem. **38**, 9 (1990)
[33] **I. Felhõsi**,
Unpublished results, Budapest (1997)
[34] **H. Abruna**, Ed.,
"*VCH chemical*", New York, 529 (1991)
[35] **T. Nomura,** and **M. Ijima**,
Anal. Chim. Acta **97**, 131 (1981)
[36] **S. Bruckenstein,** and **M. Shay**,
Electrochim. Acta **30**, 1295 (1985)
[37] **M. Benje, M. Eiermann, U. Pittermann,** and **K. G. Weil**,
Ber. Bunsen. Ges. Phys. Chem**. 90**, 435 (1986)
[38] **S. Bourkane, C. Gabrielli,** and **M. Keddam**,
Electrochim. Acta **34**, 1081 (1989)
[39] **G. Sauerbrey**,
Z. Phys., **155**, 206 (1959)
[40] **D. M. Ullevig, J. M. Evans,** and **M. G. Albrecht,**
Anal. Chem. **54,** 2341 **(**1982)
[41] **R. Borjas,** and **D. A. Buttry**,
J. Electroanal. Chem. **280**, 73 (1990)
[42] **A. Müller, M. Wicker, R. Schumacher,** and **R. N. Schindler,**
Ber. Bunsen. Ges. Phys. Chem. **92**, 1395 (1988)
[43] **C. Lu**, Ed.,
"Applications of Piezoelectric Quartz Crystal Microbalance";
Elsevier: New York, **7**, Chapter 1,2 (1984)
[44] **E. Müller,**
"Praktikum der Electrochemie", Stein-Kopp Verlag, (1953)
[45] **S. Bruckenstein** and **S. Swathirajan**,
Electrochim. Acta **30**, 851 (1985)
[46] **H. J. Schmidt, U. Pittermann, H. Schneider** and **K. G. Weil**,
Anal. Chim. Acta, **273,** 561 (1993)
[47] **Gy. Inzelt**,
J. Electroanal. Chem., **348**, 465 (1993)
[48] **A. Jardy, A. Legal Lasalle-Mulin, M. Keddam** and **H. Takenouti**,
Electrochim. Acta **37**, 2195 (1992)

http://dx.doi.org/10.14755/DIS.1999.001

[49] **D. J. Jobe, J. Sell**, **H. W. Pickering,** and **K. G. Weil**,
J. Electrochem. Soc. **142,** 2170 (1995)
[50] **M. Hepel**,
Proc. **47**th ISE meeting, Balatonfüred, Hungary, P6a-23 (1996)
[51] **J. Bácskai, V. Kertész** and **Gy. Inzelt**,
Magy. Kém Foly **98**, 310 (1992)
[52] **G. T. Cheak,** and **W. O'Grady**,
J. Electroanal. Chem. **277**, 341 (1990)
[53] **M. Volmer** and **T. Erdey-Gruz**,
Z. Phys. Chem. **150**, 203 (1930)
[54] **M. Stern,** and **A. L. Geary**,
J. Electrochem. Soc.**104**, 56 (1957)
[55] **M. Pouraix,**
"*Lectures on electrochemical corrosion*", Plenum Press, N. Y., 252 (1973)
[56] **I. Epelboin, M. Keddam** and **H. Takenouti**,
J. Appl. Electrochem. **1**, 71 (1972)
[57] **F. Mansfeld** and **W. J. Lorenz,**
"*Techniques for Characterization of Electrodes and Electrochemical Processes*", (R. Varma and J. R. Selman, ed.), John Wiley & Sons, Inc. (1991)
[58] **D. D. Macdonald**,
"*Techniques for Characterization of Electrodes and Electrochemical Processes"*, (R. Varma and J. R. Selman, ed.), John Wiley & Sons, Inc. (1991)
[59] **D. C. Silverman**,
Corrosion **46**, 589 (1990)
[60] **B. Boukamp**,
"*Equivalent Circuit (EQUIVCRT*)*",* Version (**4.51**) (1993).
[61] **J. Van den Meerakker**,
Electrochim. Acta **35**, 1267 (1990)
[62] **R. A. Heising**,
"*Quartz crystals for electric circuits*", van Nostrand, New York, (1946)
[63] **C. R. Hauser** and **W. B. Renfrow, Jr.,**
Org. Synth., Coll. Vol. **II**, 67 (1971)
[64] **R. C. West**. Ed.,
"*Handbook of Chemistry and Physics*", CRC press, Inc. **1**st Student ed. (1988)
[65} **K. Juttner, W. J. Lorenz, M. W. Kendig** and **F. Mansfield,**
J. Electrochem. Soc. **135**, 335 (1988)

http://dx.doi.org/10.14755/DIS.1999.001

Appendix.

Appendix A. EDX spectra of copper electrode in 0.1 M Na_2SO_4 with and without DBSO and also in 0.5 M NaCl with and without p-Cl-BHA..

Appendix B. Section analysis of AFM images taken on copper electrode in 0.1 M Na_2SO_4 with and without DBSO, in a wet cell.

Appendix C. Section analysis of AFM images taken on copper electrode in 0.5 M NaCl with and without p-Cl-BHA, in a wet cell.

http://dx.doi.org/10.14755/DIS.1999.001

Appendix a

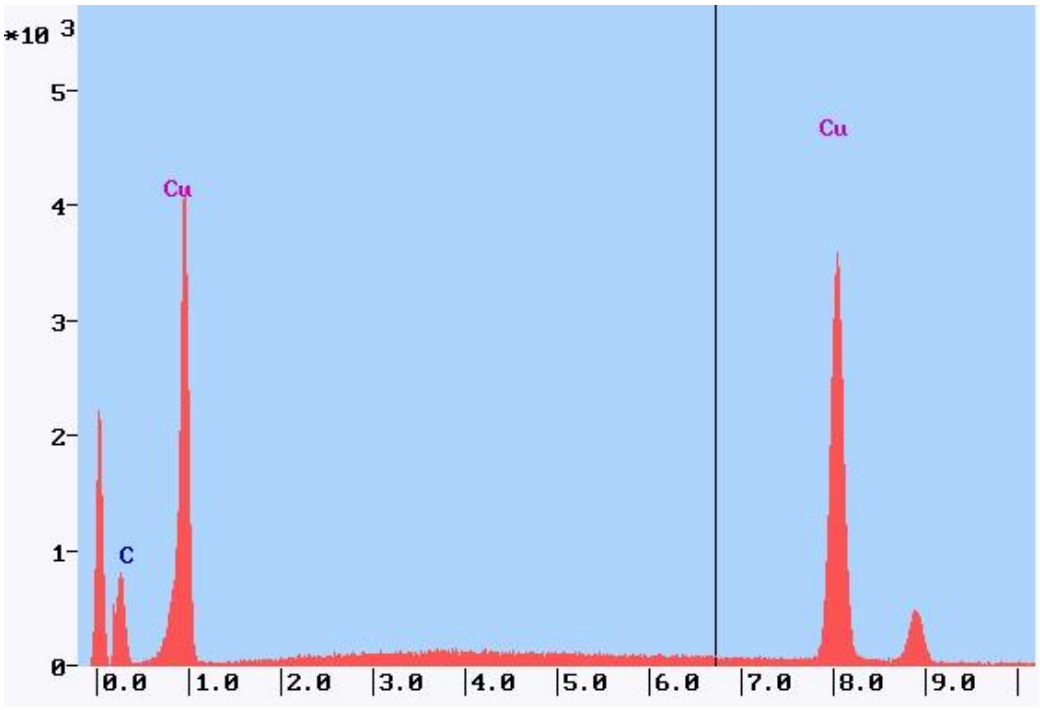

Figure A1. SEM spectrum of copper after 24 hrs in 0.1M Na_2SO4.

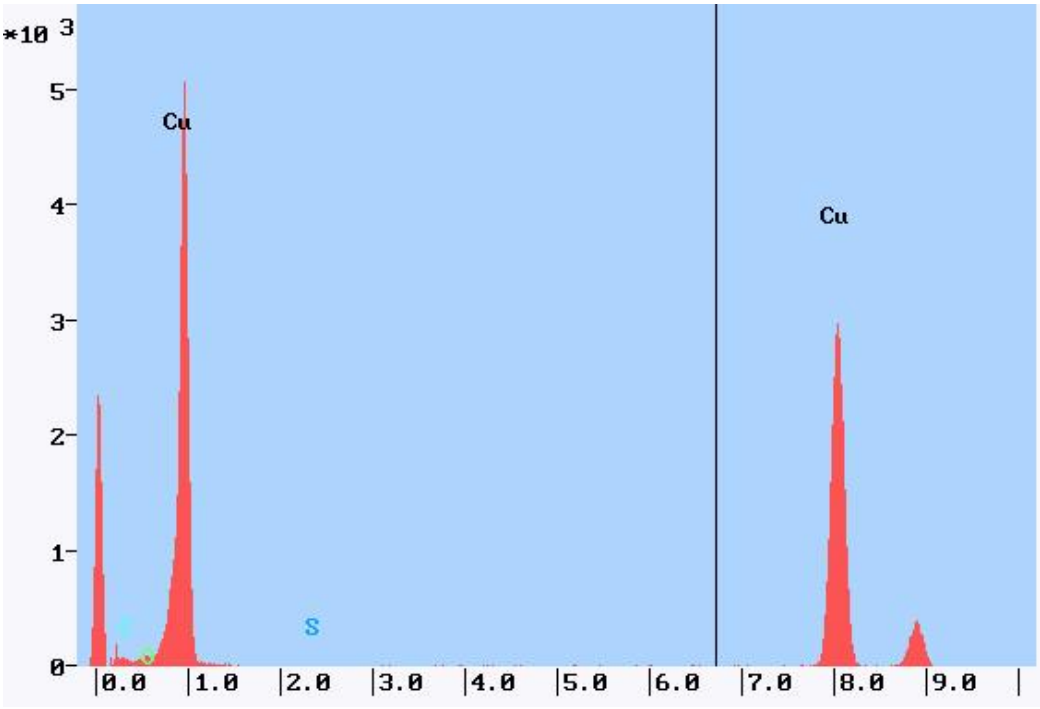

Figure A2. SEM spectrum of copper after 24 hrs in 0.1M Na_2SO4 and DBSO.

http://dx.doi.org/10.14755/DIS.1999.001

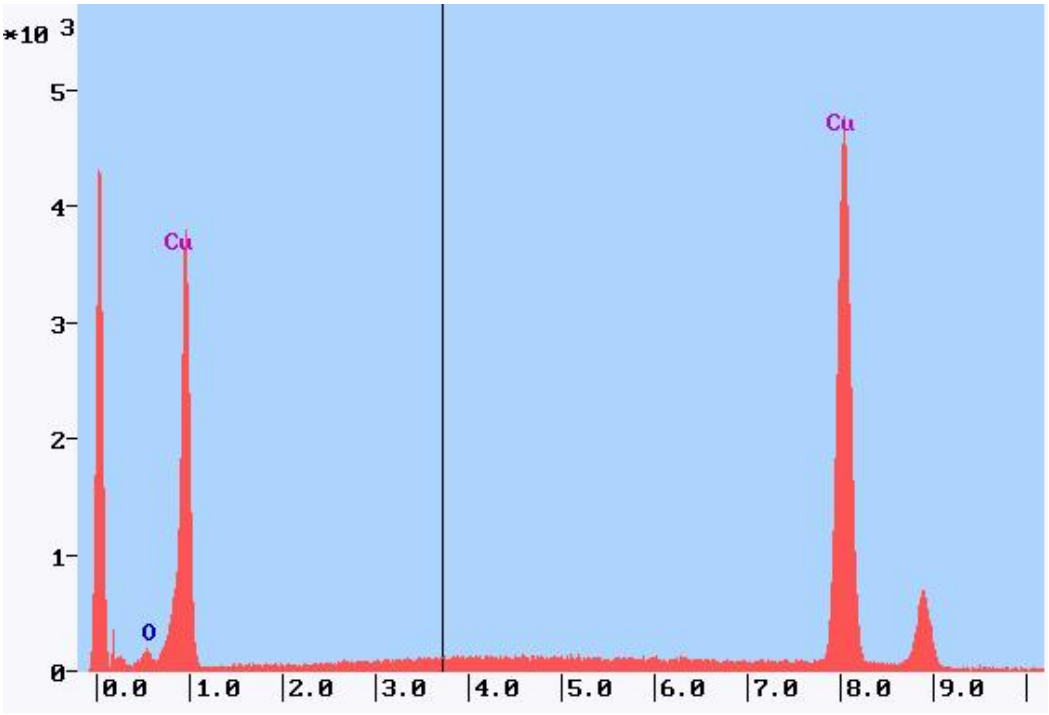

Figure A3. SEM spectrum of copper electrode after 24 hrs in 0.5M NaCl.

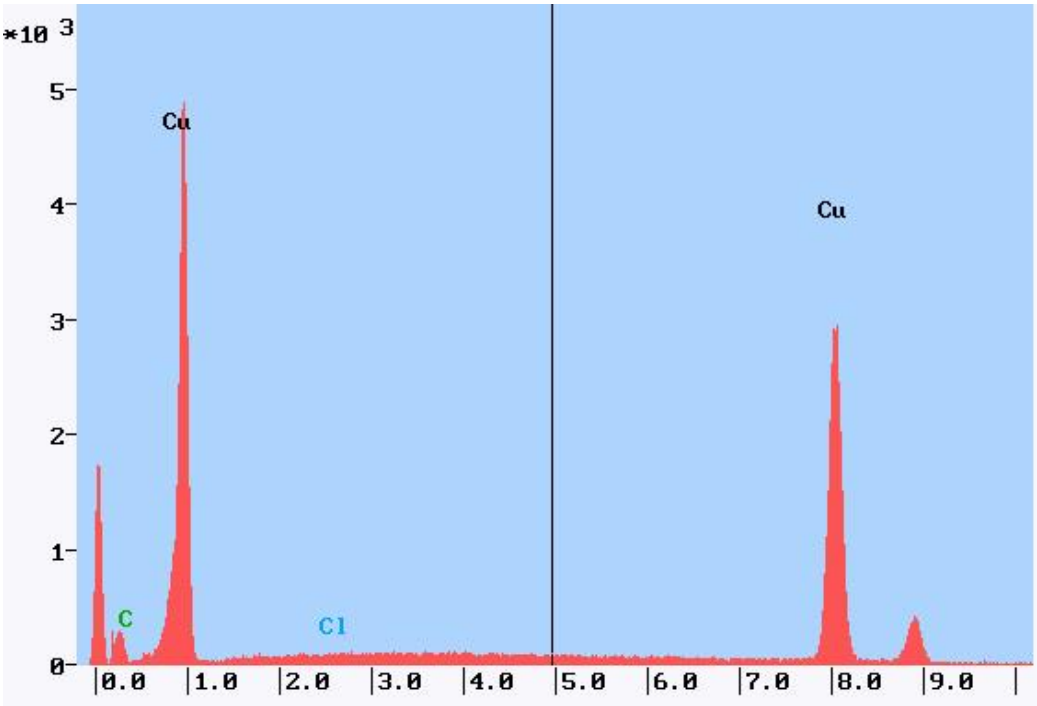

Figure A4. SEM spectrum of copper after 24 hrs in 0.5 M NaCl and p-Cl-BHA

http://dx.doi.org/10.14755/DIS.1999.001

Appendix B. **Appendix B** ***Section analysis of AFM images of copper in 0.1 Na_2SO_4***

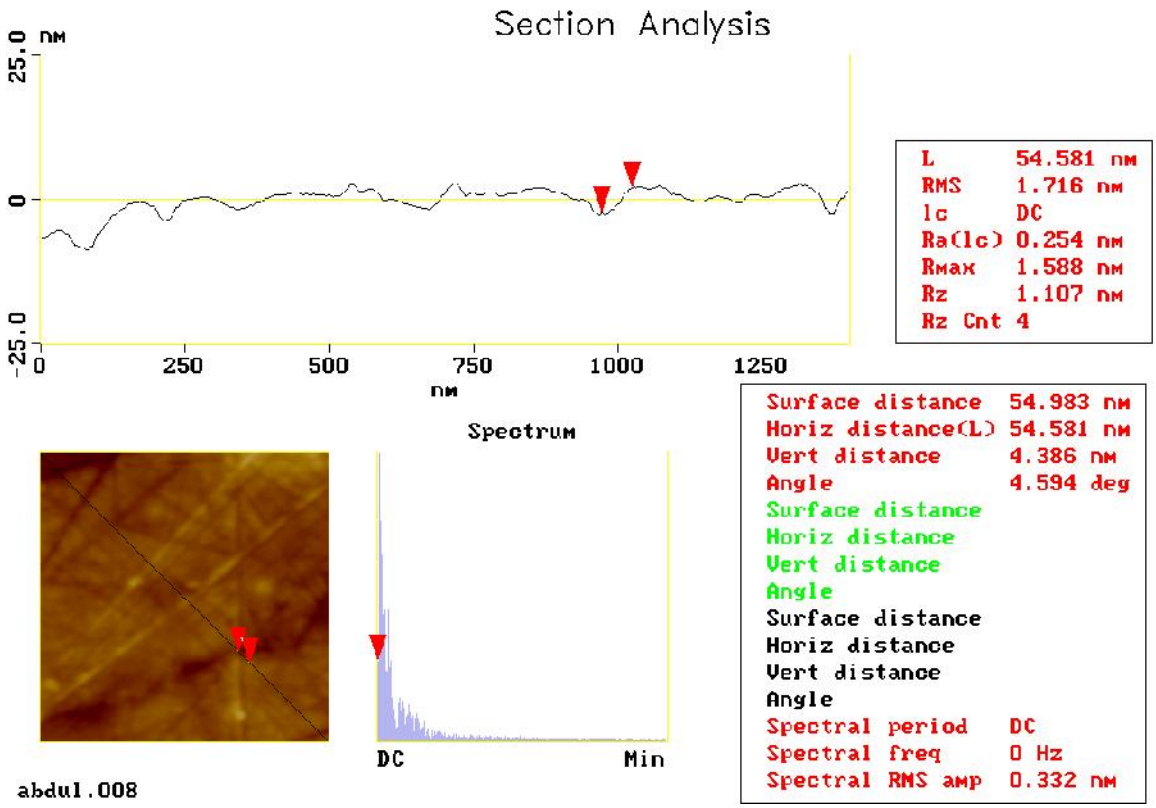

Time = 0 min.

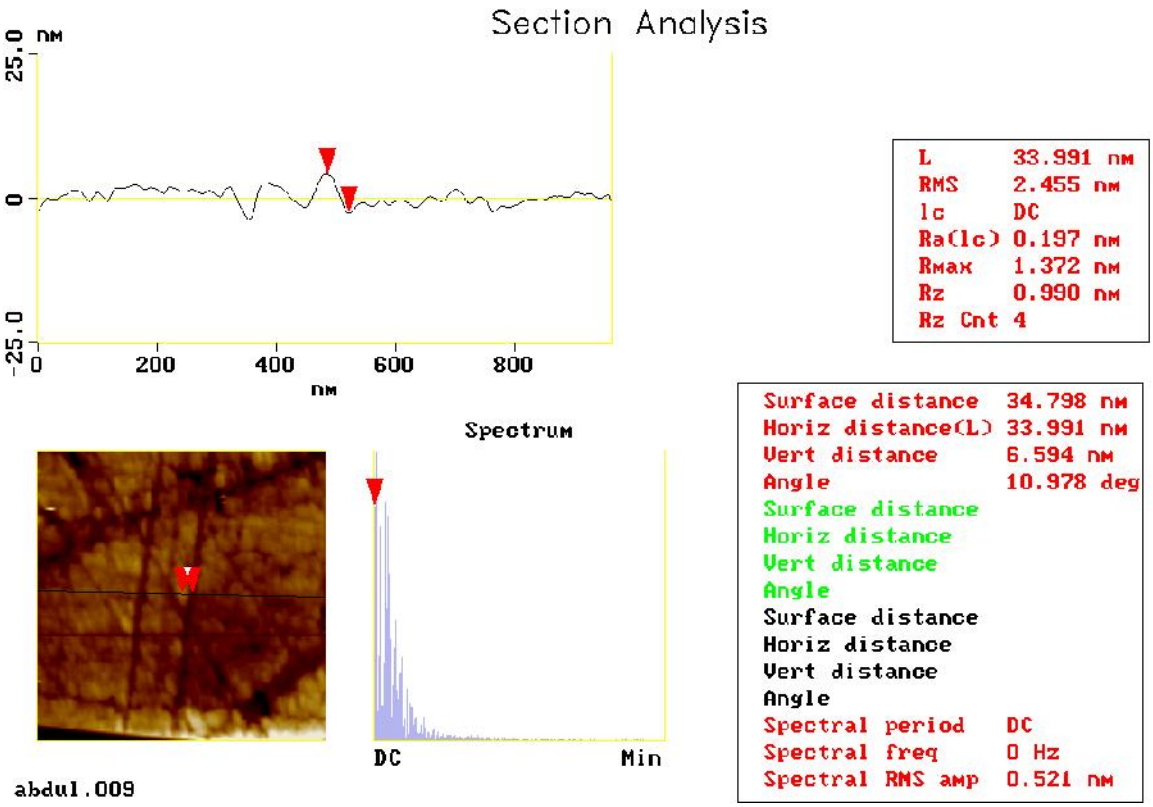

Time = 5 min.

http://dx.doi.org/10.14755/DIS.1999.001

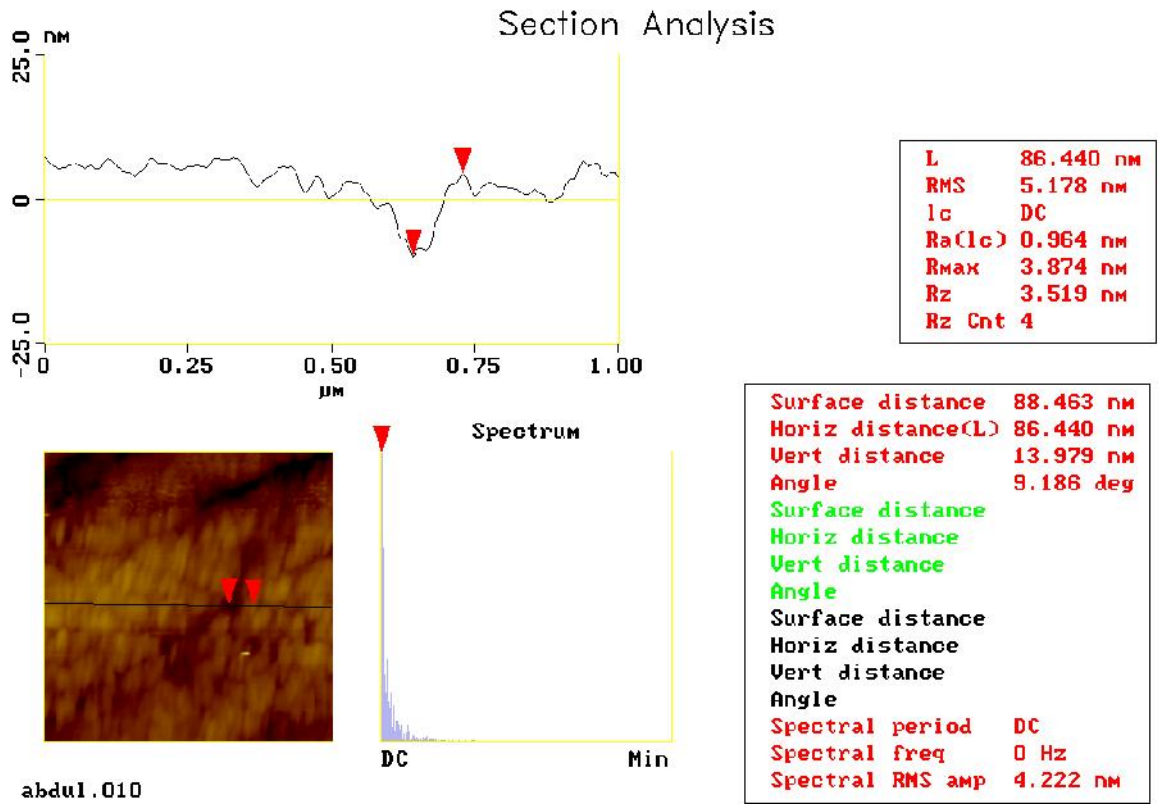

Time = 15 min.

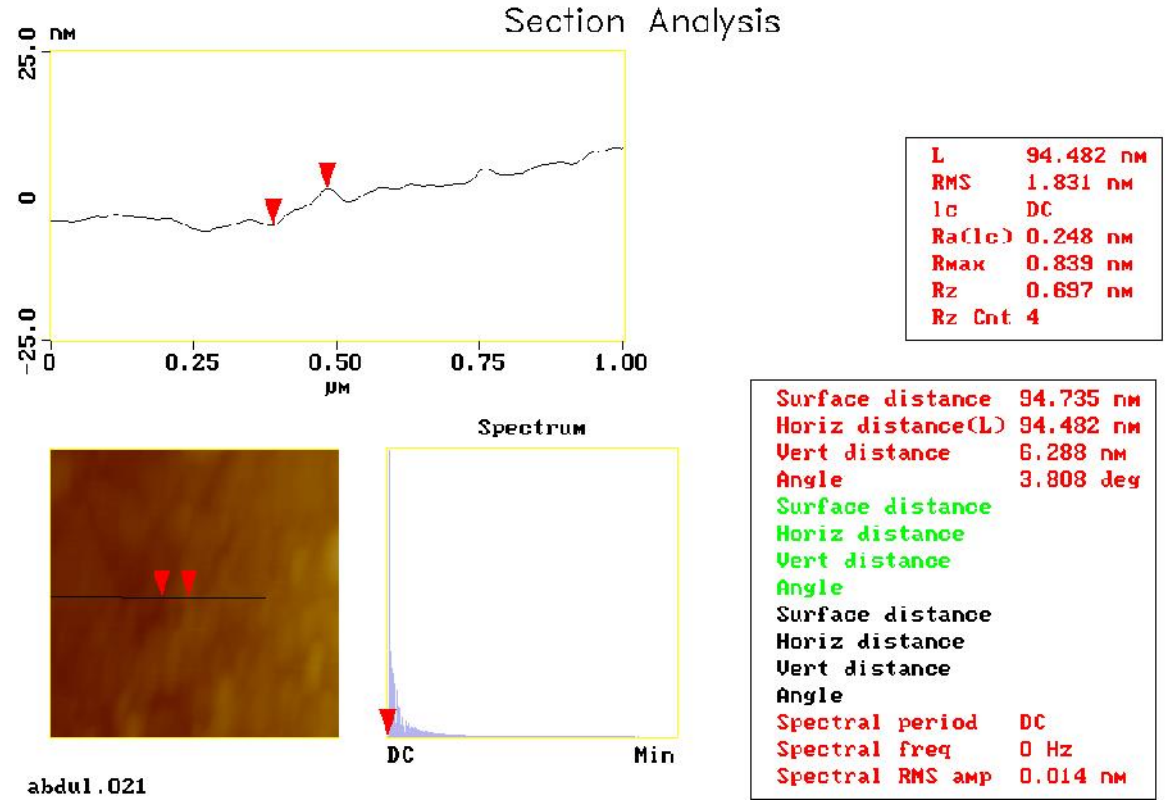

Time = 30 min.

http://dx.doi.org/10.14755/DIS.1999.001

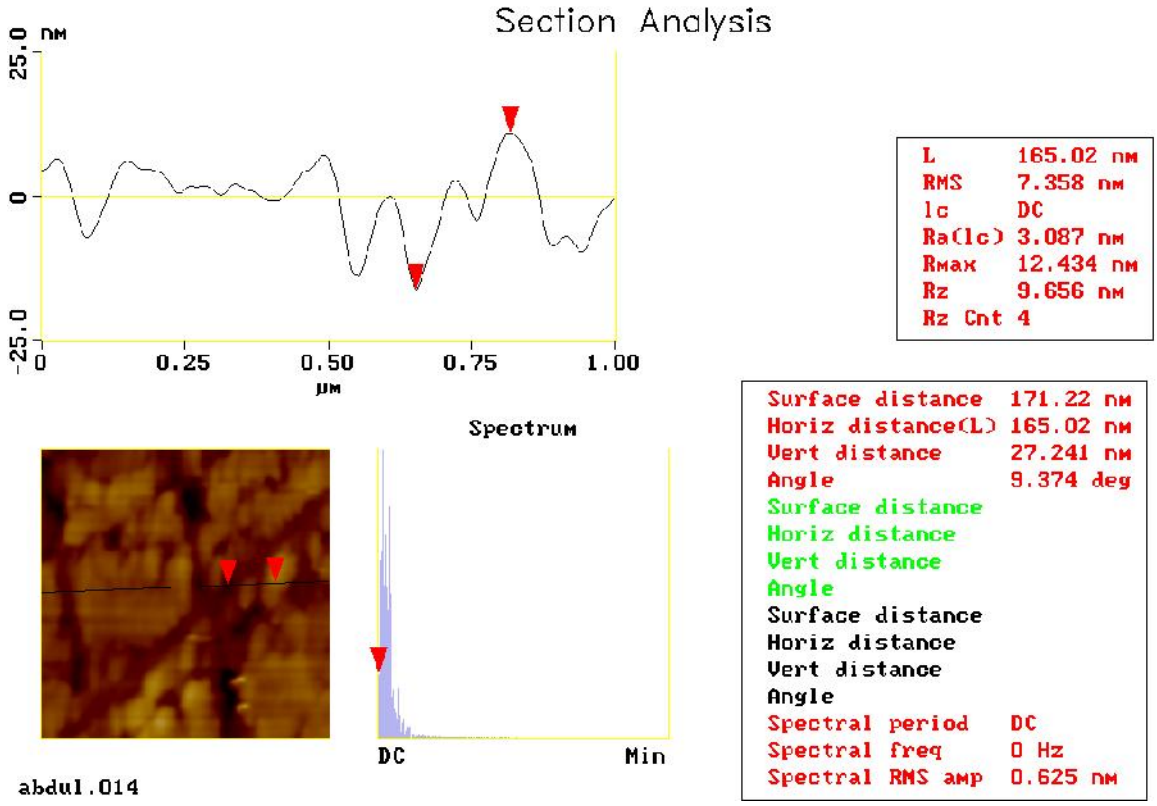

Time = 45 min.

Section analysis of AFM images of copper in 0.1 Na_2SO_4

http://dx.doi.org/10.14755/DIS.1999.001

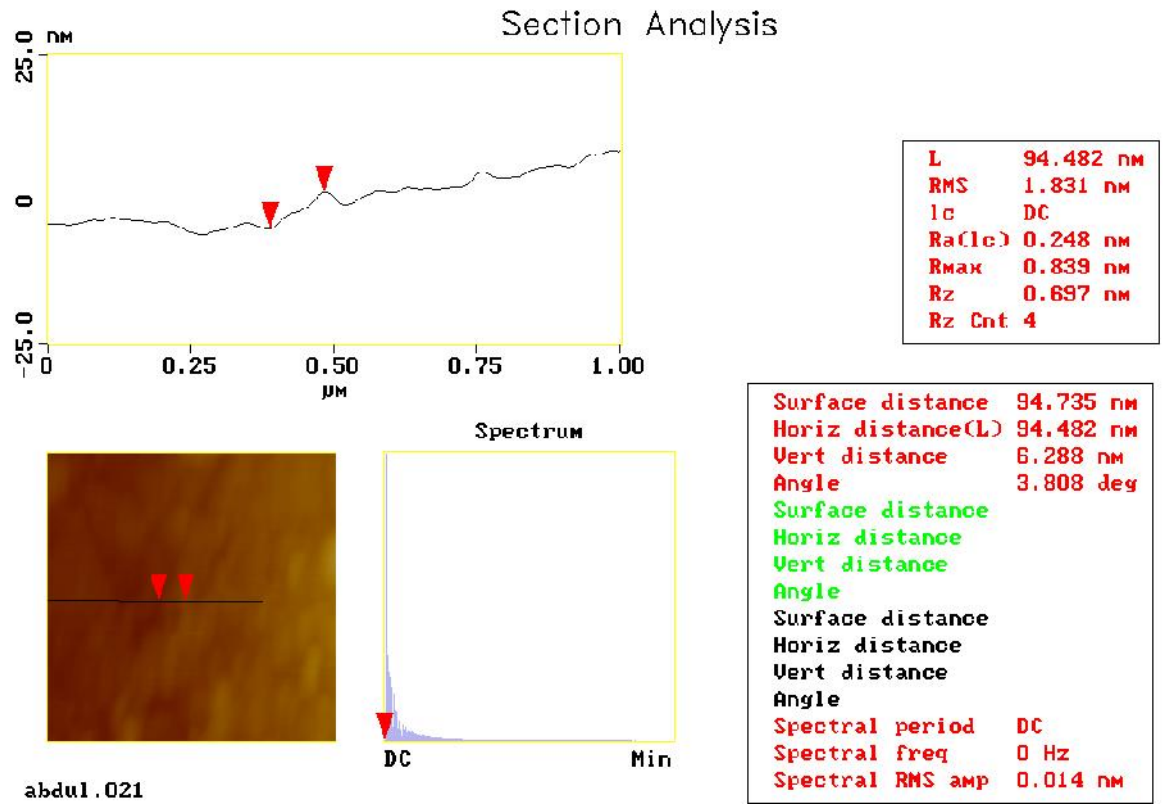

Time = 0 min.

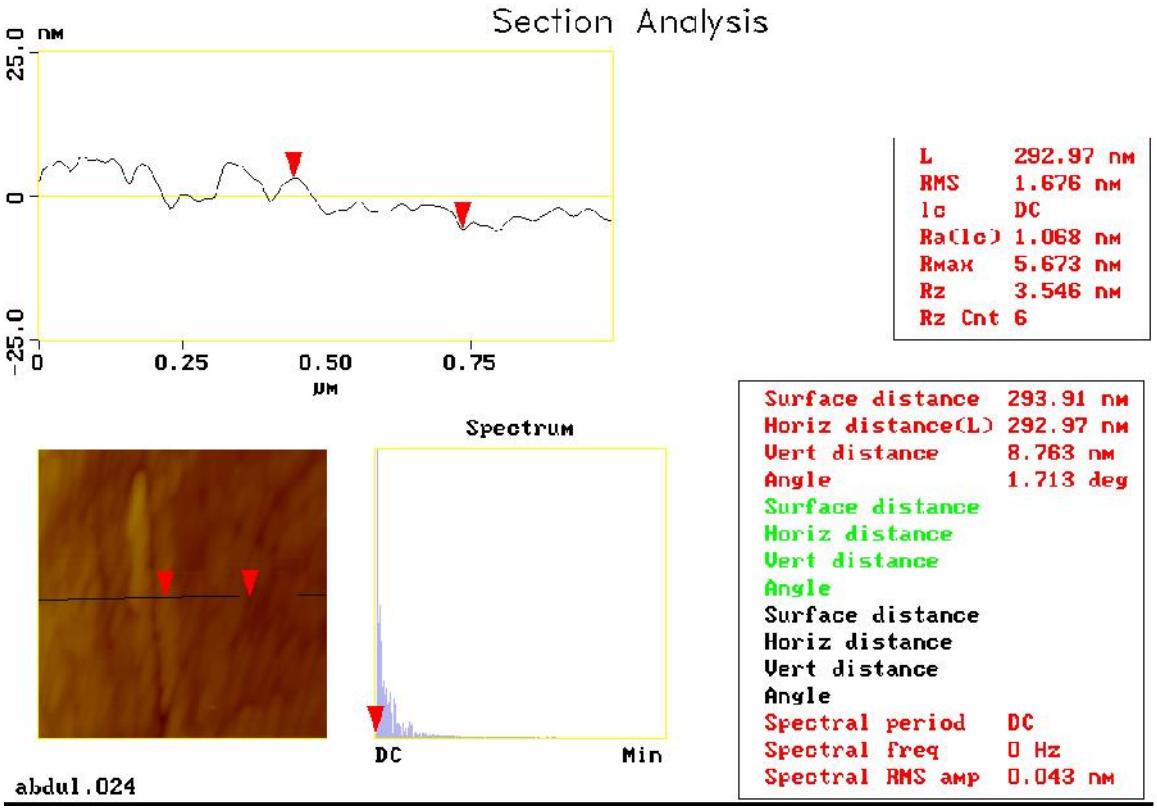

Time = 3 min.

http://dx.doi.org/10.14755/DIS.1999.001

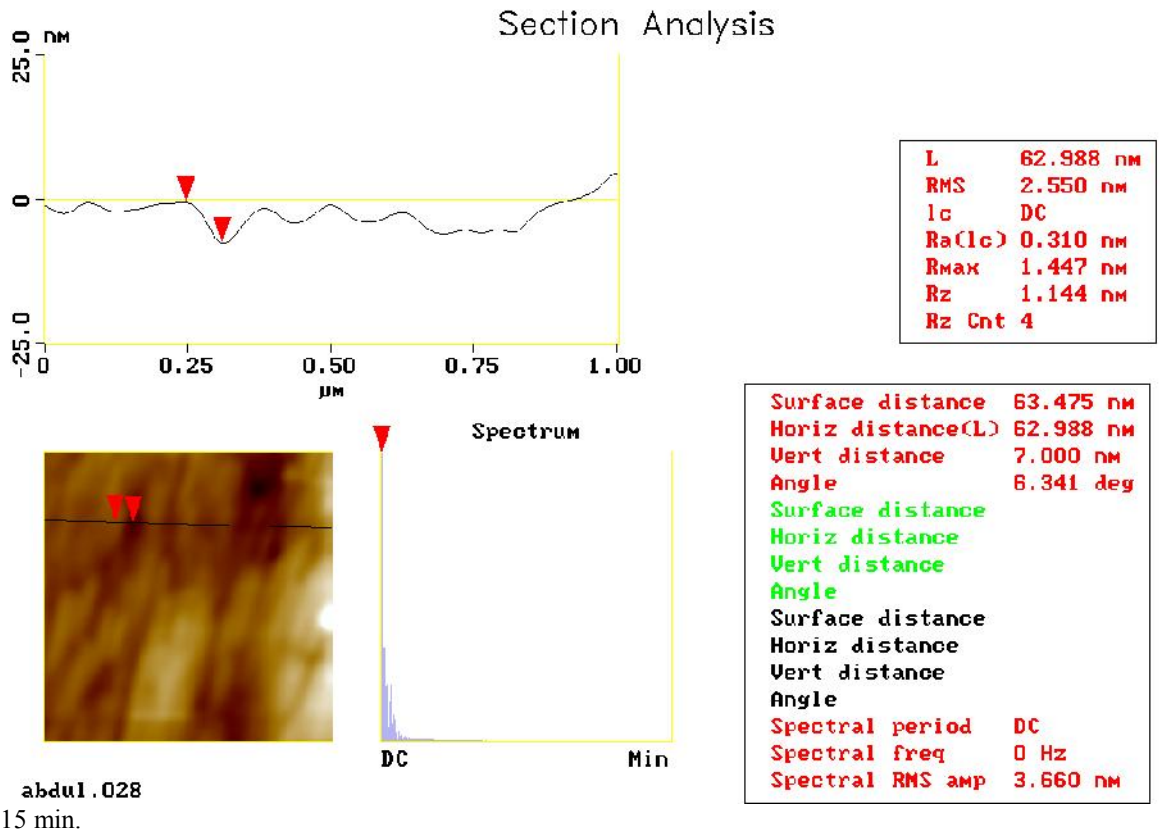

Time = 15 min.

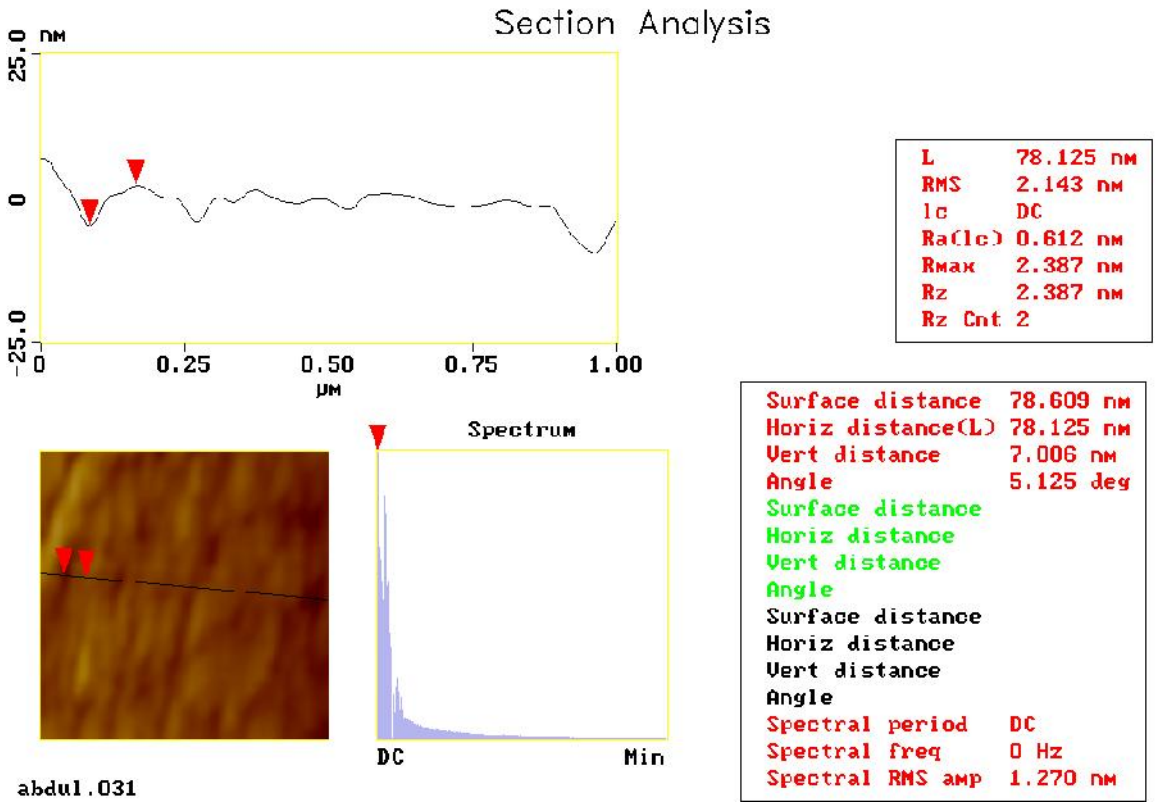

Time = 30 min.

http://dx.doi.org/10.14755/DIS.1999.001

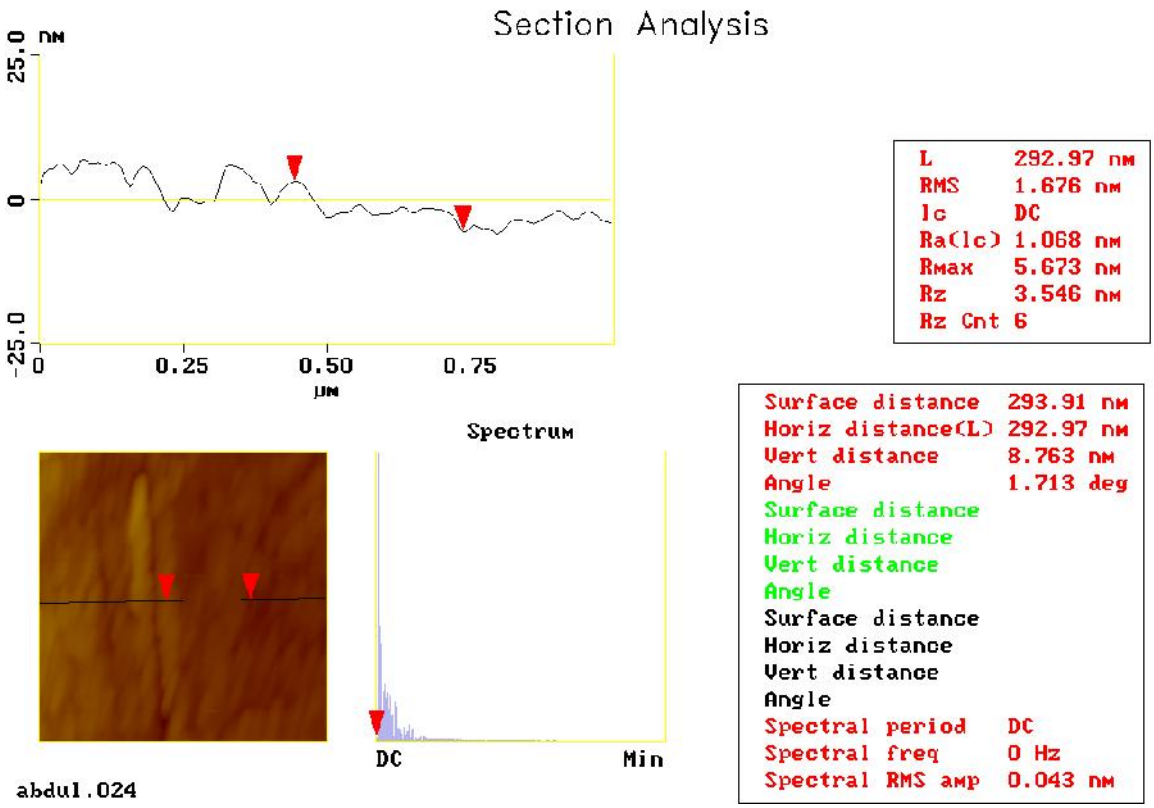

Time = 45 min.

Appendix B ***Section analysis of AFM images of copper in 0.1 Na_2SO_4 + DBSO***

http://dx.doi.org/10.14755/DIS.1999.001

Appendix C. Section analysis of AFM images of copper in 0.5 M NaCl

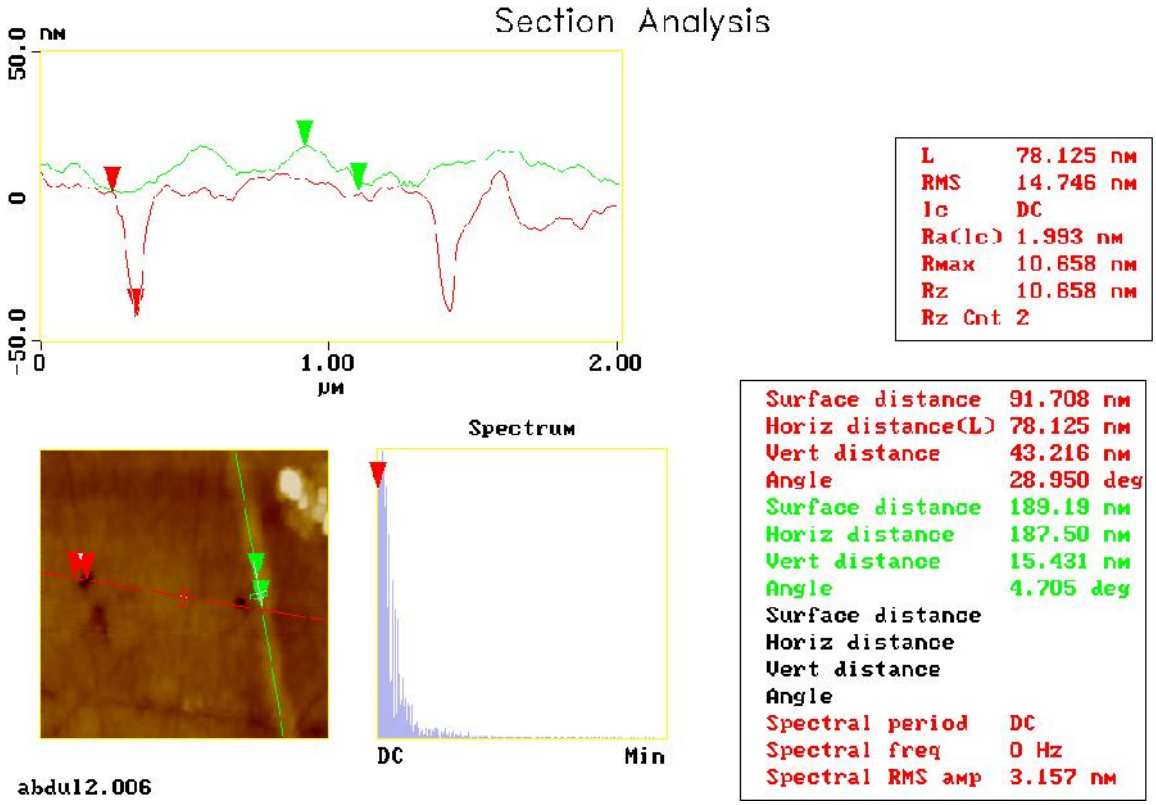

Time = 2 min.

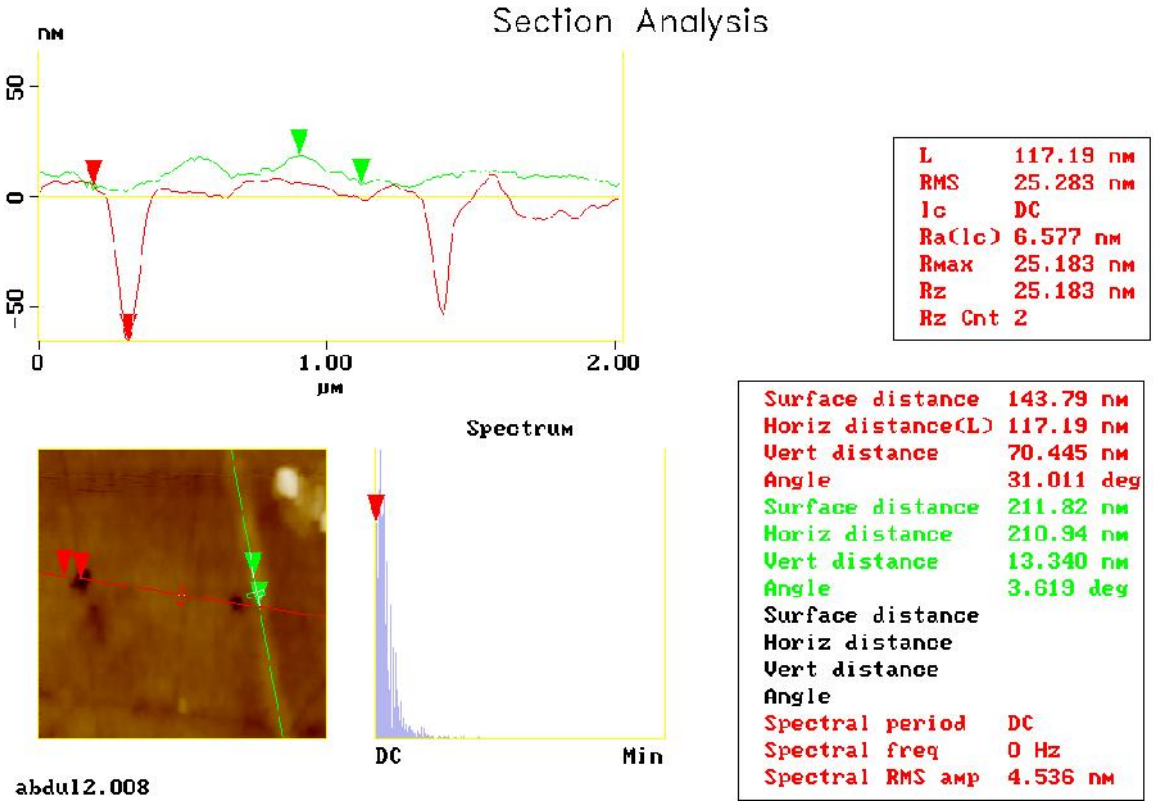

Time = 7 min.

http://dx.doi.org/10.14755/DIS.1999.001

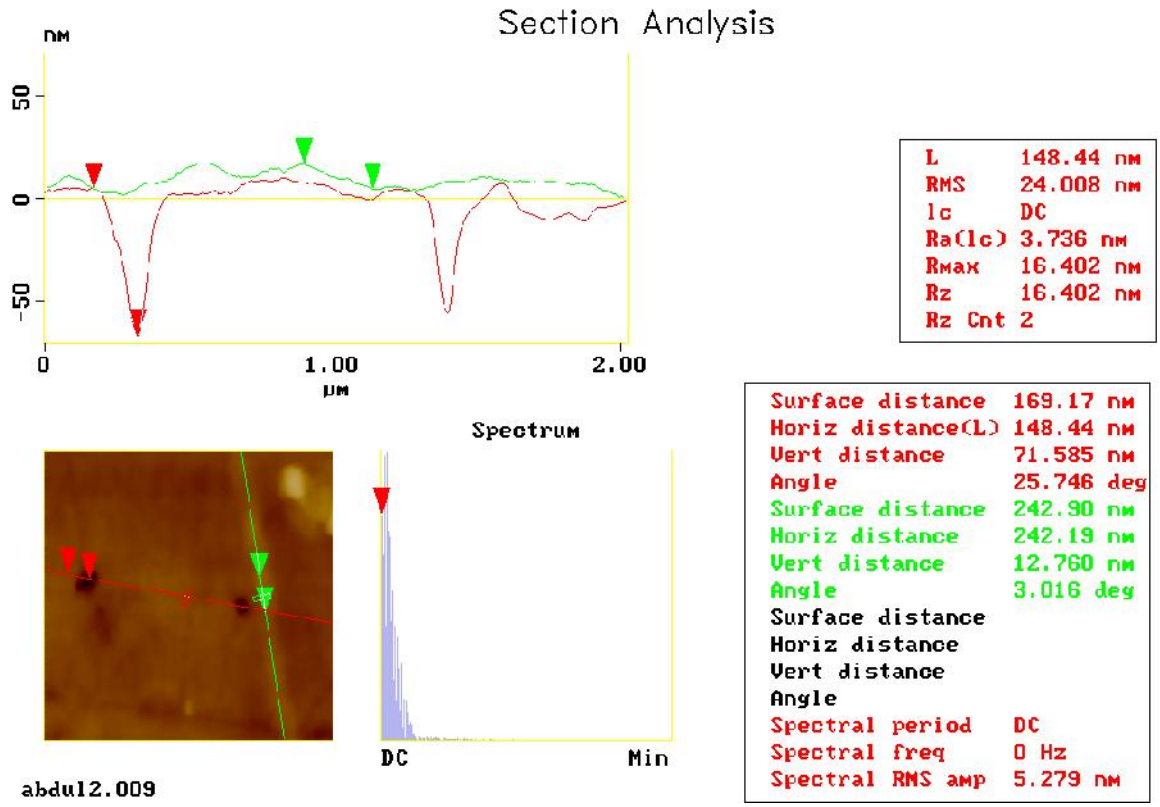

Time = 10 min.

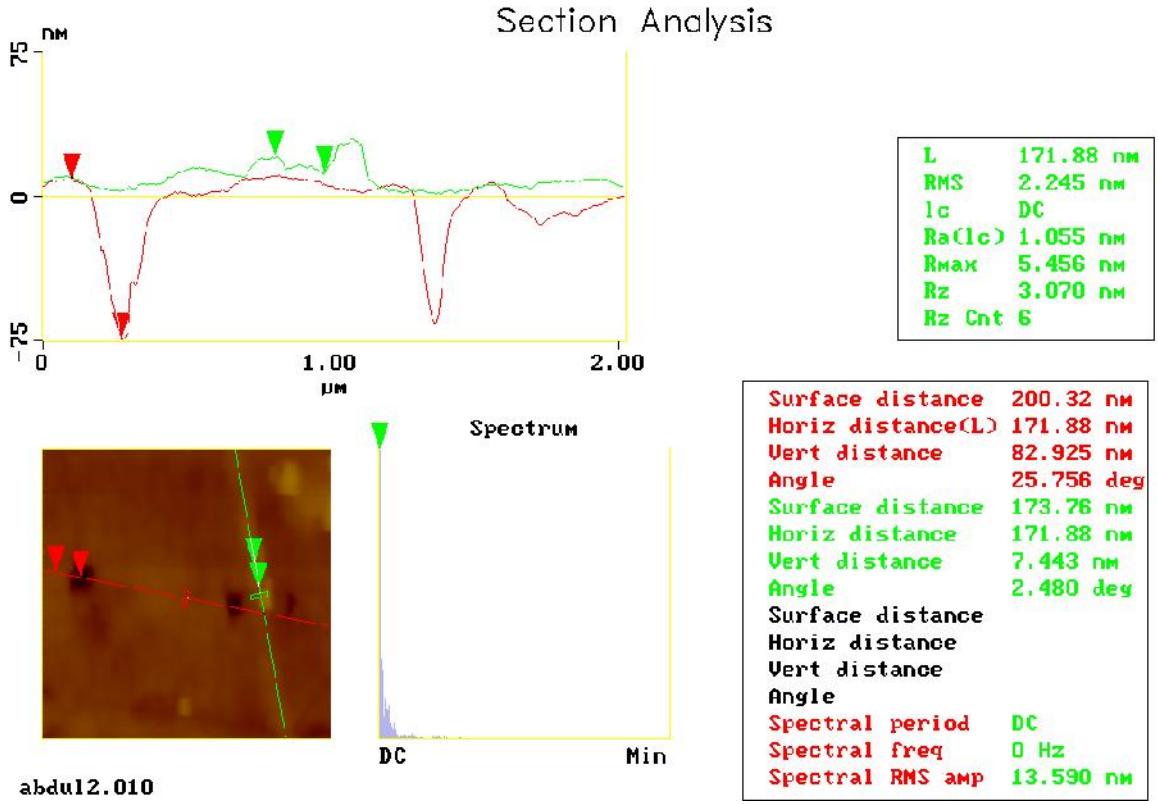

Time 15 min.

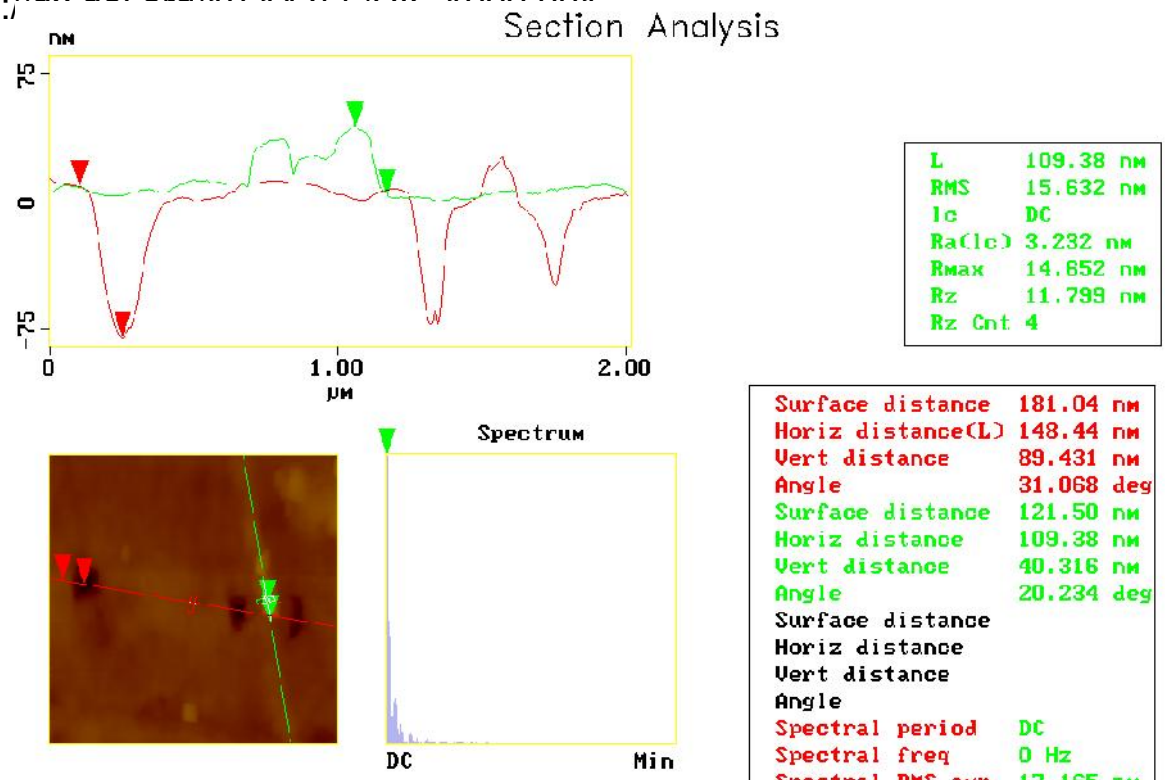

L	109.38 nm
RMS	15.632 nm
lc	DC
Ra(lc)	3.232 nm
Rmax	14.852 nm
Rz	11.799 nm
Rz Cnt	4

Surface distance	181.04 nm
Horiz distance(L)	148.44 nm
Vert distance	89.431 nm
Angle	31.068 deg
Surface distance	121.50 nm
Horiz distance	109.38 nm
Vert distance	40.316 nm
Angle	20.234 deg
Surface distance	
Horiz distance	
Vert distance	
Angle	
Spectral period	DC
Spectral freq	0 Hz
Spectral RMS amp	17.165 nm

Time = 20 min.

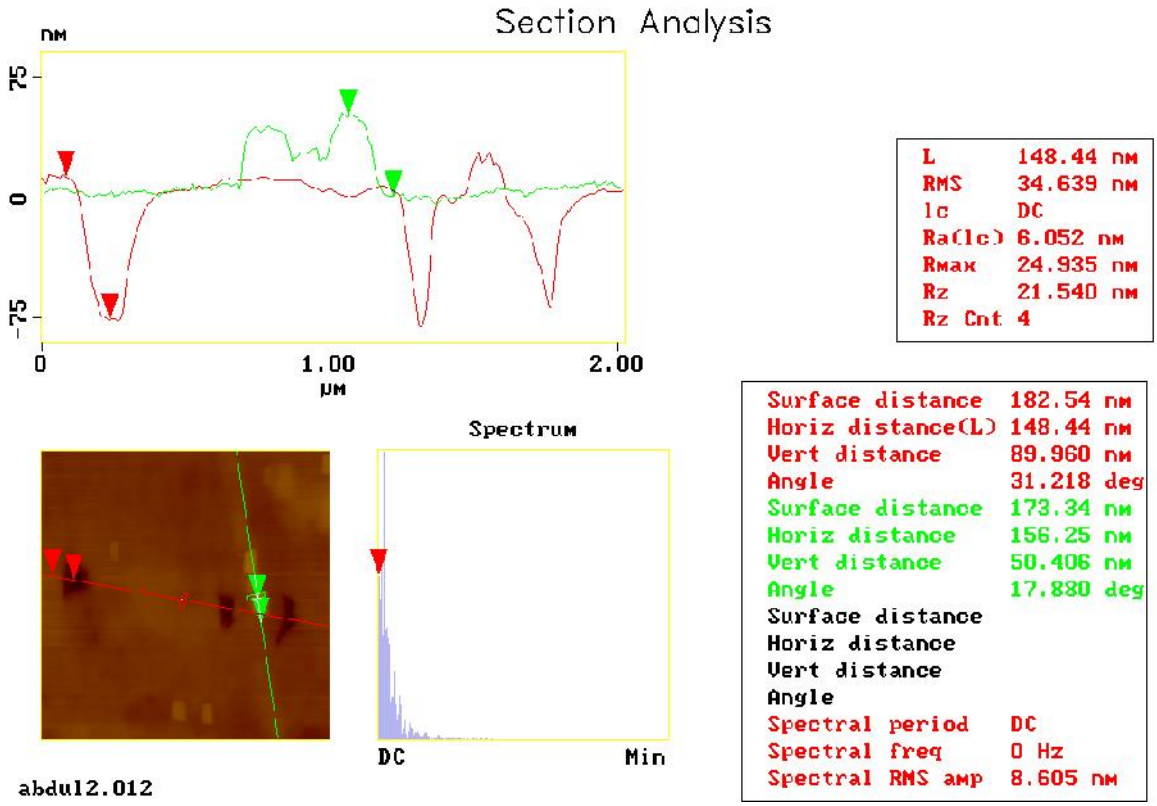

L	148.44 nm
RMS	34.639 nm
lc	DC
Ra(lc)	6.052 nm
Rmax	24.935 nm
Rz	21.540 nm
Rz Cnt	4

Surface distance	182.54 nm
Horiz distance(L)	148.44 nm
Vert distance	89.960 nm
Angle	31.218 deg
Surface distance	173.34 nm
Horiz distance	156.25 nm
Vert distance	50.406 nm
Angle	17.880 deg
Surface distance	
Horiz distance	
Vert distance	
Angle	
Spectral period	DC
Spectral freq	0 Hz
Spectral RMS amp	8.605 nm

Time = 30 min.

http://dx.doi.org/10.14755/DIS.1999.001

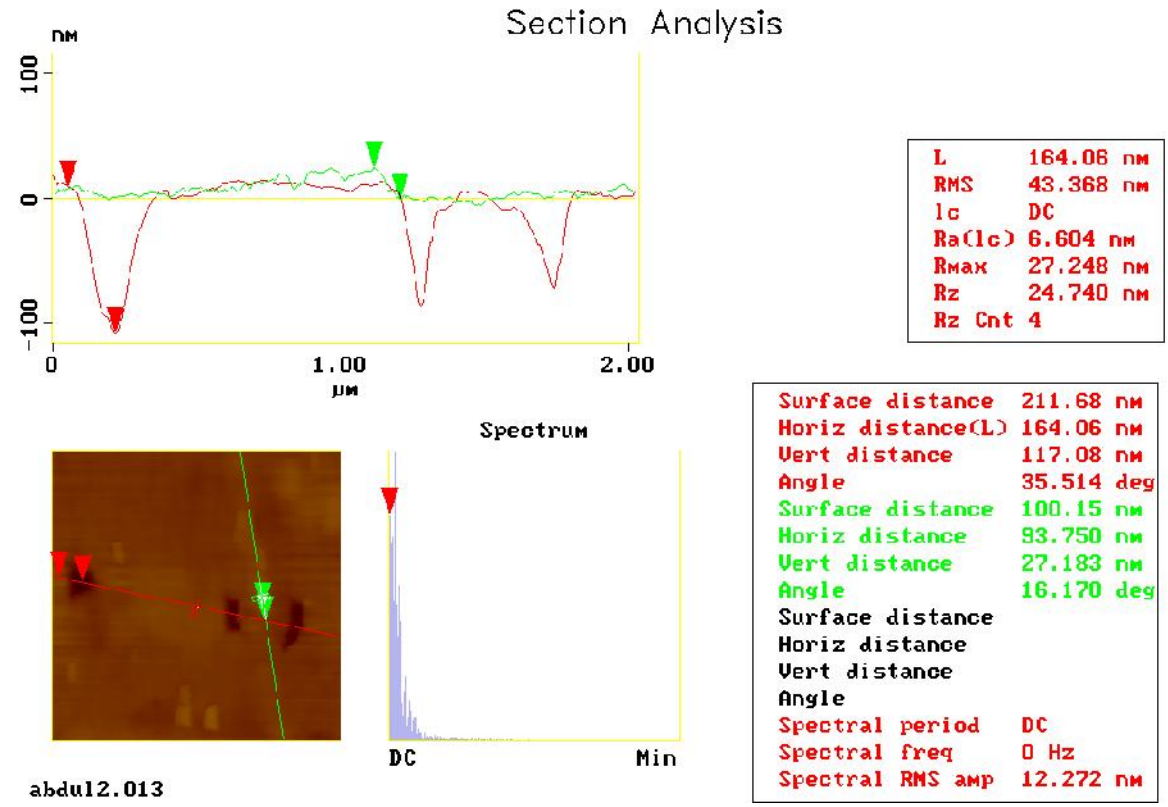

Time = 45 min.

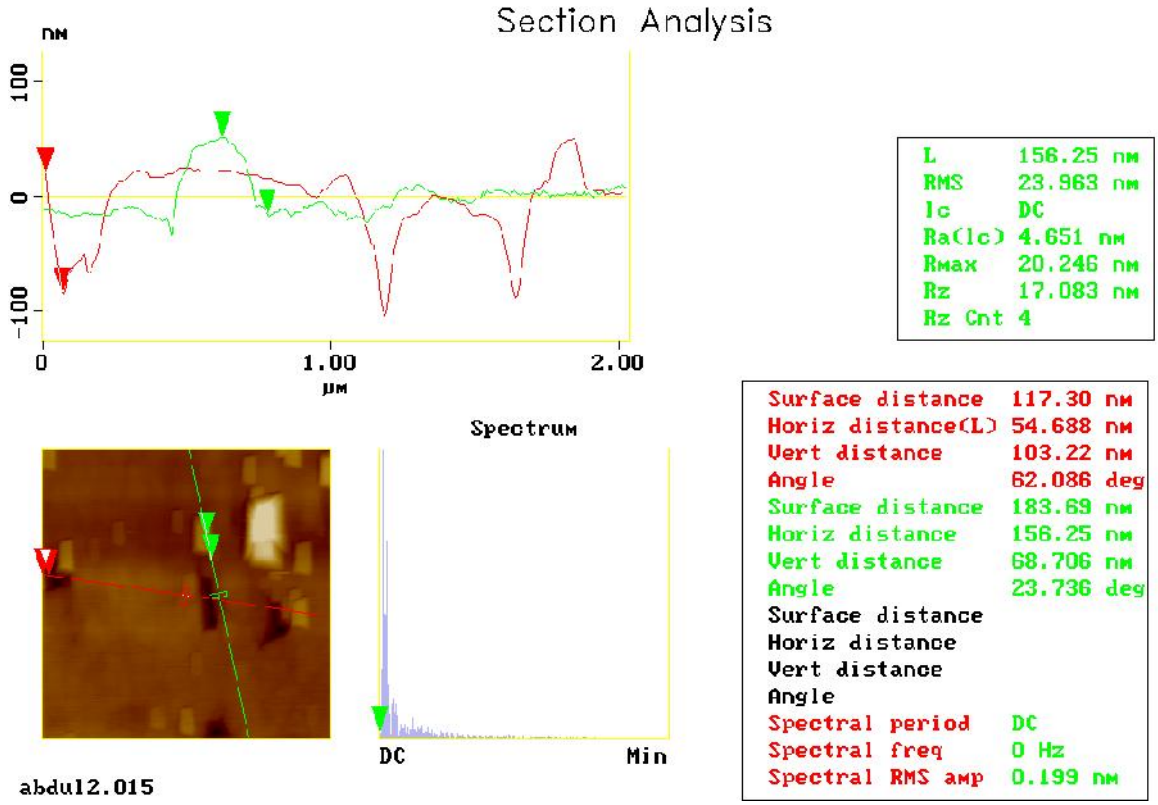

Time = 60 min.

http://dx.doi.org/10.14755/DIS.1999.001

Appendix C. Section analysis of AFM images of copper in 0.5 M NaCl + p-Cl-BHA

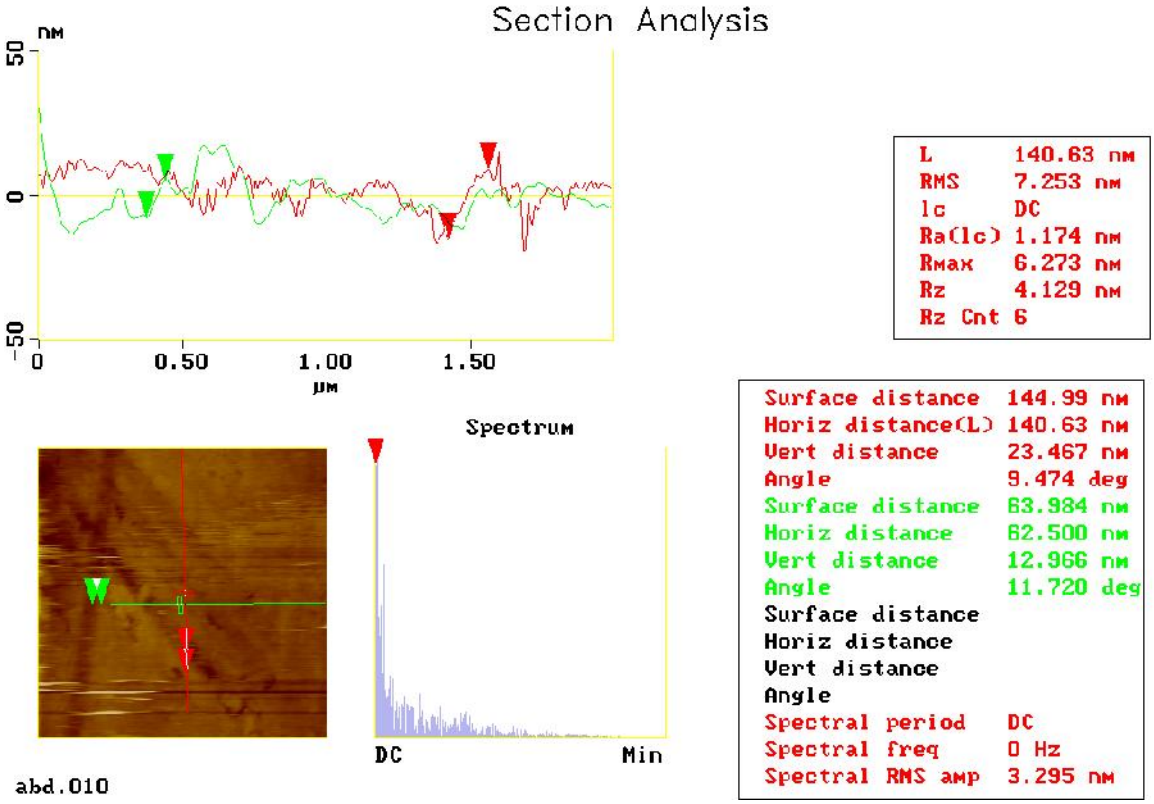

Time = 2 min

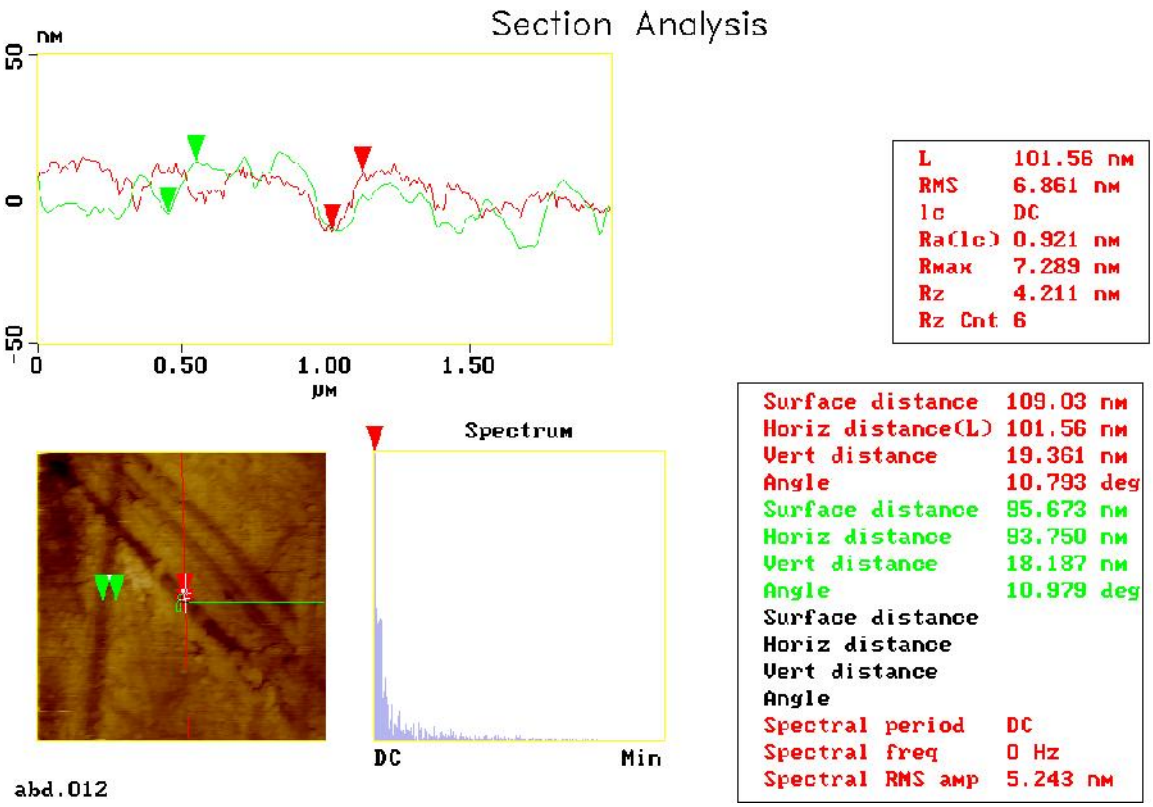

Time = 7 min.

http://dx.doi.org/10.14755/DIS.1999.001

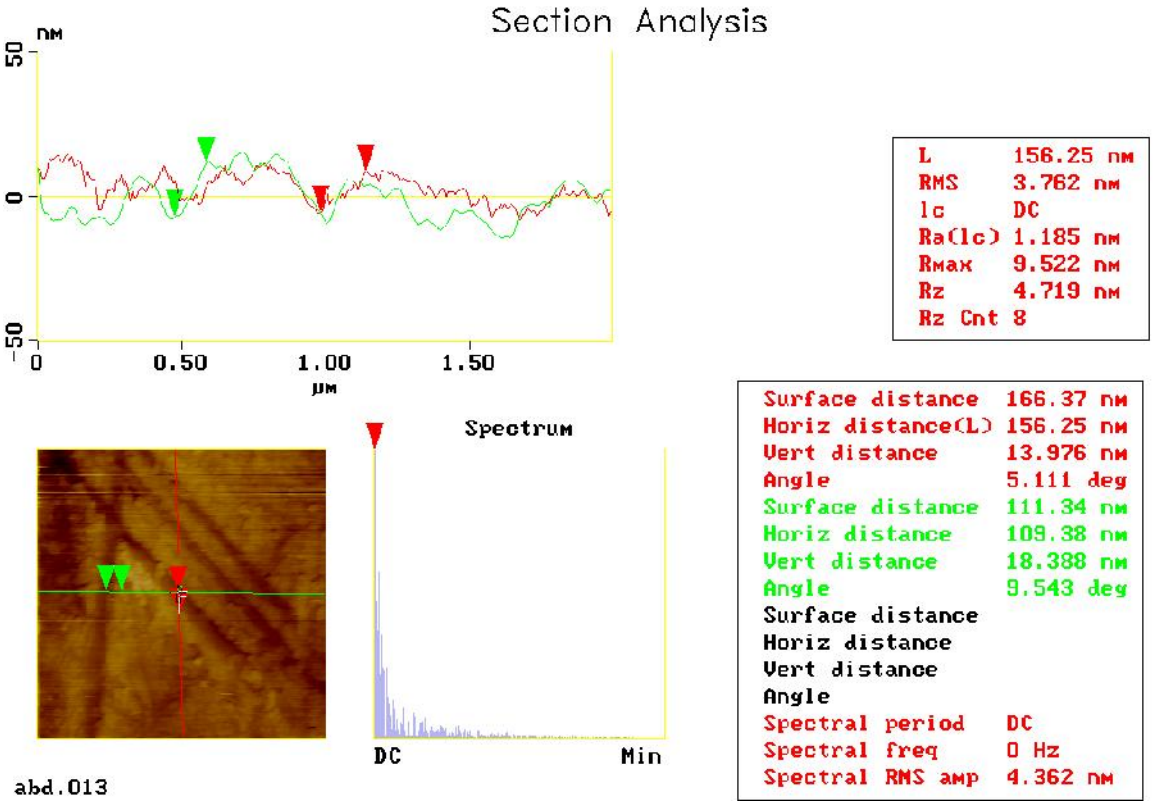

Time = 10 min.

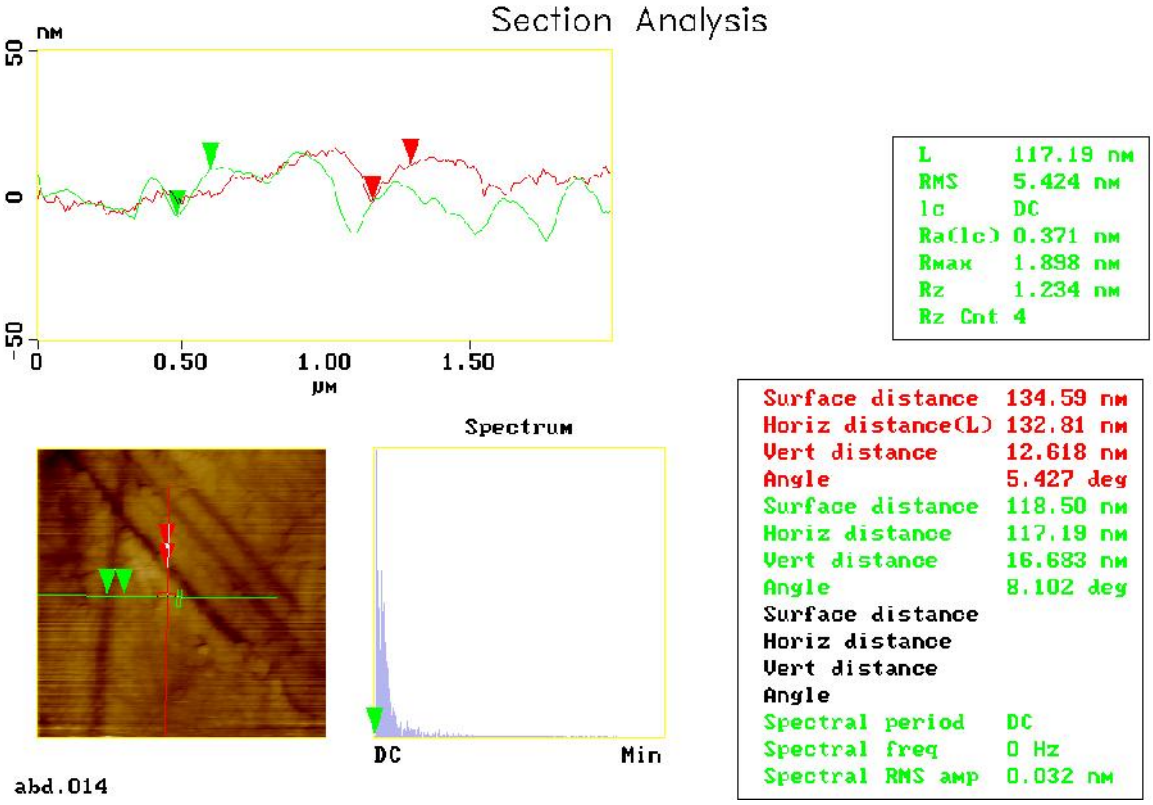

Time = 15 min.

http://dx.doi.org/10.14755/DIS.1999.001

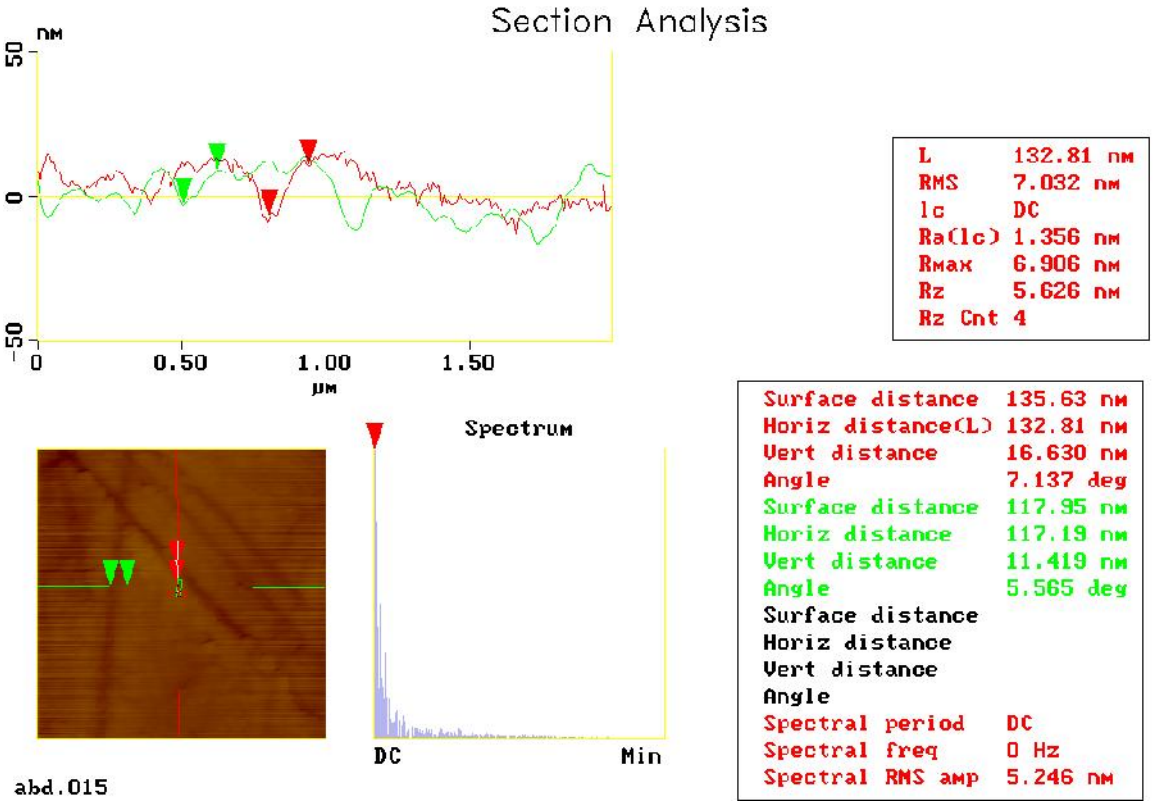

Time = 20 min.

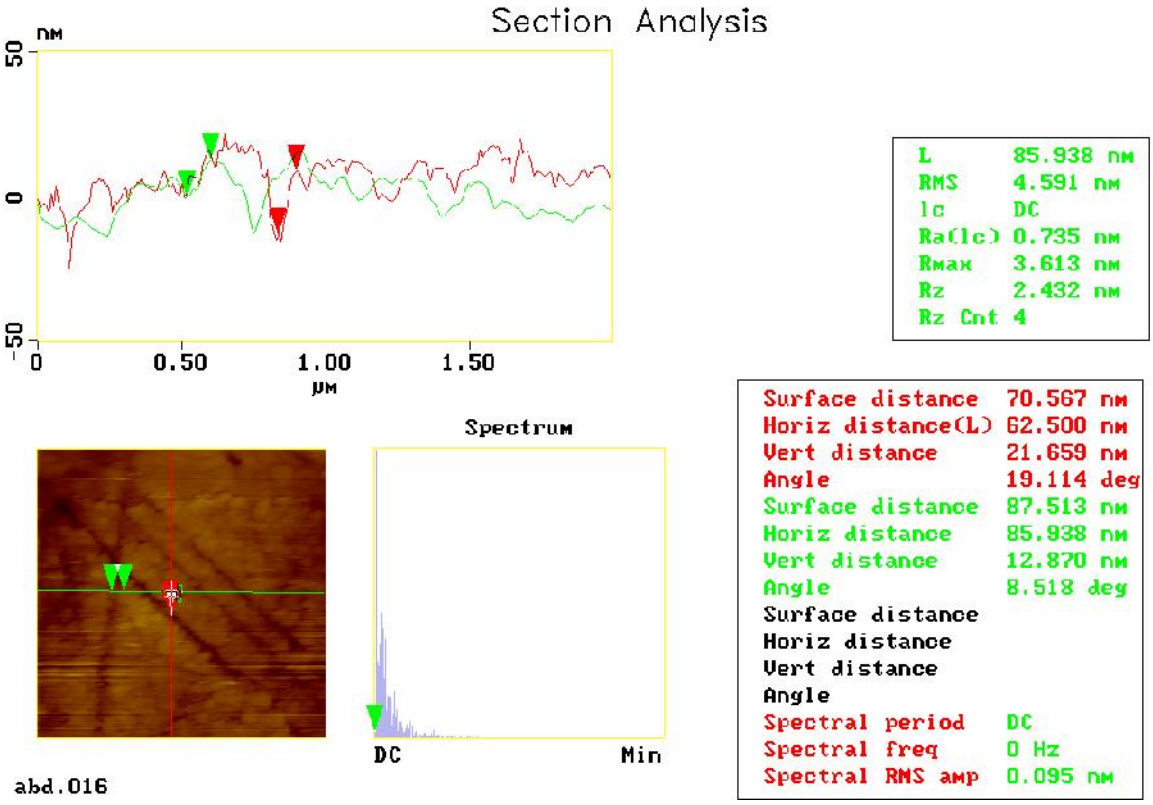

Time = 30 min.

http://dx.doi.org/10.14755/DIS.1999.001

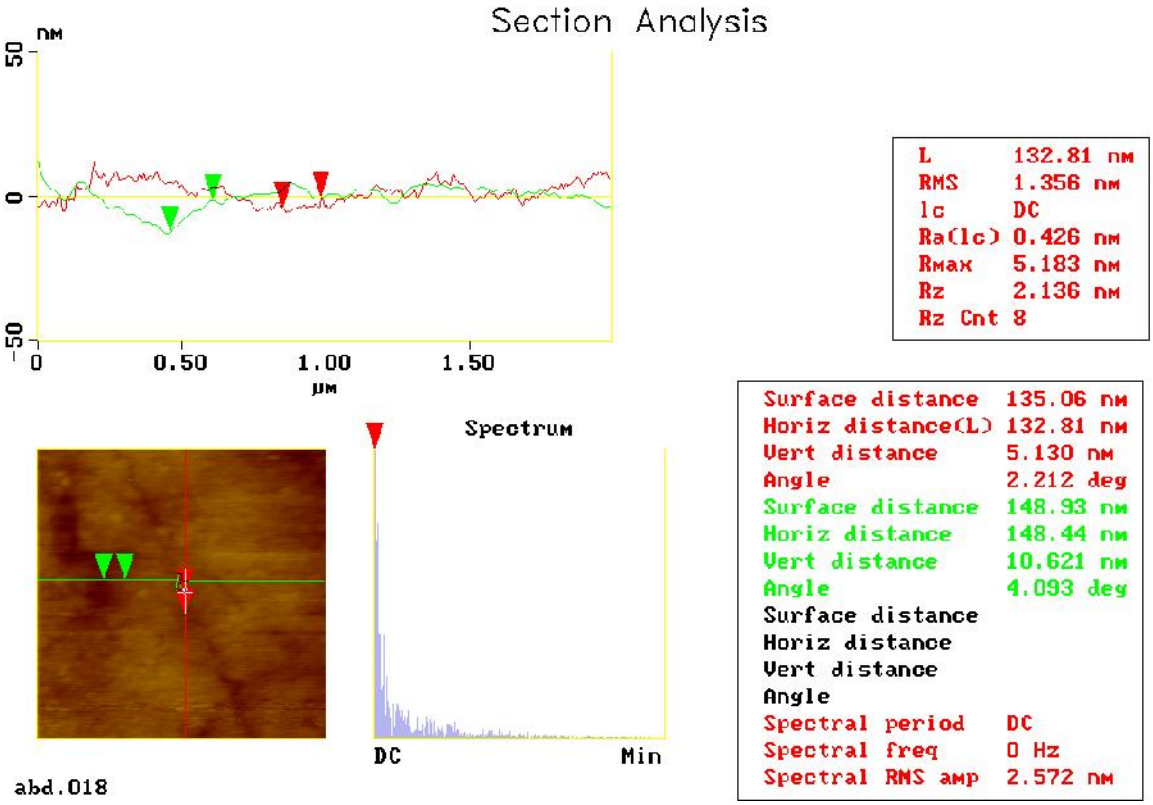

Time = 45 min.

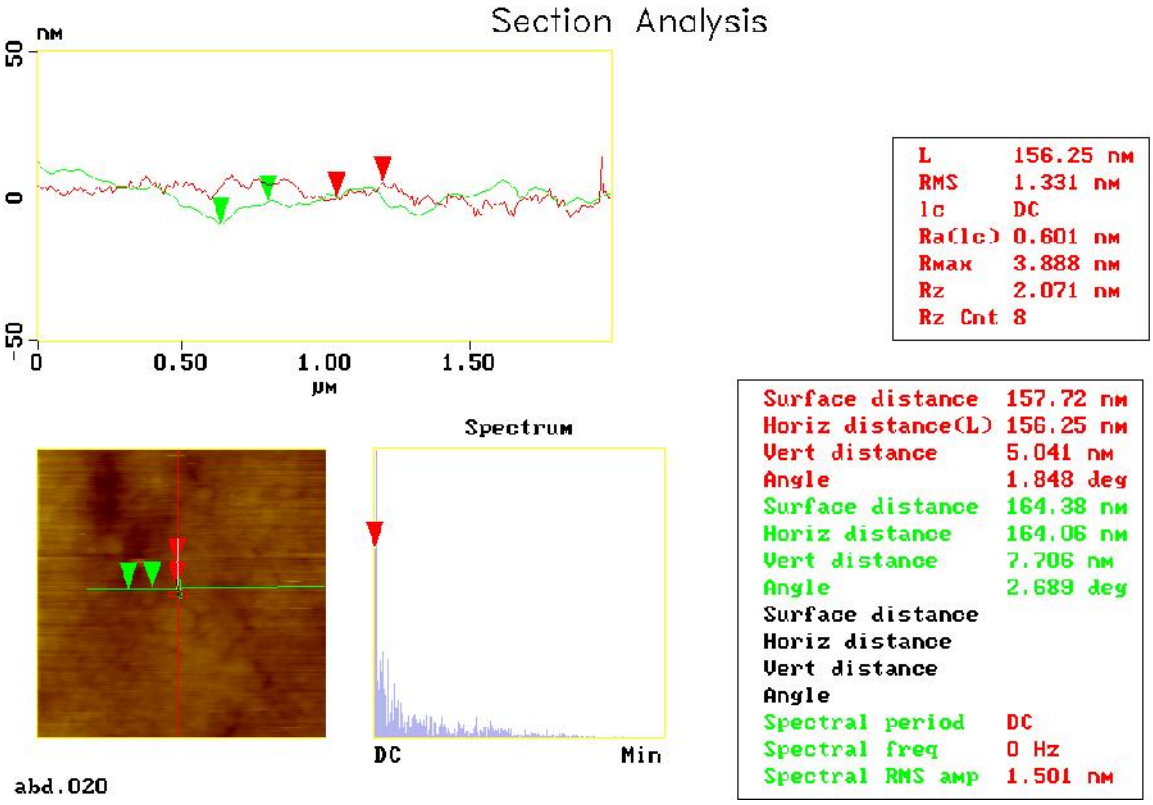

Time = 60 min.

Section analysis of AFM images of copper in 0.5M NaCl and p-Cl-BHA

http://dx.doi.org/10.14755/DIS.1999.001

Puplications.

I. Contributions in scientific journals

1. **A. Shaban**, E. Kálmán and I. Biczó
   Corros. Sci. **35**. 1463 (1993)
2. **A. Shaban**, J. Telegdi, and E. Kálmán
   "Progress in the Understanding and prevention of corrosion", Ed. J. M. Costa and A. D. Mercer, **2**, 916 (1993)
3. E. Kálmán, B. Várhegyi, I. Bakó, I. Felhösi, F. H. Kármán, **A. Shaban**
   "*Corrosion Inhibition by 1-Hydroxyl-ethane-1,1-diphosphonic Acid: An Electrochemical Impedance Spectroscopy Study"*
   J. Electrochem. Soc., **141**. 3357 (1994)
4. **A. Shaban**, J. Telegdi, S. Alexandre and E. Kálmán
   CORROSIONE, Pitture e Vernici Europe, **12**, 23 (1995)
5. Kálmán E., Várhegyi B., Felhösi I., Bakó I., Pálinkás G., Kármán F. és **A. Shaban**
   Magy. Kém. Foly., **102**, 211 (1996)
6. **A. Shaban**, E. Kálmán, and J. Telegdi
   "*An Investigation of Copper Corrosion Inhibition in Chloride Solution by Benzohydroxamic acids*", Electrochim. Acta., **43,** 159 (1998)
7. I. Lukovits, I. Bakó, **A. Shaban** and E. Kálmán
   "Polynomial Model of the Inhibition Mechanism of Thiourea Derivatives"
   Electrochim. Acta., **43**, 131 (1998)
8. **Abdul Shaban**, Kálmán Erika és Telegdi Judit
   "A rézkorrózió inhibiciója benzhidroxámsav-származékokkal vizes nátrium-klorid-oldatban", Magy. Kém. Foly., **103**, 572 (1997)
9. **A. Shaban,** J. Telegdi, E. Kálmán, G. Pálinkás, and Gy. Dóra
   "*Corrosion and Inhibition of Copper in Different Electrolyte Solutions*",
   J. Appl. Phys. A. **66.** xx (1998)
10. **A. Shaban** and E. Kálmán
    "Inhibitor of Copper Corrosion in Acidic Solutions by Various Aromatic Sulfoxides", Corrosion, submitted for publications.
11. **A. Shaban**, E. Kálmán and J. Telegdi

http://dx.doi.org/10.14755/DIS.1999.001

"*An Investigation of para-chloro-benyohydroxamic Acid as Copper Corrosion Inhibitor in 0.5 M NaCl Solution*", in preparation (1997)

II. Patents

1. "Water treating agents and additives derived from compounds containing free amino-group**", Patent No. HU 69027, 28-08-1995**

III. Contributions in local and international conferences

1. **A. Shaban**, E. Kálmán and I. Biczó,
   Proceedings, **ECASIA'91**, **4th Euro. Conf. App. Surface Analysis** Budapest, Hungary, (1991)
2. E. Kálmán, F. Kármán, I. Kónya, Gy. Litkei, **A. Shaban**, J. Telegdi, L. Várallyai
   Proceedings, **EUROCORR'91**, Budapest, Hungary, (1991)
3. **A. Shaban**, B. Várhegyi, E. Kálmán and I. Biczó
   Proceedings, **Advances in corrosion and protection**, UMIST, UK, (1992)
4. **A. Shaban**, J. Telegdi, E. Kálmán and G. Singh
   Proceeding, **10th European Corr. Congress**, Barcelona, Spain, (1993)
5. **A. Shaban**, J. Telegdi, S. Alexandre and E. Kálmán
   Proceedings, **UK CORROSION'94** and **EUROCORR'94,** Bournemouth, UK, October (1994)
6. **A. Shaban** and E. Kálmán
   Proceedings, **46th ISE** Meeting, Xiamen, China, (1995)
7. **A. Shaban**, E. Kálmán and J. Bácskai
   Proceedings, **8th Euro. Symp. Corr. Inhib. (8 SEIC)** Ann. Univ. Ferrara, N. S. Sez. v. Suppl. No. 10. (1995)
8. **A. Shaban**, J. Telegdi and E. Kálmán
   Proceedings, **47th ISE** Meeting, Balatonfüred, Hungary, (1996)
9. **A Shaban**, J. Telegdi and E. Kálmán
   Proceedings, **EUROCORR'96**, Nice, France, August (1996)
10. **A. Shaban,**
    Seminar, **HUNKOR** Meeting, ***Mátrafüred***, Hungary, March, (1997)
11. **A. Shaban**, J. Telegdi, E. Kálmán and Gy. Dóra
    Proceedings, **STM'97**, **9th Conf. STM, Spect. And Rel. Tech.**, Hamburg Germany, July (1997)
12. J. Telegdi, **A. Shaban**, Zs. Keresztes and E. Kálmán,
    Proceedings, **EMCR-VI**, Trento, Italy, August (1997)
13. **A. Shaban**, E. Kálmán and J. Telegdi, Presentation, at the **ISE'97 and Electrochemical Society**, Joint Meeting, Paris, France, September (1997).

http://dx.doi.org/10.14755/DIS.1999.001

The only way to find out how to do a PhD is to do one.

Therefore all advice is useless....

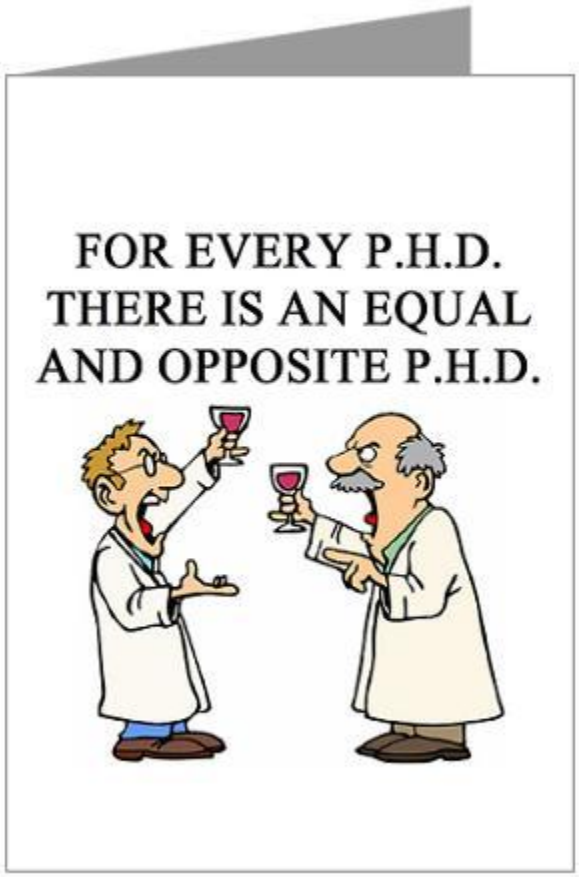

http://dx.doi.org/10.14755/DIS.1999.001

Candidate Degree

Small Thesis

Title:

PREVENTION OF COPPER CORROSION USING AROMATIC SULFOXIDES AND BENZOHYDROXAMIC ACIDS

by

ABDUL MUTTALIB SHABAN

B. Sc., M. Sc. Chemical Engineering

Supervised by

Prof. Dr. Erika Kálmán

Central Research Institute for Chemistry
of the Hungarian Academy of Sciences
Budapest, Hungary

1997

I-Foregoing and Aims.

Inorganic inhibitors such as chromates are effective but they are becoming environmentally more and more unacceptable because of the health hazards associated with its use. Due to general awareness of the environmental damage, and stricter regulations, these inhibitors are increasingly restricted. New inhibitor compounds for the 21st century require further research in order to be environment-friendly. Accordingly, attention has been diverted to the study of new inhibitors compounds which could be classified as green inhibitors. Despite considerable advances in the study of the mechanisms of corrosion and inhibition, there are many unsolved questions. The difficulties arise because of the complexity of the factors controlling corrosion and its inhibition. The major factors are as follows:

- the surface conditions of the metal,
- composition of the medium near to the metal surface, and
- changes of the environment.

Copper and its alloys behave relatively noble in neutral aqueous solutions, however, it is susceptible to corrosion by acids and strong alkaline solutions, especially in the presence of oxygen or oxidants. One major application of copper is in the acid cleaning installations. In the pH range between two and five, the dissolution of copper is very rapid and the formation of a stable surface-oxide layer, which can passivate metal surfaces, is impossible. Copper can only passivate by forming an oxide surface layer in weak acid or alkaline solutions. Accordingly, a proper copper corrosion protection method must been taken into consideration.

http://dx.doi.org/10.14755/DIS.1999.001

One of the protection methods applied is the application of corrosion inhibitors.On the other hand, copper and its alloys are applied extensively in marine environments due to their high corrosion resistance in harsh seawaters. In addition, copper dissolution in chloride solutions is very important in the electropolishing and electro-machining industries. Due to those reasons, attention has been focused on the behavior of copper in chloride solutions. Even if copper corrosion in near neutral aqueous solutions seems to be low, the dissolved copper ions can induce corrosion of other less noble materials present in the system. Accordingly, an inhibitor must be added to the environment in order to modify or hinder the reactions involved in the process. Several chemical compounds could be applied as corrosion inhibitors for copper corrosion but only few formulations have been thoroughly investigated. Generally, it can be stated that inhibitors molecules containing atoms as nitrogen and sulfur are the most effective.

Among the tested inhibitor molecules, a new group compounds, hydroxamic acid derivatives and some aromatic sulfoxide molecules have been found as most effective.

Considering the above mentioned review, the present investigation focuses on the following aims:

1. to find a sensitive and rapid tool for investigation of the corrosion inhibition performance of copper corrosion inhibitors, in both the acidic and neutral media
2. the study of the inhibition of copper corrosion by different chemical compounds in acidic or neutral media in order to find an environmentally friendly inhibitor.
3. the study of inhibition mechanisms of copper corrosion inhibition and suggesting different models to illustrate the actions.

II. Experimental Methods

In the development of new inhibitors, it is always important, irrespective of the nature of the investigation, to estimate quantitatively the effect of the inhibitor on the corrosive process. A series of measurements of corrosion rates must be made even to answer the question, whether a given substance is, or is not, a corrosion inhibitor. The gravimetric method is that most often used to measure corrosion rate and inhibitor efficiency.

The applied experimental techniques should provide information to determine both the metal corrosion rate and monitor inhibitor adsorption on the copper electrode surface. The electrochemical quartz crystal microbalance (EQCM) was proved very useful tool for corrosion investigations. Film thickness variations due to adsorption of the inhibitor or the mass loss due to corrosion can be monitored in real time. This method delivers some advantages over the classical gravimetrical method due to its high sensitivity. EQCM could detect mass changes in the nanogram range, thus a mono-molecular layer can be detected. The behavior of the copper electrode in the presence of different inhibitors in neutral environment is investigated for the first time using a quartz microbalance.

Beside this technique, AC (electrochemical impedance spectroscopy) and DC (potentiostatic polarization) electrochemical techniques, and different surface techniques (atomic force microscopy (AFM) and scanning electron

http://dx.doi.org/10.14755/DIS.1999.001

microscopy (SEM-EDX)) were applied.

AFM imaging is a new applied method to monitor surface changes due to corrosion or inhibition processes. This method is very useful when applied to investigate samples in electrolytes.

In case of copper corrosion in 0.5 M NaCl, several benzohydroxamic acid derivatives (BHA) were tested for inhibition properties. Benzohydroxamic acids were synthesized from their appropriate carboxylic acid chloride and hydroxylamin. In this series of benzohydroxamic, benzoic acid chloride and its substituted derivatives (o-Cl, p-Cl, p-NO_2, o-CH_3) provided the hydroxamic acids. For copper corrosion in 0.1 Na_2SO_4, aromatic sulfoxides (DBSO, DPSO and DPTSO) were investigated.

III. RESULTS

1. GRAVIMETRIC RESULTS

Corrosion rates and inhibition efficiencies were calculated using self-developed software. The concentration of inhibitor needed for maximum protection is also determined.

1.a. Aromatic Sulfoxides in 0.1 M Na_2SO_4

The gravimetric results for this part showed that the average optimal inhibitor concentration for the best inhibition was $5x10^{-4}$ M. One must take into consideration that the tested aromatic sulfoxides had a low solubility and precipitation could take place as in the case of DPSO. That is why the sulfoxides were dissolved in 20 ml of ethanol first and then were added to electrolyte solutions.

The order of the inhibition efficiency of the tested sulfoxides was as follows:

DBSO > DPTSO > DPSO

1.b. Benzohydroxamic Acids in 0.5 M NaCl

The optimum inhibitor concentration was $1x10^{-3}$ M. This concentration was applied throughout all investigations. At higher concentrations, precipitation of the inhibitors could occur due to their low solubility.

The preliminary experiments using the gravimetrical method produced the starting step of this investigation. The initial compounds tested as potential inhibitors for copper corrosion in 0.5 M NaCl, were:

1. Benzohydroxamic acid (BHA)
2. Orto-chloro-benzo-hydroxamic acid (o-Cl-BHA)
3. Para-chloro-benzo-hydroxamic acid (p-Cl-BHA)
4. Orto-hydroxil-benzo-hydroxamic acid (o-H-BHA)
5. Orto-carboxyl-benzo-hydroxamic acid (o-C-BHA)
6. Para-nitro-benzo-hydroxamic acid (p-N-BHA)
7. O-methyl benzohydroxamic acid (o-M-BHA)
8. Orto, orto, para-tri-methyl benzo-hydroxamic acid (o, o', p-M-BHA),

Based on the preliminary experiments results, four inhibitors, p-Cl-BHA, p-N-BHA, o-M-BHA, and o-Cl-BHA were selected for further investigations. A comparison between o-Cl-BHA and p-Cl-BHA shows the effect of the positioning of the substituent the inhibition effect. As the ortho- and para-postion, from charge distribution (electronic) point of view, are equivalent, the improved inhibition of p-Cl-BHA is only due to its more hydrophobic characters.

2. EQCM RESULTS

Most of the classical methods in electrochemistry lack the high sensitivity in determining corrosion rates or inhibition efficiencies. The EQCM provides

http://dx.doi.org/10.14755/DIS.1999.001

a very high sensitive tool to measure mass changes in real time. Although this method is considered as a density scale, nevertheless changes in the range of 10^{-10}g could be detected. The possibility to measure corrosion rates in real time is also a new dimension in monitoring corrosion. Performing long time-range experiments shows the applicability of this method in practical situations. Results of the EQCM tests are obtained as mass changes or frequency changes.

During copper deposition, the frequency decreased linearly and this was used for the calibration of the crystal where the sensitivity constant can be determined.

The EQCM results are divided into two parts, one deals with experiments of copper electrode in acidic sodium sulfate solution with the addition of aromatic sulfoxides and the other in sodium chloride solution with the addition of benzohydroxamic acid derivatives.

2.a. Aromatic Sulfoxides in 0.1 M Na_2SO_4

The electrolyte, used for these tests, was 0.1 M Na_2SO_4 with a pH ≈ 3 and the investigated potential inhibitors for copper corrosion in 0.1 M Na_2SO_4, were the following aromatic sulfoxides:

1 - di-benzyl-sulfoxide (DBSO);

2 - di-phenyl-sulfoxide (DPSO); and

3 – di-p-tolyl-sulfoxide (DPTSO)

The inhibitors were applied in a concentration of $1x10^{-3}$M. Three intervals were used, the first was in blank solution, the second in solution containing an inhibitor and the third is the same as in interval one. Differences in copper dissolution rates in the first and second intervals produced the inhibition efficiencies.

During the first interval (exposure to the aggressive solution), all experiments showed similar behavior: a frequency increases ≈ 2.4 kHz/h, which represents a mass loss on the crystal surface. The similar results for the first interval are expected because of similar conditions. Minor deviations of the frequency change during this interval could be traced back to differences in surface roughness during copper deposition.

Table 1. Thickness reduction rate of copper in 0.1M Na_2SO_4 with the addition of different sulfoxides

	Thickness Reduction Rate (μm/yr)			IE
Sulfoxide	**Interval I**	**Interval II**	**Interval III**	**(%)**
DBSO	710	152	314	78
DPSO	705	528	528	25
DPTSO	704	239	352	66

The addition of the electrolyte containing DBSO showed a steady decrease in the quartz crystal frequency due to the corrosion inhibition. The frequency increase rate in the presence of DBSO was the lowest among the investigated inhibitors. The thickness reduction rate was determined for all intervals by converting frequencies changes to mass changes using Sauerbrey equation. The inhibition efficiency was determined, using the thickness reduction rates of intervals I and II for each inhibitor, and are listed in Table 1

2.b. Benzohydroxamic Acids in 0.5 M NaCl

Results of benzohydroxamic acids investigations in 0.5 M NaCl solution are expressed as mass change (μg. cm^{-2}) vs. time (min), so the corrosion rate could be represented by the slope of the curve at

http://dx.doi.org/10.14755/DIS.1999.001

any particular time. At the time of addition of the different electrolytes, the mass removal or loss from the electrode surface varied.

The aggressive solution without any additive showed very high mass decrease rate before reaching a stable value. Small increase in mass on the electrode was noticed which is due to accumulation of some corrosion products. The addition of the electrolyte containing p-Cl-BHA hindered the decrease of the electrode mass. By the end of the experiment, the electrode mass kept on increasing to a stable value due to adsorption of the inhibitor. The solution containing o-Cl-BHA resulted in a behavior similar to that of the p-Cl-BHA but not as efficient.

All curves represent high mass-loss region, followed by a relaxed region and then a flattened region. Only the electrolyte containing p-Cl-BHA showed different behavior in mass increase on the electrode due probably to adsorption.

The order of protection for the tested BHAs evaluated from the EQCM is: p-Cl-BHA > p-N-BHA > o-Cl-BHA > o-M-BHA.

3. ELECTROCHEMICAL AC AND DC TECHNIQUES

The potentiostatic polarization and impedance spectroscopy measurements have been used in this study. The polarization curves give information on the behavior of the inhibitor in altering the corrosion current and potential.

AC impedance measurements give results in the form of frequency {Hz}, real and imaginary values of amplitude {Ω} and phase shift {degrees}. Using these data, Nyquist plots are constructed as real vs. imaginary parts of the polarization resistance (amplitude). From the Nyquist plots relaxation time constants could be realized. The relaxation time constants could give some indication of the process type, if it is chemical, diffusion, or charge controlled. Semi-circles could be visualized and the intersection of the semicircle at low frequency and the real part axis gives the polarization resistance value. This polarization resistance value is used to evaluate effectiveness of the inhibitors.

3.1. POTENTIOSTATIC POLARIZATION RESULTS

Polarization measurements were conducted to investigate the effect of inhibitors (sulfoxides and benzohydroxamic acids) on copper corrosion in different environments. Corrosion current density (i_{corr}) and corrosion potential E_{corr} and thus the inhibition efficiency are determined.

3.1.a. Sulfoxides in 0.1 M Na_2SO_4 solution

DBSO shifted the OCP toward more cathodic value while, DPTSO shifted it to more anodic value. DPSO did not show a significant change in behavior comparing to the blank solution. In more details, the polarization curves could be separated into anodic and cathodic parts. In the anodic part, which represents the metal dissolution, all curves showed similar behavior at potential values higher than 400 mV. The current density decreased slightly. The addition of DBSO influenced all regions of the graph. DPSO did not significantly influence the reactions, neither anodically nor cathodically.

http://dx.doi.org/10.14755/DIS.1999.001

Table 2. Potentiostatic polarization results for copper in 0.1M Na_2SO_4 with and without the addition of sulfoxides

Inhibitor	Corrosion current Density ($\mu A/cm^2$)	IE (DC) (%)
Blank	6.61	-
DBSO	1.25	81
DPSO	4.78	27
DPTSO	2.61	60

Normally, one is able to observe a region where the slope is nearly constant, the so-called Tafel region. However, the presence of the inhibitors led to a total deviation from the Tafel behavior. A summary of data for copper, in 0.1 M Na_2SO_4 without and with the addition of the investigated sulfoxides, obtained from the polarization curves is tabulated in Table 2.

At the end of each polarization experiment, visual observations were made. Colored surface films appeared beginning at a potential of about 450 mV. Some products grew with time and eventually fell off the electrode. These surface films could be easily rinsed off with distilled water. The observations are tabulated in the following Table 3.

3.1.b. Benzohydoxamic Acids in 0.5 M NaCl Solution

Polarization curves of the investigated benzohydroxamic acids show shifts of open circuit potential (OCP) to more cathodic values. Anodically all curves exhibit three distinct regions. A Tafel region at lower-over-potentials extending to a peak current density (i_{peak}). Then a region of decreasing current until a minimum value i_{min} is reached. Finally, a region of sudden increase in current density leading to a limiting value (i_{lim}) was observed.

Table 3. Visual observations after polarization measurements of copper in 0.1 M Na_2SO_4 without and with the addition of sulfoxides.

Inhibitor	Observations
0.1 M Na_2SO_4	Greenish solution, uniform attack
DBSO	Dark gray film, removed easily by water, uniform attack
DPSO	Black layer formed, solution was greenish
DPTSO	Dark brown layer on the electrode, some pits

The addition of the inhibitors to the corrosive medium shifted the polarization curves toward lower i_{lim}, i_{min} and i_{peak}. The extent of the shift was maximal in the case of p-Cl-BHA.

Table 4. Corrosion inhibition parameters of copper electrode in 0.5 M NaCl without and with the addition of different BHA's

Inhibitor	β_a (mV/Dec)	(i_{peak}) ($\mu A/cm^2$)	(i_{min}) ($\mu A/cm^2$)
BLANK	65	8700	3675
p-Cl-BHA	82	5620	485
o-Cl-BHA	72	7820	3935
p-N-BHA	75	7780	2265
o-M-BHA	72	7940	4345

In the cathodic region, all inhibitors reduced the current density at potential lower than the OCP. The results obtained from the polarization curves are summarized in Table 4. The order of effectiveness of the inhibitors was similar to the previous methods results.

http://dx.doi.org/10.14755/DIS.1999.001

Visual inspection was performed at the end of each experiment and observations are listed in Table 5.

Table 5. Visual observations after polarization measurements of copper in 0.5 M NaCl without and with the addition of BHAs.

Inhibitor	Observations
0.5 NaCl	Thick greenish solution resulted, pits were formed on the electrode
p-Cl-BHA	Light green color started at high potentials, uniform surface
o-Cl-BHA	Thicker dark-greenish solution, corrosion pits were noticed
o-m-BHA	Greenish solution started to form at potentials > 100 mV
p-N-BHA	white particles started to appear at potential > 0 mV.

3.2. EIS RESULTS

The EIS results are presented in the form of real vs. imaginary parts of the impedance amplitude. R_p values from the Nyquist plots are used to calculate the inhibition efficiency.

3.2.a. Copper in 0.1 Na_2SO_4 with Sulfoxides

From the Nyquist plot of data measured of copper in 0.1 M Na_2SO_4 solution (pH=3) in the absence and presence of the tested sulfoxides, a semicircle could be visualized, which intersects the real value axis at different values. This intersection represents the R_p value for each inhibitor curve. The inhibition efficiencies of the sulfoxides are listed in Table 6.

3.2.b. Copper in 0.5 M NaCl with BHA Derivatives

The Nyquist curve for copper in NaCl, obtained at the corrosion potential, shows two more-or-less poorly separated semi-circles. One semicircle is at high frequency range and another is at low frequency range. All investigated BHA produced higher R_p values than the solution without inhibitor as seen in Table 7.

Table 6. Polarization resistance values (R_p) from Nyquist plot for copper in 0.1M Na_2SO_4 without and with the addition of sulfoxides.

Inhibitor	Polarization resistance R_p (ohm cm^2)	IE (AC) (%)
Blank	120	-
DBSO	440	73
DPSO	180	33
DPTSO	340	64

Table 7. Polarization resistance values (R_p) from Nyquist plot for copper in 0.5 M NaCl without and with the addition of different BHAs

Inhibitor	Polarization resistance R_p (k ohm cm^2)	IE (AC) %
BLANK	3.5	-
p-Cl-BHA	17.2	80
o-Cl-BHA	9.7	64
p-N-BHA	13.0	72
o-M-BHA	5.5	36

Further information was obtained by the evaluation of the impedance data, which were fit to a model circuit that would describe the system physically. In order to fit the EIS data, special software, which uses a non-linear least square fit (NLLS-fit) method, was used.

http://dx.doi.org/10.14755/DIS.1999.001

For copper corrosion in 0.1 M Na_2SO_4 at pH=3, in the presence of DBSO, the EIS data were fitted by semicircles using a physical model. This model produced a good fit between the measured and simulated data. The electrochemical parameters: solution resistance; film resistance; corrosion products capacitance; electrochemical charge transfer resistance and the double layer capacitance were obtained.

For copper corrosion in 0.5 M NaCl at neutral pH range, Nyquist spectra were deconvolved using a model similar to the one presented by several authors for an inhomogeneous 3D layer. This model can simulate organic film coating behavior (i.e. p-Cl-BHA) in the presence of pits or defects in the layer. The transfer function consists of a parallel combination of the impedance of the covered surface areas (θ) and of the active surface area (1-θ), linked to the metal corrosion process.

4. SURFACE ANALYTICAL TECHNIQUES RESULTS.

4.1. Atomic Force Microscopy Data

Surface analytical methods are becoming increasingly important in characterizing the layers formed on the electrodes. AFM imaging has an advantage to be used as an *in-situ* technique to monitor changes on the surface in time. The AFM results can be represented in three different forms of images: the first is a 3D presentation of the surface image, the second is a 2D image and the third is a section analysis micrograph. The 3D presentation shows the surface morphology which is represented the RMS factors.

The images of dried copper surfaces after immersion in acidic 0.1 M Na_2SO_4 in the absence and presence of DBSO show the effectiveness of the inhibitor against the corrosion process. The same is applied for samples in 0.5 M NaCl solution in the absence and presence of p-Cl-BHA, which produced smoother surface.

In-situ measurements were performed in order to follow changes on the metal-electrolyte interface after introducing the solution without and with the added inhibitors. The injection of 0.1 M Na_2SO_4 solution demonstrate some corrosion process initiating along active boundaries such as polishing groves. Rougher surfaces was indicated by increasing the RMS values in time.

In the case of the presence of DBSO in the solution a layer started to form on the surface which smoothened the surface and plugged all the active site, caused by the mechanical polishing process. The RMS of this series of images decreased in time. Table 8 summarizes the RMS values in the absence and the presence of DBSO in the electrolyte.

A series of 3D images measured on copper electrode surface in 0.5 M NaCl in the absence of p-Cl-BHA. The effect of 0.5 M NaCl on copper showed the initiation of pitting corrosion. Pits started to develop at t = 1 min. and grew in size.

Table 8. RMS values for surfaces of copper in 0.1 M Na_2SO_4 without and with DBSO.

Time (min)		0	5	15	30	45
RMS Values	**0.1 M Na_2SO_4**	2	3	5	6	8
	+ DBSO	2	3	2	2	1

http://dx.doi.org/10.14755/DIS.1999.001

Corrosion products, most likely $CuCl_2$, accumulate on the surface. RMS value, which is an indication of pit deepness, increased sharply. The results demonstrated that p-Cl-BHA was adsorbed on the surface and plugged the active sites where pitting corrosion is most likely to take place as could be seen by the value of RMS in Table 9.

Table 9. Section analysis results for copper in 0.1 M NaCl without and with BHA.

Time	(min)	2	7	10	15	20	30	45	60
Vertical Distance (nm)	0.5 M NaCl	15	25	26	29	31	34	43	48
	0.5 M NaCl + p-Cl-BHA	7	7	4	5	7	4	2	1

4.2. Scanning Electron Microscopy-EDX Results

The morphology of the electrode surface after different pretreatments was investigated using scanning electron microscopy (SEM) with a magnification power of 3,500. The SEM is attached to an Energy Dispersive X-ray Spectrometer (EDX-spectrometer) which can provide quantitative analysis of the surface layer.

The EDX spectra did not provide any valuable quantitative results of the species on the electrode surface. This was due to the deep penetration of the analyzer beam into the surface. High concentration of copper was measured which made the rest of the components relatively negligible.

SEM results of the copper electrode surface, immersed for 20 hrs in 0.1 M Na_2SO_4, at pH=2.95, in the absence and presence of DBSO revealed that corrosion process clearly occurred along possible scratch lines but uniformly distributed. Where SEM data of copper surfaces immersed in 0.5 M NaCl solution, at pH≈7, for 20 hrs in the absence and presence of p-Cl-BHA showed that pits, due to corrosion attack, grew in the absence of inhibitor while the addition of p-Cl-BHA, localized corrosion attacks was prevented.

The study of sulfoxides proved that out of the investigated molecules, DBSO was the most efficient. Its actions are due to the conversion of the sulfoxide molecule to sulfide molecule on the electrode surface. This sulfide molecule is not so soluble in the aggressive solution. Thus it accounts for the inhibition efficiency. As for the BHA molecules; p-Cl-BHA proved to be the most effective among the tested molecules. The inhibition action is due to the attachment of the molecule to the electrode surface.

http://dx.doi.org/10.14755/DIS.1999.001

IV. NEW SCIENTIFIC RESULTS

Based on all experiments results of the dissertation, the following conclusions can be drawn:

1. The quartz microbalance is a powerful technique, which allows the determination of the corrosion rate or mass loss of copper and to monitor the effectiveness of the tested inhibitors. These measurements could be performed not only in acidic media but also in neutral media where the protective film tends to be much thicker. The high sensitivity of EQCM allows distinguishing between different processes on the electrode surface.
2. EQCM has proven to be useful as a tool for long time *in-situ* measurements where corrosion monitoring is needed. The stability of the method over a long period is advantageous.
3. The EIS results provided fast and dependable method to evaluate inhibition efficiency. The results from this method were in agreement with other experimental data.
4. AFM in contact mode, a newly applied surface imaging method could be used for monitoring processes taking place on the electrode. Pit formation rate and surface roughness can be obtained from the section analysis data.
5. The different experiments have shown that among the aromatic sulfoxides used to inhibit copper corrosion in acidic media, DBSO was the most efficient. DPTSO also produced some satisfactory results.
6. The inhibition action of DBSO on copper corrosion may be considered to be a two-steps process where the sulfoxide is first converted to sulfide, which forms a badly soluble layer on the electrode surface thus hindering the metal dissolution.
7. For copper corrosion in chloride media with different BHA inhibitors, p-Cl-BHA proved effective against copper corrosion. This inhibitor could be developed into a replacement to toxic inhibitors such as azoles. The order of inhibition efficiency among the BHA derivatives is: p-Cl-BHA > p-N-BHA > o-Cl-BHA > o-M-BHA.
8. The inhibition action of the BHA derivatives is due to complexing actions between the inhibitors and the copper chloride products.
9. The treatment of experimental data using EQCM and AFM methods presented in this thesis constitutes the basis of further research aiming to understand the mechanism of copper inhibition in different media in terms of fundamental physical-chemical phenomena. For this purpose, imaging techniques combined with surface analysis and electro-gravimetrical techniques are very promising.

http://dx.doi.org/10.14755/DIS.1999.001

PUBLICATIONS

I. Contributions in scientific journals

[P1] **A. Shaban**, E. Kálmán and I. Biczó Corros. Sci. **35**. 1463 (1993)

[P2] **A. Shaban**, J. Telegdi, and E. Kálmán, *"Progress in the Understanding and prevention of corrosion"*, Ed. J. M. Costa and A. D. Mercer, **2**, 916 (1993)

[P3] E. Kálmán, B. Várhegyi, I. Bakó, I. Felhösi, F. H. Kármán, **A. Shaban,** "*Corrosion Inhibition by 1-Hydroxyl-ethane-1,1-diphosphonic Acid: An Electrochemical Impedance Spectroscopy Study",* J. Electrochem. Soc., **141**. 3357 (1994).

[P4] **A. Shaban**, J. Telegdi, S. Alexandre and E. Kálmán, CORROSIONE, Pitture e Vernici Europe, **12**, 23 (1995).

[P5] Kálmán E., Várhegyi B., Felhösi I., Bakó I., Pálinkás G., Kármán F. és **A. Shaban** Magy. Kém. Foly., **102**, 211 (1996).

[P6] **A. Shaban**, E. Kálmán, and J. Telegdi "*An Investigation of Copper Corrosion Inhibition in Chloride Solution by Benzohydroxamic acids*", Electrochim. Acta., **43,** 159 (1998).

[P7] I. Lukovits, I. Bakó, **A. Shaban** and E. Kálmán *"Polynomial Model of the Inhibition Mechanism of Thiourea Derivatives"* Electrochim. Acta., **43**, 131 (1998).

[P8] **Abdul Shaban**, Kálmán Erika és Telegdi Judit "A rézkorrózió inhibiciója benzhidroxám - sav-származékokkal vizes nátrium-klorid-oldatban", Magy. Kém. Foly., **103**, 572 (1997)

[P9] **A. Shaban,** J. Telegdi, E. Kálmán, G. Pálinkás and Gy. Dóra, "Corrosion and Inhibition of Copper in Different Electrolyte Solutions", J. Appl. Phys., **66**. xx (1998)

[P10] **A. Shaban** and E. Kálmán *"Inhibitor of Copper Corrosion in Acidic Solutions by Various Aromatic Sulfoxides*", Corrosion, submitted for publications.

II. Patents

[PT1] "Water treating agents and additives derived from compounds containing free amino-group", Patent No. **HU 69027, 28-08-1995**

III. Contributions in local and international conferences

[C1] **A. Shaban**, E. Kálmán and I. Biczó, Proceedings, **ECASIA'91**, **4th Euro. Conf. App. Surface Analysis** Budapest, Hungary, (1991)

[C2] E. Kálmán, F. Kármán, I. Kónya, Gy. Litkei, **A. Shaban**, J. Telegdi, L. Várallyai Proceedings, **EUROCORR'91**, Budapest, Hungary, (1991)

[C3] **A. Shaban**, B. Várhegyi, E. Kálmán, I. Biczó, Proceedings, **Advances in corrosion and protection**, UMIST, UK, (1992)

[C4] **A. Shaban**, J. Telegdi, E. Kálmán, G. Singh, Proceeding, **10th European Corr. Congress**, Barcelona, Spain, (1993)

[C5] **A. Shaban**, J. Telegdi, S. Alexandre, E. Kálmán, Proceedings, **UK CORROSION'94** and **EUROCORR'94,** Bournemouth, UK, October (1994)

[C6] **A. Shaban** and E. Kálmán Proceedings, **46th ISE** Meeting, Xiamen, China, (1995)

[C7] **A. Shaban**, E. Kálmán and J. Bácskai Proceedings, **8th Euro. Symp. Corr. Inhib. (8 SEIC)** Ann. Univ. Ferrara, N. S. Sez. v. Suppl. No. 10. (1995)

[C8] **A. Shaban**, J. Telegdi and E. Kálmán Proceedings, **47th ISE** Meeting, Balatonfüred, Hungary, (1996)

[C9] **A Shaban**, J. Telegdi and E. Kálmán Proceedings, **EUROCORR'96**, Nice, France, August (1996)

[C10] **A. Shaban,** Seminar, **HUNKOR** Meeting, ***Mátrafüred***, Hungary, March, (1997)

[C11] **A. Shaban**, J. Telegdi, E. Kálmán, Gy. Dóra and G. Pálinkas, Proceedings, **STM'97**, **9th Conf. STM, Spect. And Rel. Tech.**, Hamburg, Germany, July (1997)

[C12] J. Telegdi, **A. Shaban**, Zs. Keresztes and E. Kálmán, Proceedings, **EMCR-VI**, Trento, Italy, August (1997)

[C13] **A. Shaban**, E. Kálmán and J. Telegdi Proceedings, **ISE'97 and Electrochemical Society**, Joint Meeting, Paris, France, September (1997)

http://dx.doi.org/10.14755/DIS.1999.001